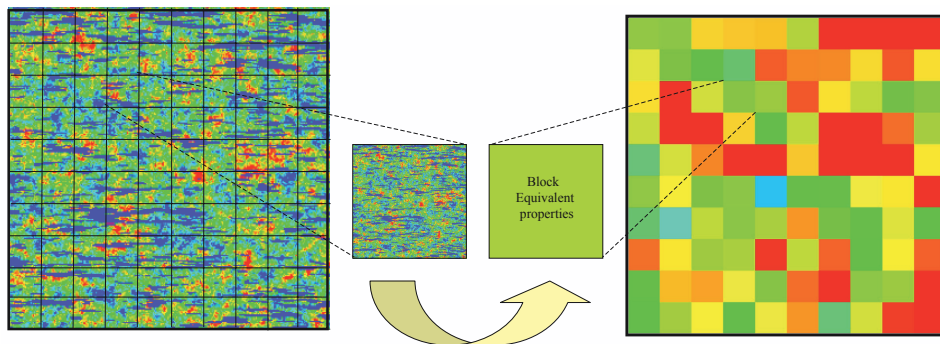




UNIVERSIDAD  
POLITECNICA  
DE VALENCIA

grupo  
de **HIDROGEOLOGIA**

## Upscaling non-reactive solute transport



PhD Thesis submitted by  
**Gerónimo Llerar-Meza**

Advisors:  
**J. Jaime Gómez-Hernández**  
**Daniel Fernández-García**



# Upscaling non-reactive solute transport

PhD Thesis submitted by  
**Gerónimo Llerar-Meza**

Advisors:  
**J. Jaime Gómez-Hernández**  
**Daniel Fernàndez-Garcia**

PhD Program:  
**Ingeniería Hidráulica y Medio Ambiente**

Department:  
**Ingeniería Hidráulica y Medio Ambiente**

**Grupo de Hidrogeología**  
**Universidad Politécnica de Valencia**  
**Valencia, Spain**

April 2009



*A Liz*



# Abstract

This thesis focuses on solute transport upscaling. Upscaling of solute transport is usually required to obtain computationally efficient numerical models in many field applications such as, remediation of aquifers, environmental risk to groundwater resources or the design of underground repositories of nuclear waste. The non-Fickian behavior observed in the field, and manifested by peaked concentration profiles with pronounced tailing, has questioned the use of the classical advection-dispersion equation to simulate solute transport at field scale using numerical models with discretizations that cannot capture the field heterogeneity. In this context, we have investigated the use of the advection-dispersion equation with mass transfer as a tool for upscaling solute transport in a general numerical modeling framework.

Solute transport by groundwater is very much affected by the presence of high and low water velocity zones, where the contaminant can be channelized or stagnant. These contrasting water velocity zones disappear in the upscaled model as soon as the scale of discretization is larger than the size of these zones. We propose, for the modeling solute transport at large scales, a phenomenological model based on the concept of memory functions, which are used to represent the unresolved processes taking place within each homogenized block in the numerical models.

We propose a new method to estimate equivalent blocks, for which transport and mass transfer parameters have to be provided. The new upscaling technique consists in replacing each heterogeneous block by a homogeneous one in which the parameters associated to a memory functions are used to represent the unresolved mass exchange between highly mobile and less mobile zones occurring within the block. Flow upscaling is based on the *Simple Laplacian with skin*, whereas transport upscaling is based in the estimation of macrodispersion and mass transfer parameters as a result of the interpretation of the residence time distribution of particles passing through a given block using fine-scale heterogeneous simulations.

The methodology proposed is applied in a Monte Carlo framework to model solute transport in several two-dimensional synthetic aquifers. The upscaled results are compared to a reference Monte Carlo analysis carried out at a smaller scale. The memory functions used to model transport at the com-

putational scale are based on the multi-rate mass transfer equations. Several formulations of the multi-rate mass transfer model, which differ in the type of memory function, were used and compared.

For the performance of the upscaled models we analyzed the reproduction of the ensemble mean behavior of the main features associated with the simulated breakthrough curves (BTCs). We examined the effect of upscaling on model uncertainty and the spatial distribution of the solute mass plume. The results showed that an appropriate description of the residence time distribution for all blocks of the numerical model provides an upscaled transport model that is capable to reproduce the ensemble mean behavior of the BTCs, but has problems in reproducing both uncertainty and plume dilution.

# Resumen

El objeto de la presente tesis es el estudio del escalado del transporte de solutos no reactivos. El escalado es usualmente aplicado para obtener modelos numéricos de acuífero, que son una herramienta alternativa altamente eficiente, para establecer estrategias en problemas tales como, la remediación de suelos y aguas subterráneas contaminadas, el diseño de almacenamientos de residuos reactivos, o la evaluación del riesgo ambiental para las aguas subterráneas.

El comportamiento anómalo (en la literatura anglosajona *non-Fickian*) observado en los resultados de ensayos de trazadores ejecutados en campo o en laboratorio, tales como los perfiles de concentración con un alto pico y una larga cola, cuestionan el uso de la clásica ecuación de advección-dispersión, para simular el transporte a escala computacional. En este contexto, se presentan las investigaciones en el uso de los modelos escalados de transferencia de masa como una herramienta alternativa para el escalado del transporte, bajo el enfoque de la modelación aplicada.

El desplazamiento de un contaminante en las aguas subterráneas es afectado por la presencia de zonas de altas y de bajas velocidades del flujo, donde el contaminante puede viajar libremente o bien puede ser retenido. Ese contraste de velocidades tiende a desaparecer en los modelos escalados, a medida que la escala de la malla de modelación sea más grande que el tamaño de esas zonas. En dichas circunstancias, para reproducir el comportamiento del transporte observado con un modelo escalado, es necesario considerar un proceso adicional de transferencia de masa entre las zonas más y menos conductivas en la ecuación de advección-dispersión.

Así, se propone como alternativa, un modelo fenomenológico basado en concepto de que el transporte puede ser simulado a gran escala usando a una malla de modelación con bloque homogéneos de gran tamaño, donde los parámetros de transporte asociado consideran alguna memoria vinculada a la heterogeneidad de las propiedades hidrogeológicas, a cuales son sometidas las partículas de contaminante a lo largo de su viaje por el medio.

De este modo, se presenta una metodología para estimar los valores equivalentes de bloque asociados a la ecuación alternativa de transporte. La nueva técnica de escalado consiste en que cada bloque con valores heterogéneos de transmisividad es reemplazado por un bloque homogéneo. A cada uno de esto

bloques se le asigna un valor equivalente de transmisividad y de los coeficientes de transferencia de masa y de dispersión, para representar los mecanismos de transporte que tienen lugar en cada uno a escala fina. Estos valores son asignados en función de los mismos en las celdas que contiene cada bloque. El valor equivalente de la transmisividad se obtiene aplicando la técnica de escalado conocida como *Simple Laplaciano con piel*. Por su parte, los coeficientes de transferencia de masa y de dispersión asociados a una función de memoria, son derivados de la interpretación de la distribución de los tiempos de residencia de las partículas que atraviesan el área delimitada por cada bloque a escala fina.

La metodología propuesta ha sido evaluada mediante simulaciones de Monte Carlo de transporte, aplicada en diversos casos sintéticos de acuíferos bidimensionales, y en cada caso usando diferentes formulaciones de transferencia de masa. Los resultados de los modelos escalados son comparados con una solución de referencia derivada a una escala fina.

El comportamiento de los modelos escalados fue evaluado desde dos perspectivas diferentes: De un lado, se analiza la reproducción del comportamiento medio de las principales características del conjunto de curvas de llegada (BTCs). Además, se determina el efecto que causa el escalado sobre la reproducción de la incertidumbre, así como en la reproducción de la distribución espacial del penacho de contaminante de referencia. Los resultados derivados del análisis estocástico indican, que una apropiada reproducción de la distribución de los tiempos de residencia en cada uno de los bloques del modelo numérico a escala gruesa, asegura que el modelo escalado es capaz de reproducir el comportamiento medio del conjunto de BTCs. Por otro lado, se muestra que los modelos escalados poseen un bajo poder predictivo para reproducir el nivel de incertidumbre y el grado de dilución del penacho de la solución de referencia.

# Resum

L'objectiu de la presente tesi és l'estudi de l'escalat del transport de soluts no reactius. L'escalat és usualment aplicat per a obtenir models numèrics d'aqüífer, que són una eina alternativa altament eficient, per establir estratègies en problemes com ara, la remediació de sòls i aigües subterrànies contaminades, el disseny d'emmagatzematges de residus reactius, o l'evaluació del risc ambiental per a les aigües subterrànies.

El comportament anòmal (referit en la literatura anglosaxona com *non-Fickian*) observat en els resultats d'assaigs de traçadors executats en camp o en laboratori, tals com els perfils de concentració amb un alt pic i una llarga cua, qüestionen l'ús de la clàssica equació d'advecció-dispersió, per simular el transport a escala computacional. En aquest context, es presenten les investigacions en l'ús dels models escalats de transferència de massa com una eina alternativa per l'escalat del transport, baix l'enfocament de la modelació aplicada.

El desplaçament d'un contaminant a les aigües subterrànies és afectat per la presència de zones d'alt i de baixes velocitats del flux, on el contaminant pot viatjar lliurement o bé pot ser retingut. Aquest contrast de velocitats tendeix a desaparèixer en els models escalats, a mesura que l'escala de la malla de modelació sigui més gran que la mida d'aquestes zones. En aquestes circumstàncies, per reproduir el comportament del transport observat amb un model escalat, cal considerar un procés addicional de transferència de massa entre les zones més i menys conductives en l'equació d'advecció-dispersió. Es proposa ací com a alternativa, un model fenomenològic basat en el concepte de que el transport pot ser simulat a gran escala utilitzant una malla de modelació amb bloc homogenis de grans dimensions, on els paràmetres de transport associats consideren alguna memòria vinculada a l'heterogeneïtat de les propietats hidrogeològiques, a quals són sotmeses les partícules de contaminant al llarg del seu viatge pel mig.

D'aquesta manera, es presenta una metodologia per estimar els valors equivalents de bloc associats a l'equació alternativa de transport. La nova tècnica d'escalat consisteix en que cada bloc amb valors heterogenis de transmissivitat és reemplaçat per un bloc homogeni. A cadascun dels blocs se li assigna un valor equivalent de transmissivitat i dels coeficients de trans-

ferència de massa i de dispersió, per representar els mecanismes de transport que tenen lloc a cada un a escala fina. Aquests valors són assignats en funció dels mateixos en les cel·les que conté cada bloc. El valor equivalent de la transmisivitat s'obté aplicant la tècnica d'escalat coneguda com *Laplaci ^ simple amb pell*. Per la seva banda, els coeficients de transferència de massa i de dispersió associats a una funció de memòria, són derivats de la interpretació de la distribució dels temps de residència de les partícules que travessen l'àrea delimitada per cada bloc a escala fina.

La metodologia proposada ha sigut avaluada mitjançant simulacions de Monte Carlo de transport, aplicada a diversos casos sintètics d'aqüífers bidimensionals, i en cada cas usant diferents formulacions de transferència de massa. Els resultats dels models escalats són comparats amb una solució de referència derivada a una escala fina.

El comportament dels models escalats va ser valorat des de dues perspectives diferents: D'una banda, s'analitza la reproducció del comportament mitjà de les principals característiques del conjunt de corbes d'arribada (BTCs). A més, es determina l'efecte que causa l'escalat sobre la reproducció de la incertesa, així com en la reproducció de la distribució espacial del plomall de contaminant de referència. Els resultats derivats de l'anàlisi estocàstic indiquen que una apropiada reproducció de la distribució dels temps de residència a cadascun dels blocs del model numèric a escala gruixuda, assegura que el model escalat és capaç de reproduir el comportament mitjà del conjunt de BTCs. D'altra banda, es mostra que els models escalats tenen un baix poder predictiu per reproduir el nivell d'incertesa i el grau de dilució del plomell de la solució de referència.

# Agradecimientos

Quiero agradecer al profesor J. Jaime Gómez-Hernández, por darme la oportunidad de desarrollar mi tesis doctoral en su grupo de Hidrogeología, así como por haber aceptado ser mi tutor y director de tesis. Le agradezco también, por otorgarme todas las facilidades durante mi estancia en Valencia, y por la confianza depositada en mi trabajo. Fue una gran experiencia y un orgullo haber trabajado con él. Gracias Jaime.

Parte de mi agradecimiento es para mi codirector profesor Daniel Fernández-García, que gracias a su entusiasmo, paciencia y generosidad me permitieron llevar acabo la presente tesis. Gracias Dani.

Agradezco también a los profesores asociados al grupo Andrés Sahuquillo Herráiz, Javier Rodrigo Ibarri y Eduardo Cassiraga, quien siempre me asesoró con las cuestiones relacionadas con el  $\text{\LaTeX}$ . A Mis compañeros Peter, Salvador, Carlos, Jianli Fu, Haiyan Zhou y Liangping Li. A Teresa Martínez Candela, por la atención prestada y por el trato recibido de su parte.

A la Facultad de Ingeniería de la Universidad Autónoma de Chihuahua, México, por otorgarme una beca PROMEP, por un período de tres años de los estudios de doctorado.

Asimismo, agradecer la financiación recibida proveniente de la Comunidad Europea a través de los proyectos integrados FUNMIG (contrato FIW6-516514) y PAMINA (contrato: FIW6-036404); y de ENRESA, Empresa Nacional de Residuos Radioactivos S.A., para la realización de esta investigación.

Por último a toda mi familia, en especial a Liz, mi esposa, por su amistad y su amor.



# Contents

<b>1</b>	<b>Introduction</b>	<b>1</b>
1.1	Motivation and Objectives . . . . .	1
1.2	Thesis Structure . . . . .	2
<b>2</b>	<b>Review of Upscaling Methodologies</b>	<b>3</b>
2.1	Introduction . . . . .	3
2.2	The Starting Point: The Advection Dispersion Equation . . . . .	4
2.3	Time-Dependent Macrodispersive Models . . . . .	7
2.4	Multi-rate Mass Transfer Models . . . . .	8
2.5	Continuous Time Random Walk Models . . . . .	11
2.6	Fractional Advection-Dispersion Transport Models . . . . .	12
2.7	Summary . . . . .	13
2.8	References . . . . .	13
<b>3</b>	<b>Upscaling Transport with Mass Transfer Model</b>	<b>17</b>
3.1	Introduction . . . . .	18
3.2	Transport Models . . . . .	20
3.2.1	The Local Transport Model . . . . .	20
3.2.2	The Upscaled Mass Transfer Model . . . . .	21
3.3	Monte Carlo Transport Simulations . . . . .	23
3.3.1	Setup . . . . .	23
3.3.2	Reference Transmissivity Fields . . . . .	24
3.3.3	Flow and Transport Solution . . . . .	26
3.4	Estimation of Block Equivalent Properties . . . . .	27
3.4.1	Methodology . . . . .	27
3.4.2	Implementation Details . . . . .	30
3.5	Numerical Results and Discussion . . . . .	31
3.5.1	Ensemble Average Behavior . . . . .	32
3.5.2	Propagation of Uncertainty . . . . .	36
3.6	Summary and Conclusions . . . . .	43
3.7	References . . . . .	45

---

<b>4</b>	<b>Modeling Solute Transport at Large Scale in Heterogeneous Media</b>	<b>51</b>
4.1	Introduction . . . . .	52
4.2	Solute Transport Experiments . . . . .	55
4.2.1	Experimental Design . . . . .	55
4.2.2	Reference Transmissivity Field . . . . .	56
4.2.3	Flow and Transport Solution . . . . .	63
4.2.4	Flow and Transport Parameters . . . . .	64
4.3	Results and discussion . . . . .	65
4.3.1	Overview of Plume Behavior . . . . .	65
4.3.2	Longitudinal Mass Distribution . . . . .	69
4.3.3	Dilution Index . . . . .	69
4.4	Summary and Conclusions . . . . .	74
4.5	References . . . . .	75
<b>5</b>	<b>Conclusions and Future Research</b>	<b>81</b>
5.1	General Conclusions . . . . .	81
5.2	Future Research . . . . .	82
	<b>Appendix</b>	<b>84</b>
<b>A</b>	<b>Calibration of Mass Transfer Parameters</b>	<b>85</b>
A.1	Reference . . . . .	86

# List of Figures

2.1	Representation of mass transfer conceptual model. . . . .	10
3.1	Illustration of the upscaling process: (a) Map of transmissivities for a given realization superposed with the discretization of the upscaled model (black lines); (b) Map of equivalent transmissivities ( $T_{xx}^v$ ). . . . .	24
3.2	Illustration of the steps involved in the stochastic generation of the composite transmissivity field, $Y(\mathbf{x}) = (1 - I(\mathbf{x}))Y_1(\mathbf{x}) + I(\mathbf{x})Y_2$ . Blue and red pixels in the $I(\mathbf{x})$ -map indicates materials $M_1$ and $M_2$ , respectively. . . . .	25
3.3	Comparison of the cumulative mass flux breakthrough curves obtained at a given $x$ -control plane ( $x = 143.3$ units) using one realization of the transmissivity field $Y_1(\mathbf{x})$ and its associated composite medium $Y(\mathbf{x})$ . . . . .	26
3.4	Map of hydraulic heads superposed with particle paths obtained from a transport simulation (only 100 particles) in an individual realization of the composite random field. . . . .	28
3.5	Calculation of residence times in a given block of the numerical model. . . . .	30
3.6	Evolution of the effective longitudinal dispersivity with travel distance . . . . .	33
3.7	Evolution with travel distance of the mean sum of square error associated with the calibrated model obtained curve-fitting $f_\tau$ with a theoretical model. . . . .	33
3.8	Evolution of the ensemble average first arrival of the BTC $T_{05}$ with travel distance. . . . .	34
3.9	Evolution of the ensemble average slope $T_{60} - T_{80}$ with travel distance. . . . .	35
3.10	Evolution of the ensemble average slope $T_{80} - T_{95}$ with travel distance. . . . .	36
3.11	Evolution of the mean concentration peak with travel distance. . . . .	37

---

3.12	Ensemble of breakthrough curves obtained at $x = 34$ units for the different upscaled models contrasted against the reference solution. The 95% confidence interval refer to the ensemble of 50 realizations. . . . .	38
3.13	Ensemble of breakthrough curves obtained at $x = 110.8$ units for the different upscaled models contrasted against the reference solution. The 95% confidence interval refer to the ensemble of 50 realizations. . . . .	39
3.14	Propagation of uncertainty: Comparison of the reference confidence interval with those obtained using the upscaled models at two different control planes. . . . .	40
3.15	Cumulative frequency distribution of the late-time slope of BTCs for the different upscaled models. The late-time slope corresponds to the region of the BTCs comprised between the 60% and 80% of the BTC total mass. . . . .	41
3.16	Cumulative frequency distribution of the early arrival time ( $T_{05}$ ) of BTCs for the different upscaled models. . . . .	42
3.17	Comparison of the simulated ensemble of BTCs obtained with and without transverse macrodispersivity. . . . .	43
4.1	Representation of the steps involved in the stochastic generation of a composite transmissivity field. . . . .	57
4.2	Illustration of the realization of the reference natural log of transmissivity $G_1(\mathbf{x})$ for the first scenario . . . . .	58
4.3	Illustration of the realization of the reference natural log of transmissivity $G_1(\mathbf{x})$ for the second scenario . . . . .	58
4.4	Transmissivity structure and histogram for the first composite field. . . . .	59
4.5	Experimental and model variograms for the $\ln T$ in the first scenario for the $x$ and $y$ directions. . . . .	59
4.6	Cumulative mass flux breakthrough curves obtained at a given x-control plane ( $x = 159.9$ units) computed on the transmissivity field $G_1(\mathbf{x})$ and on the associated composite medium $G(\mathbf{x})$ for scenario 1 . . . . .	60
4.7	Transmissivity field and histogram for the composite field in the second scenario. . . . .	60
4.8	Experimental and model variograms for the $\ln T$ in the second scenario for the $x$ and $y$ directions. . . . .	61
4.9	Cumulative mass flux breakthrough curves obtained at a given x-control plane ( $x = 159.9$ units) computed on the transmissivity field $G_1(\mathbf{x})$ and its associated second composite medium $G(\mathbf{x})$ for scenario 2. . . . .	61

---

4.10	Transmissivity field and histogram for the third composite field.	62
4.11	Cumulative mass flux breakthrough curves obtained at a given x-control plane ( $x = 159.9$ units) computed on the transmissivity fields for scenarios 2 and 3. . . . .	62
4.12	Different size of blocks used in the upscaling process . . . . .	63
4.13	Plan view of the location of the injection area and location of the control plane, at 75 units along the $x$ direction from the injection. . . . .	64
4.14	Log concentration distribution of solute mass for the three scenarios. Comparison between the simulations in the reference field and in the upscaled fields with blocks of 5 by 5 cells using two different transport models at the coarse scale. (a) First scenario, (b) second scenario and (c) third scenario. . . . .	66
4.15	Log concentration distribution of solute mass for the three scenarios. Comparison between the simulations in the reference field and in the upscaled fields with blocks of 15 by 15 cells using two different transport models at the coarse scale. (a) First scenario, (b) second scenario and (c) third scenario. . . . .	67
4.16	Comparison of the temporal evolution of relative entropy of double rate and macrodispersion models for the three scenarios. In all cases, entropy is computed relative to the reference case .	68
4.17	Longitudinal mass distribution profiles for the reference solution and the upscaled models using 5 by 5 blocks and modeling transport by double rate and enhanced macrodispersion for times $t = 300$ (left column) and $t = 600$ (right column). a) Scenario 1, b) scenario 2 and c) scenario 3. Injection point at $x = 60$ units . . . . .	70
4.18	Longitudinal mass distribution profiles for the reference solution and the upscaled models using 15 by 15 blocks and modeling transport by double rate and enhanced macrodispersion for times $t = 300$ (left column) and $t = 600$ (right column). a) Scenario 1, b) scenario 2 and c) scenario 3. Injection point at $x = 60$ units . . . . .	71
4.19	Comparison of the breakthrough curves at a control plane 75 units horizontally from the injection. (a) Scenario 1, b) scenario 2 and c) scenario 3. . . . .	72
4.20	Comparison of the temporal evolution of the dilution index. (a) Scenario 1, b) scenario 2 and c) scenario 3. . . . .	73



# List of Tables

2.1	Density Functions $f^v(\alpha)$ corresponding Memory Functions $g^v(t)$ (after Haggerty et al., 2000) . . . . .	10
3.1	Parameters to be estimated for each constitutive upscaled mass transfer model. . . . .	22



# 1

## Introduction

### 1.1 Motivation and Objectives

Solute transport models are used to predict aquifer responses to be used, for instance, in remediation studies, or in environmental risk assessment. The sophistication of today numerical models is very high, being capable of simulating complex geometries, as well as to solve for the state of the aquifer for many conceptualizations of the solute transport. However, the discrepancy between observations and numerical predictions is important, if the numerical model only incorporates the physical processes of advection and dispersion. The reason of this discrepancy is the inability of the advection-dispersion equation to reproduce the effect of heterogeneity within the, otherwise, homogeneous numerical blocks.

It is very important to capture the spatial heterogeneity of aquifer properties to model groundwater flow, and especially solute transport. Geostatistics provides a tool to characterize the spatial variability of hydrogeological properties at very small scales. Unfortunately, no matter how fast new computers are, the scale at which the aquifer parameters can be characterized is always much smaller than the scale the numerical models can handle, thus, there is a need to upscale the fine resolution description to incorporate subgrid heterogeneity at the same time that computational burden is overcome.

Solute transport is generally simulated using the advection-dispersion equation. Unfortunately, this equation has been shown not to be adequate to model solute transport at scales larger than the scale of heterogeneity. For instance,

the classical formulation of solute transport significantly underestimates the late-time behavior of breakthrough curves at observation locations. Alternative models have been proposed in the literature for modeling solute transport at the computational scale, such as continuous time random walks, fractional derivatives, and multirate mass transfer models.

We revise these alternative models and analyze how to derive the parameters needed to define them so that an upscaled, coarse scale model, can capture the unresolved heterogeneity in what respects to solute transport at the field scale. Specifically, we will focus in the use of multirate mass transfer models to mimic, using a homogeneous block, the residence times observed in a heterogeneous block.

## 1.2 Thesis Structure

This dissertation is organized as follows. The first chapter is this introduction. Chapter 2 provides a review of alternative models that have been proposed in the literature for modeling solute transport at the computational scale. We focus our attention on continuous time random walks, fractional derivatives, and multirate mass transfer models. We examine the underlying assumptions, scope and differences among these approaches.

Chapter 3 illustrates the use of mass transfer models as a tool for upscaling solute transport in a general numerical modeling framework. By comparing Monte Carlo simulations at different support scales, the performance of upscaled models was evaluated analyzing the reproduction of the ensemble mean behaviour of the main features of the breakthrough curves and the propagation of uncertainty. Furthermore, we describe how the upscaling process based on the concept of memory function, intrinsic to multirate mass transfer, is performed: each block with heterogeneous transmissivities, is replaced by a homogeneous block in which the unresolved transport processes are represented by the parameter values associated with the memory function. The parameter values are computed blockwise in order to reproduce, within each block, the residence time and spread observed at the small scale.

Chapter 4 presents some transport simulations designed to investigate the ability of upscaled models to reproduce solute transport for different types of heterogeneity. We quantify the predictive power of the upscaled models analyzing the reproduction of the dilution index and the relative entropy associated with each solute plume. It also evaluates longitudinal mass distribution profiles under different support scales. Finally, in chapter 5 we close with general conclusions and potential avenues for future research as well as questions raised during this work that need further investigation.

# 2

## Review of Upscaling Methodologies

### Abstract

Nonreactive solute transport in porous media has been conceptualized and simulated using the advection dispersion equation (ADE). However, field observations show long tails and asymmetric breakthrough curves which are contrary to the predictions by the ADE equation. For this reason, alternative conceptualizations have been proposed to model solute transport at the field scale. This chapter presents a review of four alternative.

### 2.1 Introduction

Solute transport modeling through porous media has been the focus of research in hydrogeology over several decades. Traditionally, solute transport is represented within the ADE framework, both at the local scale and at the computational scale. However, it is well documented and known from field test that ADE can not reproduce the breakthrough curves observed on site. Solute transport is affected by the presence of high and low water velocity zones, where solute can be channelized or stagnant. As soon as the numerical models uses a discretization that cannot reproduce this heterogeneity of the velocity field, transport predictions by ADE fail. Alternative approaches have been proposed to account for the effects of this velocity heterogeneity, among them we focus on the following four: Multi-rate Mass Transfer, Time-

Dependent Macrodispersive, Continuous Time Random Walk and Fractional Advection-Dispersion Transport.

## 2.2 The Starting Point: The Advection Dispersion Equation

The mass conservation equation constitutes the basis for describing the flow and solute transport in the subsurface. It is basically a mass balance equation which expresses that the net mass entering a control volume must be equal to the accumulated mass. For nonreactive solute it is written as,

$$\frac{\partial \rho(\mathbf{x}, t)}{\partial t} = -\nabla \cdot \mathbf{J}(\mathbf{x}, t) + r(\mathbf{x}, t) \quad (2.1)$$

where  $\rho(\mathbf{x}, t)$  is the solute mass per unit volume,  $\mathbf{J}(\mathbf{x}, t)$  is the total mass flux vector the magnitude of which gives the mass per unit time crossing a unit surface perpendicular to the flow direction, and  $r(\mathbf{x}, t)$  is a solute mass source/sink term. This equation is written in differential form but it is also valid for any fixed control volume in the system. Aquifer material properties in the aquifer are always determined over a given support volume. We can rewrite the above equation using a volume average operator for property  $\pi$  as,

$$\pi^v(\mathbf{x}) = \frac{1}{v} \int_{v(\mathbf{x})} \pi dV$$

being  $\mathbf{x}$  the centroid of the control volume. The mass conservation equation can be written at the support scale  $v$  as,

$$\phi \frac{\partial C^v(\mathbf{x}, t)}{\partial t} = -\nabla \cdot \mathbf{J}^v(\mathbf{x}, t) + r^v(\mathbf{x}, t) \quad (2.2)$$

where  $\phi$  is the porosity of the medium, and  $C$  is the solute concentration. The control volume denotes a given support scale, ranging from scale of measurement to the computational scale.

The mass flux is usually written in relative terms with respect to the advective contribution of mass fluxes,  $\mathbf{J}_a^v(\mathbf{x}, t)$ , which is defined as  $\mathbf{J}_a^v(\mathbf{x}, t) = \mathbf{q}^v(\mathbf{x}, t)C^v(\mathbf{x}, t)$ . The residual contribution to mass flux with respect to  $\mathbf{J}_a^v$  is denoted as  $\mathbf{J}_d^v(\mathbf{x}, t)$  and accounts for dispersive processes, i.e., the effect of velocity fluctuations about some average value,

$$\mathbf{J}_d^v(\mathbf{x}, t) = \mathbf{J}^v(\mathbf{x}, t) - \mathbf{J}_a^v(\mathbf{x}, t) \quad (2.3)$$

At the laboratory scale (the scale of core samples), denoted herein as  $v = \ell$ , the groundwater flux  $\mathbf{q}^\ell$  is given by Darcy's law

$$\mathbf{q}^\ell(\mathbf{x}, t) = -\mathbf{K}^\ell(\mathbf{x})\nabla h^\ell(\mathbf{x}, t) \quad (2.4)$$

and the dispersive mass flux  $\mathbf{J}_d^\ell(\mathbf{x}, t)$  is typically expressed through the Fickian constitutive theory, which maintains that the dispersive fluxes at a given location are proportional to the gradient of solute concentration at that location,

$$\mathbf{J}_d^\ell(\mathbf{x}, t) = -\phi\mathbf{D}^\ell(\mathbf{x})\nabla C^\ell(\mathbf{x}, t) \quad (2.5)$$

where  $\mathbf{D}^\ell$  is the local hydrodynamic dispersion tensor, which is typically defined in two or three dimensions by

$$\phi D_i^\ell = \phi D_d \tau + \alpha_i |\mathbf{q}| \quad (2.6)$$

where  $D_d$  is the molecular diffusion coefficient (assumed isotropic),  $\tau$  is the tortuosity,  $D_i^\ell$  are the eigenvalues of  $D^\ell$ , and  $\alpha_i$  are the local dispersivity coefficients, they are associated to the principal directions of the tensor, which is aligned with the directions parallel and perpendicular to flow, and referred to as longitudinal and transverse dispersivities,  $\alpha_L$  and  $\alpha_T$ .

Substituting the definitions of the advective and Fickian dispersive mass fluxes (2.5) in the mass conservation equations (2.2), the classical advection-dispersion equation is obtained, which is presumably valid at the laboratory scale,

$$\phi \frac{\partial C^\ell(\mathbf{x}, t)}{\partial t} = -\nabla \cdot (\mathbf{q}^\ell(\mathbf{x}, t)C^\ell(\mathbf{x}, t)) + \nabla \cdot (\phi\mathbf{D}^\ell(\mathbf{x})\nabla C^\ell(\mathbf{x}, t)) + r^\ell(\mathbf{x}, t) \quad (2.7)$$

Commonly, numerical models for solute transport predictions utilize the ADE equation, which is sometimes referred to as Fickian models. Unfortunately, the computational scale typically used in numerical models is significantly larger than the laboratory scale and the Fickian constitutive theory is no longer applicable.

Available alternative transport models generalize the Fickian constitutive theory by taking into account that total mass fluxes would, in general, depend on the past history of mass fluxes in space and time. This has been demonstrated by stochastic theory [Deng et al. (1993)] as well as by the volume averaging method [Wood et al. (2003)]. Under this assumption the dispersive flux is described by a convolution integral, which can be considered a generalization of Fick's equation:

$$\mathbf{J}_d^v(\mathbf{x}, t) = - \int_0^t \int_{\mathfrak{R}^3} \phi \mathbf{M}^v(s, \tau; \mathbf{x}) \nabla C^v(\mathbf{x} - s, t - \tau) ds d\tau \quad (2.8)$$

where  $\mathbf{M}^v(s, t; \mathbf{x})$  is the spatial-temporal kernel memory function, which can be seen as a weighting function of the concentration gradients. The macrodispersive flux depends on the concentration gradients throughout the space-time domain and thereby it exhibits a nonlocal dependence on the concentration gradients [Cushman and Ginn (2000)].

In general, the function  $\mathbf{M}^v(s, t; \mathbf{x})$  is block specific (conditioned to the  $\mathbf{x}$  location of the control volume centroid), and depends not only on the underlying heterogeneity but also on the numerical discretization of the domain and the size/shape of the solute plume. Hence, substituting the generalized Fickian equation (2.8) in the mass conservation equation (2.1), the alternative transport model reads.

$$\begin{aligned} \phi \frac{\partial C^v(\mathbf{x}, t)}{\partial t} = & -\nabla \cdot (\mathbf{q}^v(\mathbf{x}, t)C^v(\mathbf{x}, t)) + \\ & + \nabla \cdot \left\{ \int_0^t \int_{\mathbb{R}^3} \phi \mathbf{M}^v(s, \tau; \mathbf{x}) \nabla C^v(\mathbf{x} - s, t - \tau) ds d\tau \right\} + r^v(\mathbf{x}, t) \end{aligned} \quad (2.9)$$

Considering that for large travel distances ( $t \rightarrow \infty$ ) concentration gradients inside the integral are approximately constant at some point, the advection-dispersion equation is recovered with an equivalent dispersion coefficient given by

$$\phi \mathbf{D}^v(\mathbf{x}) = \int_0^t \int_{\mathbb{R}^3} \phi \mathbf{M}^v(s, \tau; \mathbf{x}) ds d\tau \quad (2.10)$$

This expression is sometimes written in relative terms with respect to local Fickian dispersive contribution as,

$$\phi \mathbf{D}^v(\mathbf{x}) = \phi \mathbf{D}^\ell(\mathbf{x}) + \int_0^t \int_{\mathbb{R}^3} \phi \mathbf{M}_m^v(s, \tau; \mathbf{x}) ds d\tau \quad (2.11)$$

where  $\phi \mathbf{M}_m^v(s, \tau; \mathbf{x}) = \phi \mathbf{M}(s, \tau; \mathbf{x}) - \phi \mathbf{D}^\ell(\mathbf{x}) \delta(x - s, t - \tau)$ . The subscript  $m$  refers to the macrodispersive kernel memory function. The first term explains the contribution of dispersive flux at local scale (assumed Fickian), whereas the second term represents an additional dispersive contribution due to heterogeneity embedded into the fixed volume  $v$ . Using small perturbation stochastic theories, Gelhar and Axness (1983) obtained the same expression in probability space. They found that for an infinite domain, large plume, and steady-state uniform flow conditions the memory function should be expressed as

$$\phi \mathbf{M}_m^\infty(s, t) = G_0(s, t) C_{\mathbf{q}\mathbf{q}}(s) \quad (2.12)$$

where  $G_0(s, t)$  is the Gaussian-shape homogeneous solution to the advection-dispersion equation and  $C_{\mathbf{q}\mathbf{q}}$  is the covariance function of the velocity field. Following this reasoning, modelers that use commercial transport codes based on advection-dispersion equation, normally need to enhance the values of the dispersivity coefficients to account for the unresolved heterogeneity not described by the model. In this context, a block equivalent dispersion tensor is introduced,  $\mathbf{D}^b$ , which can be formally expressed as

$$\phi D_i^b = \phi \tau D_d + (\alpha_i + A_a^b |\mathbf{q}|) \quad (2.13)$$

$D_i^b$  are the eigenvalues of  $\mathbf{D}^b$ , and  $A_i^b$  is the increase in block dispersivities. Here, we used the notation that  $v = b$  when referring to grid-blocks or elements of a numerical transport code. For most model discretizations, the increase in longitudinal dispersivity,  $A_L^b$ , is the dominant parameter having values much larger than  $\alpha_L$ ;  $A_L^b$  ranges from meters to kilometers [e.g. Gelhar et al. (1992)] whereas  $\alpha_L$  is in order of millimeters [e.g. Fernàndez-Garcia et al. (2004)].

Standard macrodispersion models employ enhanced block dispersivity coefficients to compensate for the homogenization. However, further research has shown that these conditions hardly occur in reality. General conditions are not Fickian. In such case, the Fickian theory tends to largely underestimate the tail of the concentration breakthrough curves even for moderate field heterogeneities and "well-behaving" multiGaussian random transmissivity fields [Fernàndez-Garcia et al. (2007)].

## 2.3 Time-Dependent Macrodispersive Models

The first approach we revise that attempts to circumvent the problems with the ADE equation is Time-Dependent Macrodispersive Models. This approach is based on the localization of the non-local Fickian equation (2.8). The non-local Fickian flux is localized about the plume center of mass. In the case that the memory kernel  $\mathbf{M}_m(s, \tau; \mathbf{x})$  dies out as  $|s|$  and  $|\tau|$  increases, the macrodispersive flux strongly depends on the concentration gradient at the current time and position and one can approximate the macrodispersive flux simply as,

$$\mathbf{J}_d^v(\mathbf{x}, t) \approx -\phi \mathbf{D}^v(\mathbf{x}, t) \nabla C^v(\mathbf{x}, t) \quad (2.14)$$

with,

$$\phi \mathbf{D}^v(\mathbf{x}, t) = \phi \mathbf{D}^\ell(\mathbf{x}) + \int_0^t \int_{\mathbb{R}^3} \phi \mathbf{M}^v(s, \tau; \mathbf{x}) ds d\tau \quad (2.15)$$

Now, using the mass conservation equation with the localized version of the macrodispersive flux (equation 2.14), the solute transport equation is written as,

$$\phi \frac{\partial C^v(\mathbf{x}, t)}{\partial t} = -\nabla \cdot (\mathbf{q}^v(\mathbf{x}, t) C^v(\mathbf{x}, t)) + \nabla \cdot (\phi \mathbf{D}^v(\mathbf{x}, t) \nabla C^v(\mathbf{x}, t)) + r^v(\mathbf{x}, t) \quad (2.16)$$

Note that this equation differs from the classical advection-dispersion equation (2.7) in the dispersion tensor  $\mathbf{D}(\mathbf{x}, t)$ , which not only depends on the spatial location but also in time. Transport models that follow this approach are referred to as time-dependent macrodispersive models.

Basically, two similar approaches have been suggested to use effective time-dependent macrodispersion tensors derived from stochastic theories for small plumes [Dagan (1991); Rajaram and Gelhar (1993); Dentz et al. (2000)]. In this case, the time-dependent macrodispersion tensors in (2.16) correspond to a solute plume with shape equal to the grid-block of the numerical model. Likewise, Rubin et al. (1999, 2003) have determined effective time-dependent macrodispersion tensors by removing the frequency spectra of velocity fluctuations in a small-perturbation expansion of macrodispersion.

Although the theoretical framework given by (2.16) is general and not restricted to small perturbations, on practice, there is still no algorithm to estimate time-dependent dispersion tensor specific to the grid-blocks of a numerical model. Moreover, closed-form analytical stochastic solutions provide time-dependent dispersion coefficients that vary with time but do not change from one grid-block to another.

## 2.4 Multi-rate Mass Transfer Models

Other equations for modeling the solute transport at computational scales larger than the characteristic length is an advection-dispersion equation (ADE) with an additional source/ sink term that accounts for the exchange between high and low conductivity zones. In other words, the domain is decomposed into a mobile zone with pore spaces filled with mobile water, transport process in this zone include advection, dispersion, and chemical reactions; and an immobile zone with pore spaces filled with stagnant water where advective transport is negligible. Figure 2.1 shows a schematic conceptualization of the mass transfer model. The rate at which solute moves between these two domains is controlled by a mass transfer coefficient  $\alpha$ . One defines  $C_m$  and  $C_{im}$ , the concentrations in the mobile and immobile zones respectively. The ADE, as it includes advection and dispersion, is used to describe  $C_m$ . The source/sink term represents the mass transfer exchange between a mobile zone

and a distribution of immobile zones leading to the non-Fickian solute mass fluxes at the computational scale,

$$\begin{aligned} \theta_m \frac{\partial C_m^v(\mathbf{x}, t)}{\partial t} + \theta_{im} \int_0^\infty f^v(\alpha) \frac{\partial C_{im}^v(\mathbf{x}, t; \alpha)}{\partial t} d\alpha \\ = -\nabla(\mathbf{q}^v(\mathbf{x}, t)C_m^v(\mathbf{x}, t)) + \nabla \cdot (\theta_m \mathbf{D}^v(\mathbf{x})\nabla C_m^v(\mathbf{x}, t)) + r^v(\mathbf{x}, t) \end{aligned} \quad (2.17)$$

The mass flux between mobile and immobile zones is driven by the concentration difference between zones as,

$$\theta_{im} \frac{\partial C_{im}^v(\mathbf{x}, t; \alpha)}{\partial t} = \alpha(C_m^v(\mathbf{x}, t) - C_{im}^v(\mathbf{x}, t; \alpha)) \quad \forall \alpha \quad (2.18)$$

where  $\alpha$  is the mass transfer coefficient,  $f^v(\alpha)$  is the density function of mass transfer rates,  $\theta_m$  and  $\theta_{im}$  are the volume fractions of the mobile and immobile zones,  $C_m$  is the concentration in mobile zones and  $C_{im}$  is the concentration in immobile zones.

Integrating the mass transfer equation (2.18) and then substituting  $C_{im}^v(\mathbf{x}, t; \alpha)$  into (2.17), one obtains a transport equation simply depending on the mobile concentration,

$$\begin{aligned} \theta_m \frac{\partial C_m^v(\mathbf{x}, t)}{\partial t} + \theta_m \cdot \beta_{tot}^v \int_0^t g^v(\tau) \frac{\partial C_m^v(\mathbf{x}, t - \tau)}{\partial t} d\tau \\ = -\nabla(\mathbf{q}^v(\mathbf{x}, t)C_m^v(\mathbf{x}, t)) + \nabla \cdot (\theta_m \mathbf{D}^v(\mathbf{x})\nabla C_m^v(\mathbf{x}, t)) + r^v(\mathbf{x}, t) \end{aligned} \quad (2.19)$$

where  $\beta_{tot}^v$  is the total maximum capacity to retain particles in the immobile zones,  $g^v(t)$  is known as the (temporal) memory function,

$$g^v(t) = \int_0^\infty \alpha f^v(\alpha) e^{-\alpha t} d\alpha \quad (2.20)$$

The memory function can be interpreted as the particle resident time distribution function in the immobile zone. Or, in other words, the memory function represents the mass flux to the immobile zones per unit volume of aquifer, for a unit change in concentration in the mobile zones [(Haggerty et al., 2000); (Carrera et al., 1998)]. The formulation of this term depends on the geometry of the immobile zones and on the variability of the mass transfer or diffusion rates (Haggerty et al., 2000). Table 2.1 shows the density functions  $f^v(\alpha)$  corresponding to the mass transfer models used in this dissertation.

Various researches [e.g. Zinn and Harvey (2003)] have demonstrated that nonreactive solute transport through heterogeneous media is often better simulated when an advection-dispersive model is used in conjunction with a

mass transfer model. Conceptually, this artificial mass term does not represent local kinetic reactions but it rather accounts for solute mass exchange between high and low velocity areas occurring at the Darcy-scale within each grid block. Although straightforward relationships between memory functions and physical properties of the aquifer are not established yet, the meaning of the memory function has been seen to strongly depend on heterogeneity. The formulation of the memory function depends on the geometry of immobile zones and on the variability of mass transfer or diffusion rates (Haggerty et al., 2000).

Model	$f^v(\alpha)$	$g^v(t)$
First-order	$\beta_{tot}\delta(\alpha - \alpha_f)$	$\alpha_f\beta_{tot}e^{-\alpha_f t}$
Multirate Series	$f^v(\alpha)$	$\int_0^\infty \alpha f^v(\alpha)e^{-\alpha t} d\alpha$
Power Law Distribution <sup>a</sup>	$\frac{\beta_{tot}(k-2)}{\alpha_{max}^{k-2} - \alpha_{min}^{k-2}} \alpha^{k-3}$	$\int_{\alpha_{min}}^{\alpha_{max}} \alpha f^v(\alpha)e^{-\alpha t} d\alpha$

<sup>a</sup> A truncated power law density function with  $k > 0, k \neq 2$ , and  $\alpha_{min} \leq \alpha \leq \alpha_{max}$ .  $\alpha_{max}$  is the maximum rate coefficient,  $\alpha_{min}$  is the minimum rate coefficient, and  $k$  is the exponent.

**Table 2.1.** Density Functions  $f^v(\alpha)$  corresponding Memory Functions  $g^v(t)$  (after Haggerty et al., 2000)

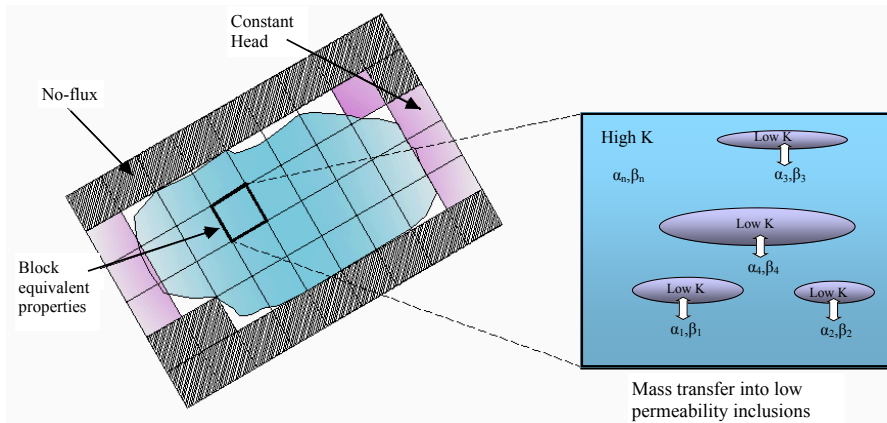


**Figure 2.1.** Representation of mass transfer conceptual model.

## 2.5 Continuous Time Random Walk Models

The continuous time random walk (CTRW) is a generalization of the standard (discrete) random walk. It is based on the idea that not only the length of a particle jump is random (not necessarily following a Gaussian distribution as the standard random walk) but also the particle undergoes a random waiting time between two successive jumps. The length of a given jump and the waiting time are drawn from a joint pdf  $\psi(\mathbf{x}, t)$ , which is known as the jump pdf. From the joint pdf  $\psi(\mathbf{x}, t)$ , the jump length pdf and the waiting time pdf can be derived as marginal distributions,

$$\lambda(\mathbf{x}) = \int_0^{\infty} \psi(\mathbf{x}, t) dt \quad (2.21)$$

and

$$\omega(t) = \int_{-\infty}^{\infty} \psi(\mathbf{x}, t) d\mathbf{x} \quad (2.22)$$

Following Metzler and Klafter (2000), different types of CTRW processes can be defined by the characteristic waiting time and jump length second moment,

$$T = \int_0^{\infty} t\omega(t) dt \quad (2.23)$$

$$\Sigma_{ij}^2 = \int_{-\infty}^{\infty} x_i x_j \lambda(\mathbf{x}) d\mathbf{x} \quad (2.24)$$

Anomalous dispersion takes place when either the characteristic waiting time or characteristic jump length are not finite. The continuous time random walk method provides a general framework in the sense that both the fractional-dispersion transport models and the mass transfer models haven demonstrated to be particular cases of the CRTW formalism (Dentz and Berkowitz, 2003; Cushman and Ginn, 2000). Most frequently, for simplicity, the CTRW formalism is simplified by considering the waiting time and jump length mutually independent. In this case, assuming a finite characteristic jump length but undefined characteristic waiting time, the transport equation governing the movement of particles under steady state flow condition is (Dentz and Berkowitz, 2003)

$$\phi \frac{\partial C_m^v(\mathbf{x}, t)}{\partial t} = -\nabla \cdot \left\{ \int_0^t M^v(t) \mathbf{q}^v(\mathbf{x}) C^v(\mathbf{x}, t) - M^t(v) \mathbf{D}^v(\mathbf{x}) \nabla C^v(\mathbf{x}, t) dt \right\} + r^v(\mathbf{x}) \quad (2.25)$$

with  $M(t)$  being the memory function which is typically expressed in the Laplace domain as

$$M(p) = Tp \frac{\psi(p)}{1 - \psi(p)} \quad (2.26)$$

where  $p$  is the Laplace variable. The memory function serves to capture the non-Fickian transport induced by the heterogeneity not represented by the model.

## 2.6 Fractional Advection-Dispersion Transport Models

Fractional advection-dispersion transport models have been used in recent years [e.g. Metzler and Klafter (2000); Schumer et al. (2003); Benson et al. (2000)] as a way to generalize the advection-dispersion equation with the objective to better describe the power-law scaling behavior in the spread of solute plume observed in the field. Mathematically, fractional dispersion can be viewed as a specific case of continuous time random walk in which the transition displacement distribution of particles  $p(\mathbf{s})$  is described by a Lévy distribution. A Lévy distribution is a generalization of the Gaussian distribution. It is defined in the Fourier space as

$$f(\mathbf{k}) = e^{(|\sigma k|)^\alpha} \quad (2.27)$$

where  $k$  is the Fourier variable,  $\alpha$  is the magnitude of the Lévy flight and  $\alpha$  is the Lévy index. For  $\alpha < 2$  the variance of the distribution function is undefined, for  $\alpha < 1$  the mean of the distribution function is also undefined. For  $\alpha = 1$  we recover the standard Gaussian distribution and the inverse of The Fourier Transform has an explicit expression.

The transport equation is defined as

$$\phi \frac{\partial C_m^v(\mathbf{x}, t)}{\partial t} = -\nabla \cdot (\mathbf{q}^v(\mathbf{x}, t) C^v(\mathbf{x}, t)) + \nabla \cdot (\phi \mathbf{D}_{\alpha-1}^v(\mathbf{x}) \nabla^{\alpha-1} C^v(\mathbf{x}, t)) + r^v(\mathbf{x}, t) \quad (2.28)$$

where the term  $\mathbf{D}_{\alpha-1}^v(\mathbf{x}) \nabla^{\alpha-1} C^v(\mathbf{x}, t)$  is defined in the Fourier space as

$$\mathfrak{F}[\mathbf{D}_\alpha^v(\mathbf{x}) \nabla^\alpha C^v(\mathbf{x}, t)] = -\mathbf{D}_\alpha^v(\mathbf{x}) |\mathbf{k}|^\alpha C^v(\mathbf{k}, t) \quad (2.29)$$

Note that this expression is a generalization of the Fourier Transform of a derivative for noninteger numbers. In order to emphasize the relationship between this model and the previous discussion, we will use the convenient

result that the fractional advection-dispersion equation can be obtained as a special case of the nonlocal Fickian transport equation (2.8). That is, Cushman and Ginn (2000) demonstrated that the fractional advection-dispersion equation is recovered from CTRW when the kernel memory term is given by the following specific form, which in one-dimension reads as,

$$M(s, \tau) = \frac{D_{\alpha-1}^v \delta(\tau) H(s)}{\Gamma(2 - \alpha) s^{\alpha-1}} \quad (2.30)$$

where  $D_{\alpha-1}^v$  is constant,  $\delta(\tau)$  is the Dirac delta, and  $H(s)$  is Heaviside function on  $(0, \infty)$ . The important point here is to note that the Dirac delta function serves to localize the flux in time, so that the fractional advection dispersion equation only nonlocal in space (Cushman and Ginn, 2000). Also, the Heaviside function serves to restrict the nonlocality in space to positive  $s$  values, which corresponds to an upstream weighting memory function.

## 2.7 Summary

A review of mass transport formulations to simulate solute transport at the field scale has been presented. The emphasis of this review has been placed on the theoretical framework of each approach. These models provide alternative ways to predict contaminant transport. Transport problems always require a greater detail of heterogeneity than flow problems, the issue we will address is how to replace the loss of within-block heterogeneity by an alternative formulation to the ADE. We will propose an upscaling technique to address this problem.

## 2.8 References

- Benson, D. A., S. W. Wheatcraft, and M. M. Meerschaer (2000), The fractional-order governing equation of Lévy motion, *Water Resources Research*, 36(6), 1413–1424.
- Carrera, J., X. Sánchez-Vila, I. Benet, A. Medina, G. Galarza, and J. Guimerà (1998), On matrix diffusion: formulations, solution methods and qualitative effects, *Hydrogeology Journal*, 6, 178–190.
- Cushman, J. H., and T. R. Ginn (2000), Fractional advection-dispersion equation: A classical mass balance with convolution-Fickian flux, *Water Resources Research*, 36(12):3763–3766.

- Dagan, G. (1991), Dispersion of a passive solute in non-ergodic transport by steady velocity fields in heterogeneous formation, *J. Fluid Mech.*, 233, 197–210
- Deng, F. W., J. H. Chusman, and J.W. Delleur (1993), A fast fourier transform stochastic analysis of the contaminant transport problem , *Water Resources Research*, 29(9), 3421–3247.
- Dentz, M., Kinzelbach H., Attringer S., Kinzelbach (2000), Temporal behavior of a solute cloud in a heterogeneous porous medium 1. Point-like injection, *Water Resources Research*, 39(12),3591–3604
- Dentz, M., and B. Berkowitz (2003), Transport behavior of a passive solute in continuous time random walks and multirate mass transfer, *Water Resources Research*, 39(5), 1111, doi:10.1029/2001WR001163.
- Gelhar, L. W., and C. L. Axness (1983), Three-dimensional stochastic analysis of macrodispersion in aquifer, *Water Resources Research*, 19(1), 161–180.
- Gelhar, L. W., C. Welty, and K. Rehfeld (1992), A critical review of data on field-scale dispersion aquifers, *Water Resources Research*, 28(7), 1955–1974.
- Fernàndez-Garcia, D., T. H. Illangasekare, and H. Rajaram (2004), Conservative and sorptive forced-gradient and uniform flow tracer test in a three-dimensional laboratory test aquifer, *Water Resources Research*, 40, W10103, doi:10.1029/2004WR003112.
- Fernàndez-Garcia and Gómez-Hernández (2007), Impact of upscaling on solute transport: travel times, scale-dependence of dispersivity and uncertainty, *Water Resources Research*, VOL. 43, W02423, doi:10.1029/2005WR004727, 2007.
- Guswa, A. J., and D. L. Freyberg (2000), Slow advection and diffusion through low permeability inclusions, *Journal of Contaminant Hydrology*, 46, 205–232.
- Haggerty, R., S.A. McKenna, and L. C. Meigs (2000), On the late-time behaviour of tracer test breakthrough curves, *Water Resources Research*, 36(12), 3467–3479.
- Metzler, R. and J. Klafter (2000), The random walk’s guide to anomalous diffusion: A fractional dynamics approach, *Physical reports*, 339, 1–77.
- Neuman, S. P., D. M. Tartakovsky (2008), Perspective on theories of non-Fickian transport in heterogeneous media, *Advances Water Resources*, in press.

- Rajaram, H., and L. W. Gelhar (1993), Plume scale-dependent dispersion in heterogeneous aquifers 2. Eulerian analysis and three-dimensional aquifers, *Water Resources Research*, 29(9), 3261–3276
- Rubin, Y., A. Sun, Maxwell, and A. Bellin (1993), The concept of block effective macrodispersivity and a unified approach for grid-scale- and plume-scale-dependent transport, *J. Fluid Mech.*, 395, 161–180
- Rubin, Y., A. Bellin, and L. E. Lawrence (2003), On the use of block-effective macrodispersion for numerical simulations of transport in heterogeneous formations, *Water Resources Research*, 39(9), 1242, doi:10.1029/2002WR001727.
- Schumer, R., D. A. Benson, M. M. Meerschaert, and B. Baeumer (2003), Fractal mobile/immobile solute transport, *Water Resources Research*, 39(10), 1–12, doi:10.1029/2003WRR002141.
- Wood, B. D., F. Cherblan, M. Quintard, and S. Whitaker (2003), Volume averaging for determining the effective dispersion tensor: Closure using periodic unit cells and comparison with ensemble averaging, *Water Resources Research*, 39(8), 1210, doi:10.1029/2002WR001729.
- Zinn, B., and C. F. Harvey (2003), When good statistical models of aquifer heterogeneity go bad: A comparison of flow, dispersion, and mass transfer in connected and multivariate Gaussian hydraulic conductivity fields, *Water Resources Research*, 39(3), 1051, doi:10.1029/2001WR0



# 3

## Upscaling Transport with Mass Transfer Model

### Abstract

The ambiguity associated with the choice of an adequate conceptual transport model constitutes a major challenge associated with the upscaling of solute transport. Among the different alternatives to the classical advection-dispersion model, the (multirate) mass transfer model has been proposed as a valuable and convenient alternative to model the large-scale behavior of solute transport. Here, we evaluate the use of mass transfer models as a constitutive equation for upscaling solute transport. To achieve this, we compare Monte Carlo simulations of solute transport at two different support scales. Transport simulations performed at the smallest scale represent a set of reference transport solutions, which are contrasted against transport simulations obtained using an upscaled model. Several formulations of the multi-rate mass transfer model, which differ in the type of memory function, are used as a constitutive transport equation. The large scale scenario represents an operational model obtained by partially homogenizing the reference solution. Results show that, albeit the double-rate and the truncated power-law mass transfer models were capable to properly describe the ensemble average behavior of the main features associated with the integrated breakthrough curves, the uncertainty associated with the upscaled mass transfer models was still substantially smaller than that attributed to the reference solution. Importantly, the corresponding cumulative distribution function of concentrations (CDF) associated with the

upscaled model follows a distribution similar to the reference solution but with smaller dispersion. The reason is that while appropriate memory functions can be used to preserve the residence time distribution of mass particles during upscaling, the lack of memory in space prevents the model from reproducing mass fluxes in all directions. Specifically, the reproduction of mass fluxes taking place at the interface between two homogenized blocks of the upscaled model are not satisfied, thus providing a poor description of the spatial distribution of mass particles.

### 3.1 Introduction

Albeit different approaches can be used to generate high-resolution maps of aquifer attributes by means of geostatistics or related tools, still, in practice, due to computational efficiencies, some sort of upscaling (i.e., transfer of small-scale information into a larger support volume) is usually necessary to construct a numerical transport model. In subsurface hydrology, the large spatial variability observed in aquifer attributes, being the hydraulic conductivity an attribute that varies several orders of magnitude within an aquifer, largely influences solute transport predictions and drastically complicates the upscaling of solute transport.

Among the effects of heterogeneity, the usual observation of anomalous (non-Fickian) transport, manifested in the field by peaked concentration profiles having long back-tails, has questioned the use of the classical advection-dispersion equation (ADE) to model transport phenomena at the usual computational scale of a numerical model (Mackay et al., 1986; Adams and Gelhar, 1992; Riva et al., 2008; Gouze et al., 2008; Haggerty et al., 2000). These field observations are supported by laboratory experiments (Levy and Berkowitz, 2003; Fernández-García et al., 2005c), numerical simulations of solute transport in heterogeneous media (Zinn and Harvey, 2003; Feehley et al., 2000; Fernández-García et al., 2005a, 2007; Salamon et al., 2007), and fundamental statistical theory.

By modeling hydraulic conductivity (defined at a small support scale) as a correlated random space function, stochastic theories have succeeded in demonstrating that mean mass fluxes at the  $\mathbf{x}$  location and time  $t$  should not in general be exclusively dependent on the mean concentration gradients at that location and time, as it is expressed by Fick's law. Instead, dispersive mass fluxes should depend on the past values of the mean concentration gradients over the entire space-time domain (Hu et al., 1995; Morales-Casique et al., 2006), thus rendering memory to the transport equation.

In response to this lack of Fickianity, several alternative transport models have been proposed in the literature to properly describe transport phenomena

at a large support scale. Promising alternatives contemplate continuous time random walks (CTRW) (Berkowitz and Scher, 1998), fractional derivatives (Benson et al., 2000), and multirate mass transfer models (MRMT) (Haggerty and Gorelick, 1995; Carrera et al., 1998) among others. Comprehensive reviews of the theories of anomalous transport in heterogeneous media are provided by Berkowitz et al. (2006) and Neuman and Tartakovsky (2008). Interestingly, the CTRW formalism supposes a more general framework, but simplifies to the MRMT model in its most common adopted form (Dentz and Berkowitz, 2003). Still, the MRMT model has the advantage that its formulation and physical interpretation is well-known by practitioners, and many numerical transport codes based on the MRMT model are already available for field applications (Zheng and Wang, 1999; Carrera et al., 1998; Salamon et al., 2006; Willmann et al., 2008). Alternatively, the stochastic ADE equation, defined over a small support volume, can be used to directly provide the conditional low-order moments (mean and covariance) of concentrations and solute fluxes (Morales-Casique et al., 2006). Interestingly, upon considering no statistical interdependence of the velocity field, the mean transport equation reduces to the CTRW model (Neuman and Tartakovsky, 2008).

Here, we focus on the use of MRMT models as a constitutive equation for upscaling solute transport. Various researches (e.g., Guswa and Freyberg, 2002; Carrera et al., 1998; Harvey and Gorelick, 2000; Zinn and Harvey, 2003; Liu et al., 2004; Riva et al., 2008; Willmann et al., 2008) have shown that large-scale non-reactive solute transport phenomena observed in a heterogeneous medium is often better represented when a mass transfer equation is coupled with the ADE.

Conceptually, this artificial mass transfer equation does not represent local kinetic reactions or diffusive mass transfer processes but it rather accounts for subgrid heterogeneity (Zinn and Harvey, 2003; Willmann et al., 2008). In this context, we compare Monte Carlo simulations of solute transport obtained at two different support scales with the aim to evaluate the adequacy of MRMT models as a tool for upscaling. Transport simulations performed at the smallest scale represent a set of reference solutions defined on the basis of a local ADE. At the large scale, several formulations of the MRMT model are evaluated as potential constitutive transport equations.

The upscaled model scenario represents an operational or a functional model obtained by partially "homogenizing" the reference geological system (defined over a fine-scale) so that it ultimately consists of various homogeneous regions. We emphasize the word "partial homogenization" to be in contrast with most previous analysis of upscaling of solute transport (e.g., Harvey and Gorelick, 2000; Zinn and Harvey, 2003; Willmann et al., 2008) in which the system is completely homogenized. The distinctive aim of this work is that: (1) we look at the process of transferring subgrid information to finite blocks

or homogeneous regions of a numerical model by means of MRMT models; (2) we seek for a more comprehensive understanding of the interplay between the (homogenized) regions of an upscaled transport model; and (3) we evaluate how uncertainty is affected by the change of the support scale when the MRMT model is selected for upscaling.

## 3.2 Transport Models

### 3.2.1 The Local Transport Model

At the local scale, denoted herein as  $\omega$ , we considered solute transport to be governed by the advective-dispersion equation (ADE). Neglecting the changes in porosity with time and disregarding the source/sink term, this is written as

$$\theta^\omega \frac{\partial c^\omega}{\partial t} = -\nabla \cdot (\mathbf{q}^\omega c^\omega - \theta^\omega \mathbf{D}^\omega \nabla c^\omega), \quad (3.1)$$

where the first term in the divergence operator is the advective mass flux and the second term accounts for dispersive fluxes.  $c^\omega$  is the volume average concentration of solute in  $\omega$ , and  $\mathbf{q}^\omega$  is the Darcy flux. This equation is based on the mass conservation principle and assumes that the dispersive mass fluxes can be described by Fick's law at some small scale  $\omega$ , i.e., mass fluxes at point  $\mathbf{x}$  and time  $t$  are proportional to concentration gradients at point  $\mathbf{x}$  and time  $t$ ,

$$\mathbf{J}_d^\omega(\mathbf{x}, t) = -\theta^\omega \mathbf{D}_d^\omega \nabla c^\omega(\mathbf{x}, t). \quad (3.2)$$

This assumption has been challenged by several authors. In general, in the absence of dead-end-pores, Fick's law can be argued to be valid for sufficiently small support volumes (Neuman and Tartakovsky, 2008). In any case, from a practical point of view, our analysis is based on the fact that the non-Fickian transport behavior observed at the Lauswiesen site (Riva et al., 2008) and at the MADE site (Salamon et al., 2007) has been adequately modeled using an ADE (defined over a small support volume) in conjunction with a high-resolution description of heterogeneity. This is precisely the situation we consider here.

The local dispersion tensor,  $\mathbf{D}_d^\omega$ , is the sum of the effective molecular diffusion tensor,  $\mathbf{D}_{diff}^\omega$ , and the mechanical dispersion tensor,  $\mathbf{D}_{disp}^\omega$ . The latter accounts for residual fluxes at the local scale  $\omega$ , and is typically defined with eigenvectors oriented parallel and perpendicular to the direction of flow, and eigenvalues defined as

$$D_{disp,i}^\omega = \alpha_i \frac{|\mathbf{q}^\omega|}{\theta^\omega}, \quad (3.3)$$

where  $\alpha_i$  are the local dispersivity coefficients. The  $\alpha_i$  components parallel and transverse to the flow direction are usually denoted as longitudinal and transverse dispersivities,  $\alpha_L$  and  $\alpha_T$ .

### 3.2.2 The Upscaled Mass Transfer Model

At the computational scale, denoted here as  $v$  ( $v \gg \omega$ ), transport phenomena is represented by means of the MRMT model (Haggerty and Gorelick, 1995; Carrera et al., 1998; Haggerty et al., 2000). The MRMT model allows to represent a large variety of mass transfer processes taking place simultaneously over a wide range of scales, i.e., processes ranging from pore diffusion at the grain scale to matrix diffusion into fractured rocks can be simultaneously represented. This model considers an overlapped continuum media formed by a mobile domain, where advection-dispersion takes place, and many immobile domains, where mass can be transferred to and temporarily be trapped.

Here, the MRMT model is not used in strict sense to represent a variety of diffusive processes. Instead, the mobile and immobile zones are viewed as to represent areas of relatively fast and relatively slow solute movement (inside  $v$ ). Similar representations of a heterogeneous media have been considered by Zinn and Harvey (2003) and Willmann et al. (2008). Formally, the MRMT equation is essentially an ADE with a source/sink term,

$$\theta^v \frac{\partial c^v}{\partial t} = -\nabla \cdot (\mathbf{q}^v c^v - \theta^v \mathbf{D}_d^v \nabla c^v) - \theta^v \Gamma^v(\mathbf{x}, t), \quad (3.4)$$

where

$$D_{d,i}^v = D_{diff,i}^\omega + (\alpha_i + A_i) \frac{|\mathbf{q}^v|}{\theta^v} \quad (3.5)$$

$$\Gamma^v(\mathbf{x}, t) = \beta(\mathbf{x}) \int_0^t g(\mathbf{x}, \tau) \frac{\partial c^v}{\partial t}(\mathbf{x}, t - \tau) d\tau \quad (3.6)$$

The additional dispersive contribution term in (3.5),  $A_i$ , accounts for processes that can actually be represented with a Fickian model, whereas processes associated with anomalous transport are represented through the memory function  $g(\mathbf{x}, \tau)$ .

As time evolves, the memory function emphasizes the different past values of the concentration derivatives with time, thus rendering memory to solute transport. The coefficient  $\beta(\mathbf{x})$  defines the magnitude of memory effects and is known as the capacity coefficient.

Several forms of the MRMT model are found in the literature (e.g., Carrera et al., 1998; Haggerty et al., 2000). Among them, the single-rate model, the gamma model, the log-normal model, the power-law model, and the diffusion

model (with spherical, layered and cylindrical geometries) are the most commonly used. Each one of these conceptual models have been successfully employed to model field and laboratory experiments. Remarkably, the single-rate mass transfer model was successfully utilized to reproduce the tracer experiment at the Macrodispersion Experiment (MADE) site using either (partially homogenized) numerical models (Feehley et al., 2000) or (completely homogenized) analytical solutions (Harvey and Gorelick, 2000). Importantly, the quantities associated with these mass transfer models at the MADE site were shown to be mostly related to Darcy-scale heterogeneity (Salamon et al., 2007).

Here, we selected three potential upscaled constitutive equations based on a different form of the memory function: the single-rate model, a discrete multirate model with two immobile domains (double-rate), and the truncated power-law memory function. The mathematical expression of the memory function  $g(\mathbf{x}, t)$  can be generally written as

$$g(\mathbf{x}, t) = \int_0^\infty \alpha f(\mathbf{x}, \alpha) e^{-\alpha t} d\alpha \quad (3.7)$$

where  $f(\mathbf{x}, \alpha)$  is a function that can be physically interpreted as the probability distribution function of mass transfer rates associated with distinct domains of the overlapped continuum. Detail description of the three selected upscaled mass transfer models are provided in Table 3.1. We note that because our upscaled model considers a domain formed by various homogeneous regions, the mass transfer parameters in (3.6) depend also on the space location accordingly.

**Table 3.1.** Parameters to be estimated for each constitutive upscaled mass transfer model.

Model	Memory function	Parameters
First-order	$\alpha_1 e^{-\alpha_1 t}$	$\beta, \alpha_1, v_m, A_L$
Double rate <sup>a</sup>	$\alpha_1 \frac{\beta_1}{\beta} e^{-\alpha_1 t} + \alpha_2 \frac{\beta_2}{\beta} e^{-\alpha_2 t}$	$\beta_{j=1,2}, \alpha_{j=1,2}, v_m, A_L$
Power Law <sup>b</sup>	$\sim t^{1-k}$	$\beta, \alpha_{max}, \alpha_{min}, k, v_m, A_L$

<sup>a</sup>  $\beta = \beta_1 + \beta_2$

<sup>b</sup> The power law model is only defined over the interval  $\alpha_{min} \leq \alpha \leq \alpha_{max}$

In a randomly heterogeneous aquifer, stochastic theories predict that the mean dispersive flux should in general depend on the past mean concentration gradients throughout the entire space-time domain (Neuman, 1993; Morales-Casique et al., 2006; Neuman and Tartakovsky, 2008). In a similar manner, the memory function in the MRMT model operates as a weighting function that penalizes past concentration derivatives in time (but not in space). In

this context, the MRMT model should be seen as a model with a space-localized memory kernel. This is in contrast with the time-localized memory kernel associated with the fractional advection-dispersion model (Cushman and Ginn, 2000). In anyway, we note that the intend here is not to question the validity of the theoretical premises underlying the upscaled MRMT model but to directly assess the applicability of a well established model.

### 3.3 Monte Carlo Transport Simulations

#### 3.3.1 Setup

We consider a confined two-dimensional aquifer whose domain consists in a square area of  $240 \times 240$  units. Flow is driven by a mean hydraulic gradient oriented parallel to the  $x$ -direction ( $J_x = 0.01$ ,  $J_y = 0$ ) under steady-state flow conditions. Boundary conditions were no-flux for boundaries parallel to the mean flow and constant-head otherwise. Thus, groundwater flow is moving from left to right.

Aquifer heterogeneity is represented by considering the natural log of transmissivity,  $Y(\mathbf{x})$ , as a spatially varying attribute. All other properties are assumed spatially constant. A total of 50 different transport solutions were obtained by generating multiple equally likely realizations of  $Y(\mathbf{x})$ .  $Y(\mathbf{x})$  is assumed isotropic at the small support scale and is represented by uniformly discretizing the entire domain into  $240 \times 240$  square pixels of 1 unit size.

Each upscaled mas transfer model was obtained by transferring the fine-scale pixel information into a numerical model formed by  $10 \times 10$  regular homogeneous blocks. Thus, the size of each block was of  $24 \times 24$  units. Figure 3.1 shows an individual reference transmissivity field,  $Y(\mathbf{x})$ , contrasted against the corresponding depiction of the transmissivity field in the upscaled model.

To simplified the problem, at the local scale, transport is assumed purely advective so that  $\mathbf{D}_d^\omega = 0$ . The transport problem setup considers a solute plume initially distributed over a long transverse line located upgradient and having a constant concentration. This line was centered in the transverse dimension of the domain and takes up 140 units. To avoid boundary effects, the plume source was separated 21 units from the upgradient head boundary and 50 units from the impermeable boundaries.

Transport simulations were designed to efficiently calculate the global mass flux breakthrough curves observed at 14  $x$ -control planes equally distributed within the entire domain. The simulated breakthrough curves constituted the reference transport solution used to subsequently analyze the performance of upscaling by the different upscaled models.

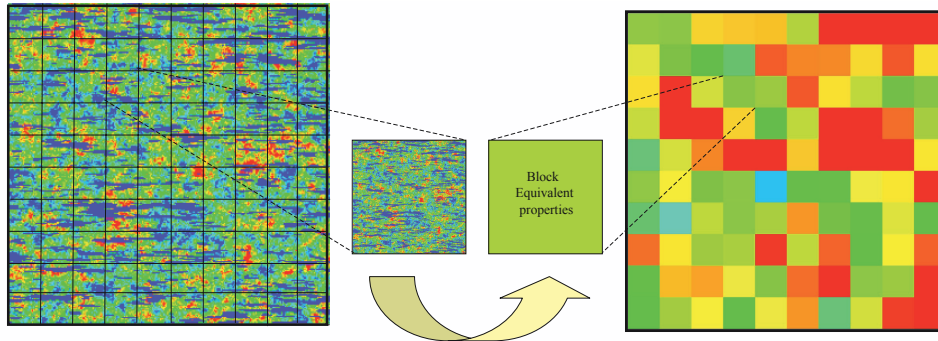


**Figure 3.1.** Illustration of the upscaling process: (a) Map of transmissivities for a given realization superposed with the discretization of the upscaled model (black lines); (b) Map of equivalent transmissivities ( $T_{xx}^v$ ).

### 3.3.2 Reference Transmissivity Fields

The reference transmissivity fields were conceptualized as an stochastic bimodal composite medium. The objective here was to test the upscaled models in a complex geological system formed by highly conductive conduits embedded in an otherwise well behaving Gaussian heterogeneous medium. Thus, we assumed that the aquifer is composed of two coexisting materials or facies ( $M_1$  and  $M_2$ ), each represented by a different random function model of the spatial distribution of the natural log of transmissivity,  $Y_1(\mathbf{x})$  and  $Y_2(\mathbf{x})$ ,

$$Y(\mathbf{x}) = (1 - I(\mathbf{x}))Y_1(\mathbf{x}) + I(\mathbf{x})Y_2(\mathbf{x}) \quad (3.8)$$

where  $I(\mathbf{x})$  is an indicator spatial random variable,

$$I(\mathbf{x}) = \begin{cases} 1 & \mathbf{x} \in M_2 \\ 0 & \text{otherwise} \end{cases} \quad (3.9)$$

The natural log of transmissivity  $Y_1(\mathbf{x})$  of the first material,  $M_1$ , follows a multiGaussian random function with a geometric mean of  $T_g=1$  and an anisotropic exponential covariance function,

$$C_{Y_1}(|\mathbf{r}|) = \sigma_{Y_1}^2 \exp \left( -\sqrt{\left(\frac{r_x}{\lambda_x^{Y_1}}\right)^2 + \left(\frac{r_y}{\lambda_y^{Y_1}}\right)^2} \right) \quad (3.10)$$

where  $\mathbf{r} = (r_x, r_y)$  is the separation vector between two points of the aquifer,  $\sigma_{Y_1}^2$  is the variance of  $Y_1(\mathbf{x}) = \ln T_1(\mathbf{x})$  assumed as 9, and  $\lambda_x^{Y_1}$  and  $\lambda_y^{Y_1}$  are the longitudinal and transverse correlation scales set to 40 and 4 units, respectively. The second material,  $M_2$ , represents a family of highly conductive

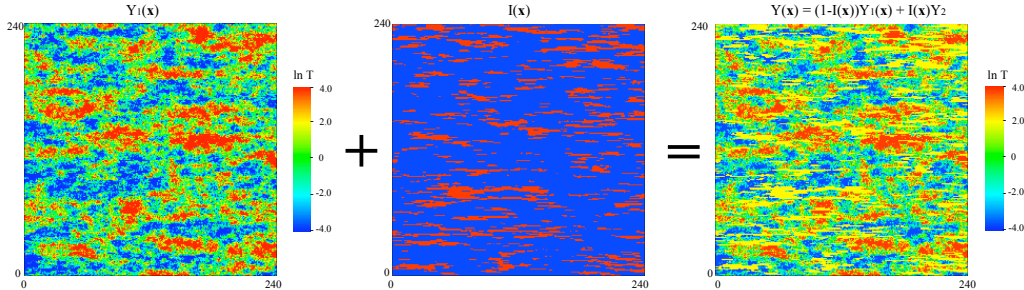


**Figure 3.2.** Illustration of the steps involved in the stochastic generation of the composite transmissivity field,  $Y(\mathbf{x}) = (1 - I(\mathbf{x}))Y_1(\mathbf{x}) + I(\mathbf{x})Y_2$ . Blue and red pixels in the  $I(\mathbf{x})$ -map indicates materials  $M_1$  and  $M_2$ , respectively.

conduits. We considered that the variation of  $Y_2(\mathbf{x})$  is of minor importance compared with  $Y_1(\mathbf{x})$ , and we therefore assigned a deterministic constant transmissivity value to  $Y_2(\mathbf{x})$ , i.e.,  $Y_2(\mathbf{x}) = Y_2 = 2.0$ . Figure 3.2 illustrates the steps involved in the stochastic generation of the composite random field for a given realization of  $Y(\mathbf{x})$ .

In a bimodal media, the volumetric proportion of material  $M_2$ , denoted as  $p_2$ , defines the mean and variance of the indicator random variable, respectively written as  $\langle I(\mathbf{x}) \rangle = p_2$  and  $\sigma_I^2 = p_2 p_1$ , where  $p_1$  is the volumetric proportion of  $M_1$  ( $p_1 = 1 - p_2$ ). We consider that the family of highly conductive conduits (material  $M_2$ ) occupies 20% of the domain, i.e.,  $p_2 = 0.2$  and  $p_1 = 0.8$ . This choice allowed us to obtain transmissivity fields leading to breakthrough curves with long back-tailing during transport simulations. Figure 3.3 compares the cumulative mass flux breakthrough curves obtained at a given  $x$ -control plane using one realization of  $Y_1(\mathbf{x})$  and its associated composite medium,  $Y(\mathbf{x})$ . Note that the slope of the late-time behavior observed for  $Y_1(\mathbf{x})$  is substantially more elongated than that observed for  $Y(\mathbf{x})$ . The indicator variable was further characterized with an anisotropic covariance function,

$$C_I(|\mathbf{r}|) = \sigma_I^2 \exp \left( -\sqrt{\left(\frac{r_x}{\lambda_x^I}\right)^2 + \left(\frac{r_y}{\lambda_y^I}\right)^2} \right) \quad (3.11)$$

where  $\lambda_x^I$  and  $\lambda_y^I$  are the longitudinal and transverse correlation scales of the indicator variable set to 16 units and 1 unit, respectively. Following (Rubin and Journel, 1991; Rubin, 1995), we assumed that the spatial distribution of  $Y_1(\mathbf{x})$  and  $I(\mathbf{x})$  are mutually uncorrelated. Based on this and according to Rubin (1995) and Lu and Zhang (2002), the resulting composite random field,  $Y(\mathbf{x})$ , displays a theoretical mean, variance and covariance function given by,

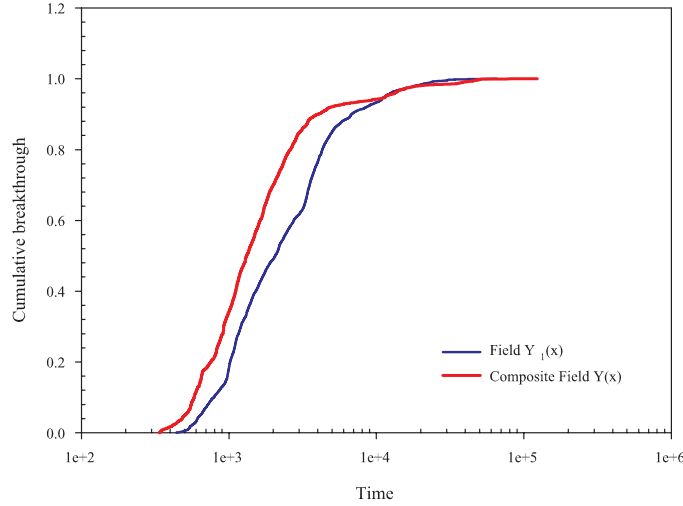


**Figure 3.3.** Comparison of the cumulative mass flux breakthrough curves obtained at a given  $x$ -control plane ( $x = 143.3$  units) using one realization of the transmissivity field  $Y_1(\mathbf{x})$  and its associated composite medium  $Y(\mathbf{x})$ .

$$\langle Y(\mathbf{x}) \rangle = p_1 \langle Y_1 \rangle + p_2 Y_2 \quad (3.12)$$

$$C_Y(|\mathbf{r}|) = [C_I(|\mathbf{r}|) + p_1^2] C_{Y_1}(|\mathbf{r}|) + (\langle Y_1 \rangle - Y_2)^2 C_I(|\mathbf{r}|) \quad (3.13)$$

$$\sigma_Y^2 = [p_1 p_2 + p_1^2] \sigma_{Y_1}^2 + (\langle Y_1 \rangle - Y_2)^2 p_1 p_2 \quad (3.14)$$

Thus, the statistical properties of the final composite media are  $\langle Y(\mathbf{x}) \rangle = 0.4$  and  $\sigma_Y^2 = 7.84$ , having integral scales in the  $x$  and  $y$  directions of  $\lambda_x^Y = 32.8$  units and  $\lambda_y^Y = 3.2$  units. Because  $Y_1(\mathbf{x})$  and  $I(\mathbf{x})$  are not correlated, the stochastic generation of  $Y_1(\mathbf{x})$  and  $I(\mathbf{x})$  was performed independently. Thus, for each realization of  $Y(\mathbf{x})$ , we separately generated  $I(\mathbf{x})$  using an indicator sequential simulation program, ISIM3D (Gómez-Hernández and Srivastava, 1990), and  $Y_1(\mathbf{x})$  using a sequential gaussian simulation program, GCOSIM3D (Gómez-Hernández and Journel, 1993). The composite media is finally obtained from  $Y(\mathbf{x}) = (1 - I(\mathbf{x}))Y_1(\mathbf{x}) + I(\mathbf{x})Y_2$ .

### 3.3.3 Flow and Transport Solution

A finite difference ground-water flow model, MODFLOW2000 (Harbaugh et al., 2000), was used to solve the flow problem at both scales. The discretization

of the numerical grid was given by the discretization of the spatial distribution of transmissivities. The model calculates the flow rates at grid interfaces. These velocity fields were then used in a transport code based on the Random Walk Particle Method, RW3D (Fernández-García et al., 2005a,b), to simulate either conservative solute transport needed to obtain fine-scale transport solutions or solute transport coupled with multirate mass transfer to obtain the corresponding upscaled model solutions (coarse-scale).

The particle tracking methodology presented by Salamon et al. (2006) was employed to simulate multirate mass transfer processes. Essentially, transport is simulated by injecting a large number of mass particles into the system; each particle representing a small portion of the solute plume. Advection is simulated by moving particles along flowlines, whereas dispersion is emulated by a Brownian motion. Mass-transfer processes are efficiently incorporated by switching the state of the particle between mobile/immobile states according to appropriate transition probabilities.

Transport simulations start by injecting a large number of particles (10,000) equidistantly distributed in a line transverse to the mean flow direction with size 140 units. For each movement, the time step was adapted based on a grid Courant number of 0.01 (Wen and Gómez-Hernández, 1996). A unit mass was assigned to each particle. The first arrival time and the position of particles passing through 14 control planes transverse to the mean flow direction and located at several distances away from the source were tracked until particles exited the last control plane. Figure 3.4 shows the map of hydraulic heads superposed with the pathlines of particles obtained in an individual realization of  $Y(\mathbf{x})$ . Only the movement of 100 particles are depicted so that the figure can be easily understood.

## 3.4 Estimation of Block Equivalent Properties

### 3.4.1 Methodology

In the upscaled model, flow is still driven by Darcy's law but we use an equivalent anisotropic transmissivity tensor,  $\mathbf{T}^v$ , to represent the heterogeneous medium inside  $v$ . For each block,  $\mathbf{T}^v$ , was calculated based on the simple Laplacian method with skin (Gómez-Hernández, 1991; Wen and Gómez-Hernández, 1996) as

$$T_{ii}^v = \frac{\int_v q_i^\omega(\mathbf{u}) d\mathbf{u}}{-\int_v \partial h^\omega / \partial x_i(\mathbf{u}) d\mathbf{u}}. \quad (3.15)$$

This methodology yields flow fluxes in the upscaled model,  $\mathbf{q}^v(\mathbf{x})$ , that represent block spatial average quantities,

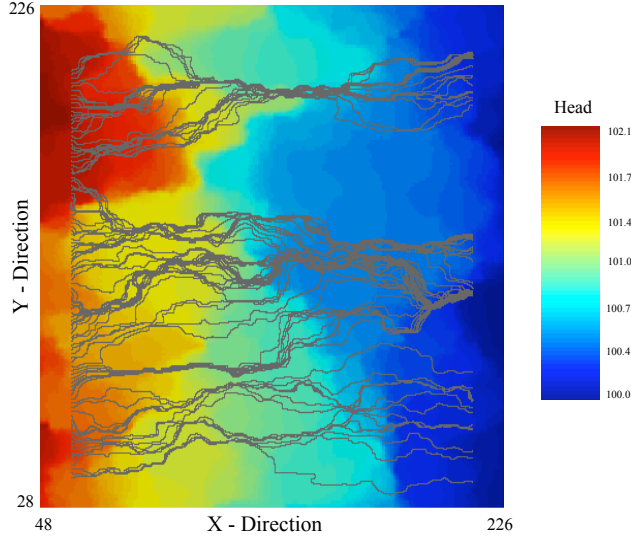


**Figure 3.4.** Map of hydraulic heads superposed with particle paths obtained from a transport simulation (only 100 particles) in an individual realization of the composite random field.

$$\mathbf{q}^v = \frac{1}{v} \int_v \mathbf{q}^\omega(\mathbf{u}) d\mathbf{u}. \quad (3.16)$$

Then, we estimated the appropriate mass transfer parameters of the up-scaled transport model by using a methodology conducive to preserve the residence time distribution of solute mass particles in each block. This seems a natural approach when using the up-scaled MRMT model because the memory function, which plays a central role, can be physically interpreted as the residence time distribution of solute mass in the immobile domains (slow velocity areas) (Haggerty et al., 2000). Essentially, the up-scaled parameters were estimated by curve-fitting the residence time distribution (numerically obtained from fine-scale transport simulations) with a theoretical MRMT model. When transport takes place according to the MRMT model in an equivalent homogeneous medium (i.e., a block of the up-scaled model), the cumulative residence time distribution,  $F_\tau(\tau)$ , can be approximately written in Laplace space as

$$\widehat{F}_\tau(p) \approx \frac{1}{p} \exp \left[ L_b \left( \frac{1}{2A_\ell} - \sqrt{\frac{1}{4A_\ell^2} + \frac{\psi(p)}{A_\ell v_m}} \right) \right] \quad (3.17)$$

$$\psi(p) = p + \beta \int_0^\infty f(\alpha) \frac{p\alpha}{p + \alpha} d\alpha \quad (3.18)$$

where  $A_\ell$  is the effective longitudinal dispersivity coefficient,  $L_b$  is the mean travel displacement of solute mass particles in  $v$ , and  $v_m$  is the mobile velocity. Here, we have assumed that  $F_\tau$  is not significantly influenced by transverse dispersion since we are measuring integrated mass fluxes over a surface.

The effective velocity of the solute inside  $v$  moving through the mobile domain (preferential channels) is the mobile velocity,  $v_m$ . This is an important concept here because the solute plume is not necessarily sampling the entire region of a given block. Moreover,  $\theta^v$  does not represent the void ratio of the entire aquifer ( $\theta^\omega$ ), but only defines the pore volume fraction associated with the mobile domain. The parameters obtained from curve-fitting are:  $v_m$ ,  $\beta$  and those characterizing  $f(\alpha)$  (see Table 3.1). From them, we estimated  $\theta^v$  so that the mean residence time,  $\bar{\tau}$ , is preserved during upscaling,

$$\theta^v = \frac{\theta^\omega}{1 + \beta} C_\tau, \quad (3.19)$$

where  $C_\tau$  is

$$C_\tau = \frac{\bar{\tau}}{\tau^v}, \quad \tau^v = \frac{\theta^\omega L_b}{|\mathbf{q}^v|}, \quad (3.20)$$

and  $\bar{\tau}$  is the mean residence time

$$\bar{\tau} = \int \tau f_\tau(\tau) d\tau, \quad f_\tau = \frac{dF_\tau}{d\tau}, \quad (3.21)$$

being  $f_\tau$  the frequency distribution function of residence times. The parameter  $C_\tau$  takes into consideration that the mean residence time,  $\bar{\tau}$ , is not necessary given by the averaged spatial velocity inside  $v$ . This term can be also related to the noncontributing capacity coefficient ( $\beta_{nc}$ ) introduced by Zinn and Harvey (2003) as

$$C_\tau = \frac{1 + \beta_{nc} + \beta}{1 + \beta}. \quad (3.22)$$

A block equivalent transverse macrodispersivity value associated with the MRMT model was estimated using the method of moments as

$$A_t = \frac{\sigma_y^2}{2L_b} \quad (3.23)$$

where  $\sigma_y^2$  is the variance of transverse displacements of the particles moving through  $v$ .

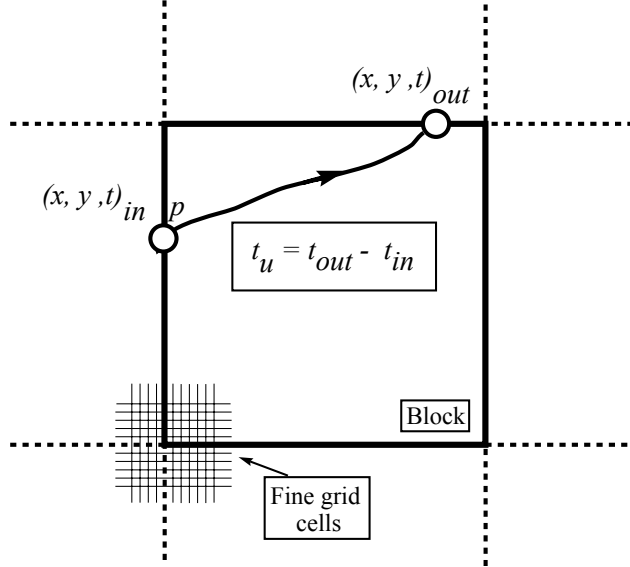


**Figure 3.5.** Calculation of residence times in a given block of the numerical model.

### 3.4.2 Implementation Details

Numerically, the residence time distributions,  $f_\tau(\tau)$  and  $F_\tau(\tau)$ , were obtained by recording the first passage time ( $t_{in}$ ) and the exiting time ( $t_{out}$ ) of a particle passing through a given block during fine-scale simulations (see Figure 3.5). The distribution of residence times was estimated by reconstructing the (cumulative) frequency distribution of residence times  $\{\tau_i, i = 1, \dots, N_p\}$ , where  $N_p$  is the number of particles traveling through the block, and  $\tau_i = t_{out} - t_{in}$  is the residence time of the  $i$ -th mass particle. The mean residence time  $\bar{\tau}$  was estimated as

$$\bar{\tau} = \int \tau f_\tau(\tau) d\tau \approx \frac{1}{N_p} \sum_{i=1}^{N_p} \tau_i \quad (3.24)$$

The time-domain solution of (3.17) was calculated using the STAMMT-L code (Haggerty and Reeves, 2002). An optimization program, PEST (Doherty, 2004), was utilized to calibrate the mass transfer parameters associated with  $F_\tau(\tau)$ . The minimized objective function by PEST included the estimates of the cumulative distribution function obtained at different times as well as the low-order temporal moments of  $f_\tau(\tau)$  (see appendix).

The fact that the residence time distribution at each block is preserved during upscaling renders the upscaled mass transfer model a promising tool to couple solute transport with chemical reactions controlled by residence times.

Yet, from a practical point of view, we recognize that the proposed upscaling methodology can be computationally expensive because it requires to solve flow and transport at a small-scale. This is only justifiable when the upscaled model is used afterwards to solve a more computationally demanding problem (e.g., reactive transport involving many species and reactions). Nevertheless, several approaches to reduce the computational burden can be considered. Similar to what is known for upscaling hydraulic conductivity (Sánchez-Vila et al., 1995; Wen and Gómez-Hernández, 1996; Sánchez-Vila et al., 2006), instead of solving the flow and transport problem over the entire domain, the equations can be iteratively solved over smaller support volumes, which contain  $v$  plus a "skin" region.

The skin ensures a more realistic flow and transport boundary condition associated with each block. Importantly, in this case, we note that the injection of solute should be placed in the skin region so that enough memory effects are retained. Anyhow, noticing that the objective of this chapter is not to present an upscaling methodology but to evaluate the adequacy of an alternative constitutive transport model, we employed the most exact version of the upscaling methodology, which is to resolve  $f_\tau$  and  $F_\tau$  directly from global fine-scale simulations.

### 3.5 Numerical Results and Discussion

The evaluation of each constitutive upscaled transport model was performed by contrasting the Monte Carlo simulated BTCs obtained using the upscaled models against the reference BTCs solution. In addition to the upscaled mass transfer models, we further compare the results with the well-known macrodispersive model and the purely advective upscaled model. The purely advective model does not account for macrodispersive fluxes and memory effects, and serves to illustrate the effects of smoothing the heterogeneous  $Y(\mathbf{x})$ -field by upscaling.

The macrodispersive model is defined as a particular case of the MRMT model in which  $\psi(p) = 0$  in (3.17) and serves to compare the upscaled mass transfer model with a Fickian model. The structure of the discussion is as follows. First, we analyzed the reproduction of the ensemble average behavior of BTCs and its associated uncertainty with  $A_T = 0$ . This avoids mass transfer effects between blocks Fernández-García et al. (2007) and allows to focus on the longitudinal component of dispersive fluxes. Then, we discuss the effect of including  $A_T \neq 0$  into the upscaled models.

### 3.5.1 Ensemble Average Behavior

We start by looking at the ensemble average behavior of the main features associated with the simulated BTCs, which we characterized by: (a) the early arrival time (the time at which 5% of the mass arrives at the  $x$ -location, denoted as  $T_{05}$ ); (b) the maximum value of concentrations (peak); (c) the late-time slope of BTCs; and (d) the spreading of BTCs. The spreading of BTCs is measured by means of an effective longitudinal dispersivity coefficient estimated as

$$A^{eff}(x) = \frac{x}{2} \left\langle \frac{\mu_2(x)}{(\mu'_1(x))^2} \right\rangle \quad (3.25)$$

where the brackets denote the expected operator,  $x$  is the coordinate of the control plane in the mean flow direction, and  $\mu'_1$  and  $\mu_2$  the first two temporal moments of BTCs, written as

$$\mu'_1 = \frac{\int_0^\infty tC(t)dt}{\int_0^\infty C(t)dt} \quad (3.26)$$

$$\mu_2 = \frac{\int_0^\infty (t - \mu'_1)^2 C(t)dt}{\int_0^\infty C(t)dt} = \frac{\int_0^\infty t^2 C(t)dt}{\int_0^\infty C(t)dt} - (\mu'_1)^2 \quad (3.27)$$

where  $C(t)$  denotes flux-concentrations. Figure 3.6 displays  $A^{eff}$  as a function of travel distance for the different upscaled models. Remarkably, we see that the inclusion of memory in the transport equation allows an accurate reproduction of effective spreading when either a discrete MRMT model with more than two immobile domains are considered or a continuous distribution of mass transfer rates is described with a truncated power-law.

This is in contrast with the macrodispersive model and the single-rate mass transfer model results which largely underestimate  $A^{eff}$ . The reason for this is that the memory function associated with these models are too simple to properly describe the heterogeneous processes taking place within a block. This is shown in Figure 3.7 which depicts the mean sum of square errors (SSE) associated with the calibrated model obtained after curve-fitting the block residence time distribution with the theoretical model. Note that the ultimate SSE values for the single-rate model are substantially larger than those associated with the truncated power-law and the double-rate model.

Spreading by itself does not provide enough information about the complete distribution of concentrations. The interest on the different characteristic behaviors of the BTC depends on the type of application. The early-time of BTCs usually displays a sharp rising limb and can be characterized by its early arrival time,  $T_{05}$ . In practice, this parameter is important for designing underground radioactive repositories. Figure 3.8 compares the simulated mean  $T_{05}$

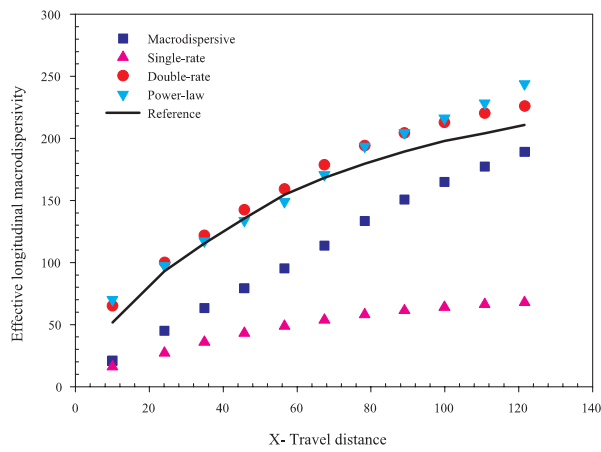


Figure 3.6. Evolution of the effective longitudinal dispersivity with travel distance .

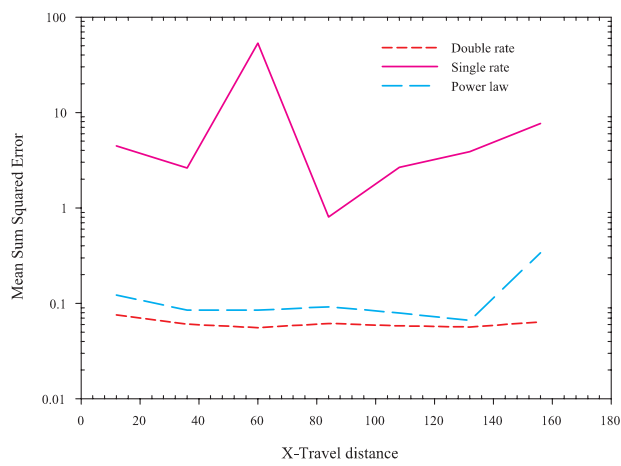
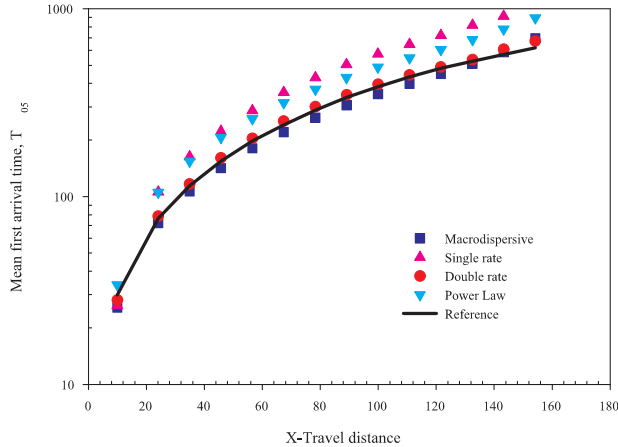


Figure 3.7. Evolution with travel distance of the mean sum of square error associated with the calibrated model obtained curve-fitting  $f_\tau$  with a theoretical model.



**Figure 3.8.** Evolution of the ensemble average first arrival of the BTC  $T_{05}$  with travel distance.

value obtained at the small support scale to its corresponding upscaled model solution. As expected, the upscaled advective model yields not conservative estimates of travel times, i.e., the upscaled model overestimates  $T_{05}$ . Most remarkably, in this case, even though the double-rate and the power-law model are described with the same number of parameters (degrees of freedom), the truncated power-law model can largely underestimate  $T_{05}$ .

A proper representation of the late-time behavior of BTCs has recently received much attention for being indicative of anomalous transport (e.g., Haggerty et al., 2000; Harvey and Gorelick, 2000; Salamon et al., 2007; Riva et al., 2008; Willmann et al., 2008). It also constitutes an important parameter for the calculation of clean-up times needed to remediate contaminated aquifers. Typically, BTCs are observed to behave as a power law at late times (i.e.,  $C(t) \sim t^{-m}$ ), where  $m$  is the slope of the BTC on double log-scale. The mechanisms by which the presence of slow and fast channels (heterogeneity) affects the slope  $m$  have been recently studied by Willmann et al. (2008), who found that, for conservative solutes moving in a heterogeneous medium, the slope mainly depends on "connectivity" rather than the classical statistical properties of the aquifer (variance of  $\ln T$ ).

Here, we do not concentrate on the fundamental nature of the slope but we look at the capability of upscaled mass transfer models to reproduce tailing. In other words, we evaluate whether a proper description of residence times,  $f_{\tau}$ , at each block of a numerical model assures the reproduction of the late-time behavior of BTCs. To do this, we concentrate on the simulated slope attained over two time intervals of the BTCs:  $(T_{60}, T_{80})$  and  $(T_{80}, T_{95})$ , where

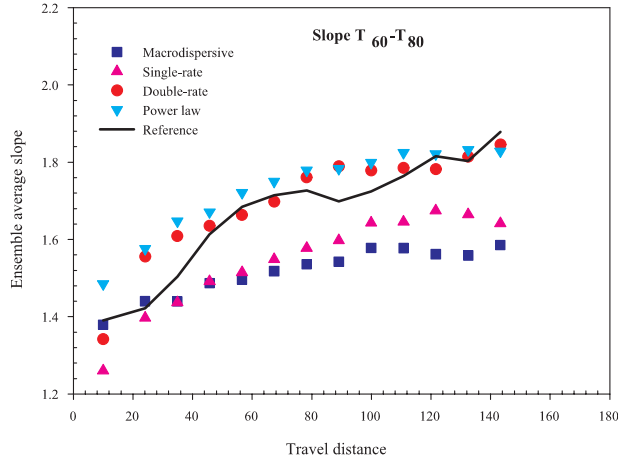


**Figure 3.9.** Evolution of the ensemble average slope  $T_{60} - T_{80}$  with travel distance.

$T_{60}$  denotes the time at which 60% of the mass passes through the observation location and so on. The slope was estimated by using least square regression of the corresponding BTC values plotted in a double log-scale. The ensemble average behavior of the slope as a function of travel distance is shown in Figures 3.9 and 3.10.

For all models and time scales, the slope slowly increases with travel distances and thus tends to a more Fickian-like behavior. As expected, the upscaled mass transfer models provide a better description of the late-time behavior of BTCs, being the macrodispersive model a less adequate model for this matter. In this context, we see that while the truncated power-law model can accurately simulate the late-time behavior of BTCs at all time scales (the two intervals of time), the double-rate model is only capable to describe the late-time behavior over the time interval  $(T_{60}, T_{80})$ . This is consistent with theory, Carrera et al. (1998) demonstrated that the late-time behavior of BTCs associated with MRMT models is the result of an infinite superposition of single-rate mass transfer modes (Carrera et al., 1998). Thus, a proper description beyond  $t > T_{80}$  in this case requires a discrete mass transfer model with more than two modes.

Interestingly, the slope reproduced by the macrodispersive model is small compared to the reference solution. This points out an important conceptual limitations of the macrodispersive model, which is back-dispersion. Close to the source, where concentration gradients are usually higher, the macrodispersive model creates dispersive mass fluxes oriented in the opposite direction to flow, which are not physically possible. Due to this mechanism, particles close

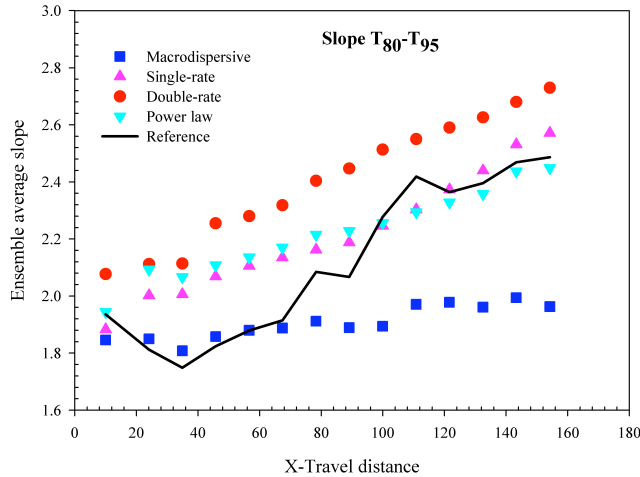


**Figure 3.10.** Evolution of the ensemble average slope  $T_{80} - T_{95}$  with travel distance.

to the source were susceptible to be trapped in low velocity regions during simulations, causing the presence of very slow particles.

Another important characteristic parameter of a BTC is the concentration peak. When groundwater is the source for drinking water, this water is required to meet certain drinking water standards. This standard is typically contrasted against a maximum concentration threshold. Figure 3.11 shows the performance of the upscaled models in terms of the peak of concentrations associated with the simulated BTCs. Now, we see that, albeit both models are described with the same number of degrees of freedom, a discrete MRMT model with only two modes provides a better description of the maximum value of concentrations than the the truncated power-law model.

### 3.5.2 Propagation of Uncertainty

The lack of complete knowledge of an aquifer on the one hand and the large spatial variability of the aquifer attributes on the other makes deterministic models to be highly inadequate for representing solute transport in heterogeneous media. Alternatively, multiple possible scenarios should be considered (see (Riva et al., 2008) for an illustrative field example). In this context, the transfer of information from one scale to another by upscaling should also require the proper propagation of model uncertainty.

Here, we evaluate the reproduction of uncertainty by qualitatively examining the 95%-confidence interval associated with the ensemble of BTCs. Figures 3.12 and 3.13 compares the ensemble of Monte Carlo-based BTCs obtained using the reference transmissivity fields to those associated with each upscaled

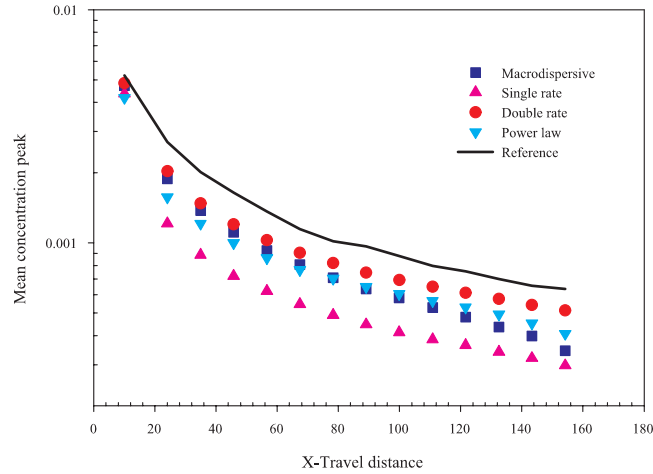


**Figure 3.11.** Evolution of the mean concentration peak with travel distance.

mass transfer model at two control planes ( $x = 34$  units and  $x = 110$  units). By comparing the ensemble of BTCs to the 95%-confidence interval associated with the fine-scale model, it is clear that all the upscaled mass transfer models exhibit a reduction of uncertainty to a certain degree. This reduction is more apparent for late times (slow particles) and small travel distances. The latter is shown in Figure 3.14, which displays the 95%-confidence intervals of the BTCs obtained at two different control planes.

A complete evaluation of uncertainty is provided by examining the cumulative frequency distribution function (CDF) of the main features associated with the BTCs obtained at a given control plane.

Figures 3.15 and 3.16 respectively show the CDF of the slope ( $T_{60} - T_{80}$ ) and the first arrival ( $T_{05}$ ) associated with the simulated BTCs obtained at  $x = 34.9$  units and  $x = 110.8$  units. Interestingly, at early times, when particles have still not pass through few blocks, the integrated BTC is simply the superposition of residence time distributions of all sample blocks, and therefore, for small travel distances, the CDF of the late-time slope associated with the double-rate and the truncated power-law model is adequately reproduced.

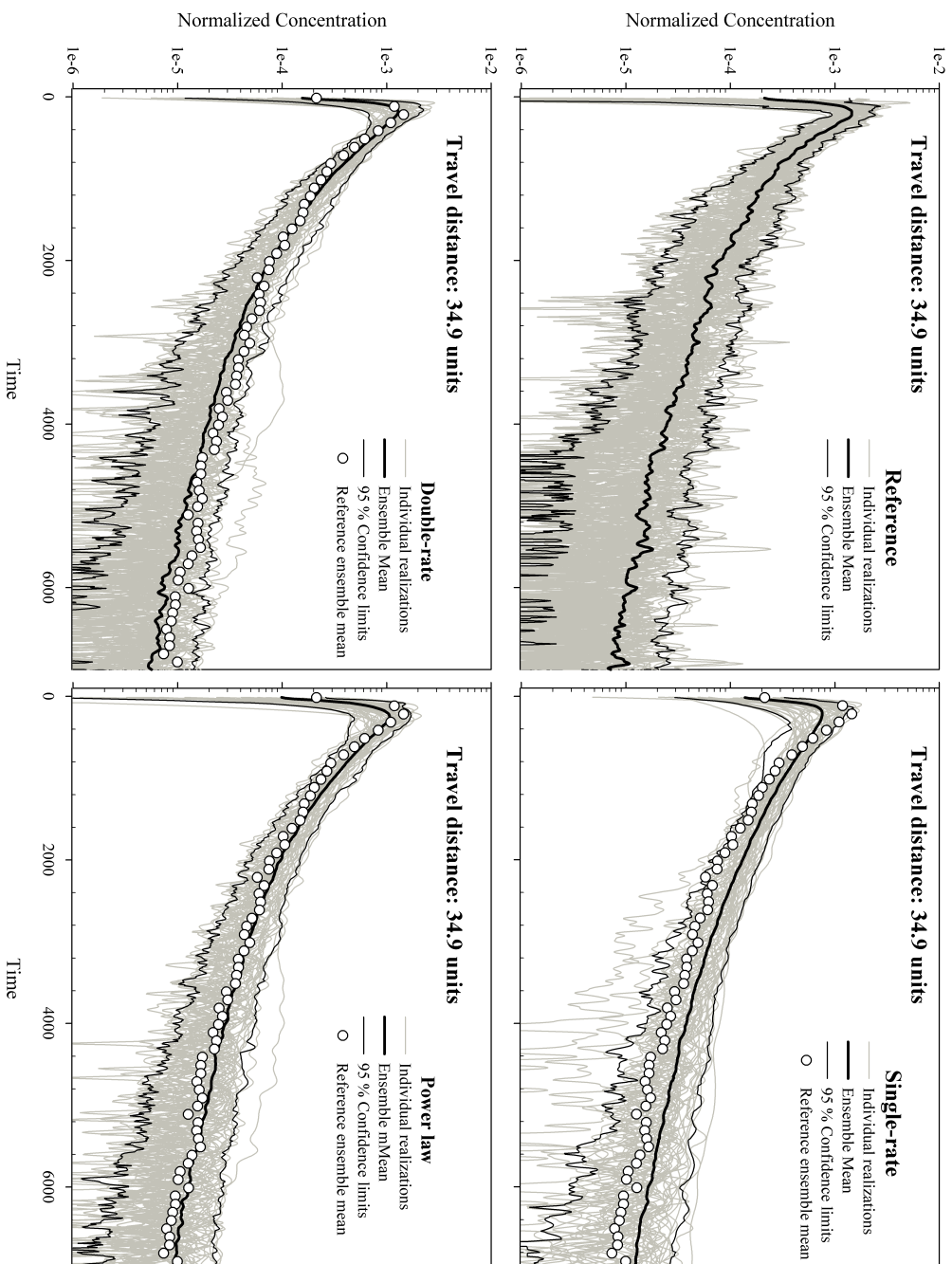


**Figure 3.12.** Ensemble of breakthrough curves obtained at  $x = 34$  units for the different upscaled models contrasted against the reference solution. The 95% confidence interval refer to the ensemble of 50 realizations.

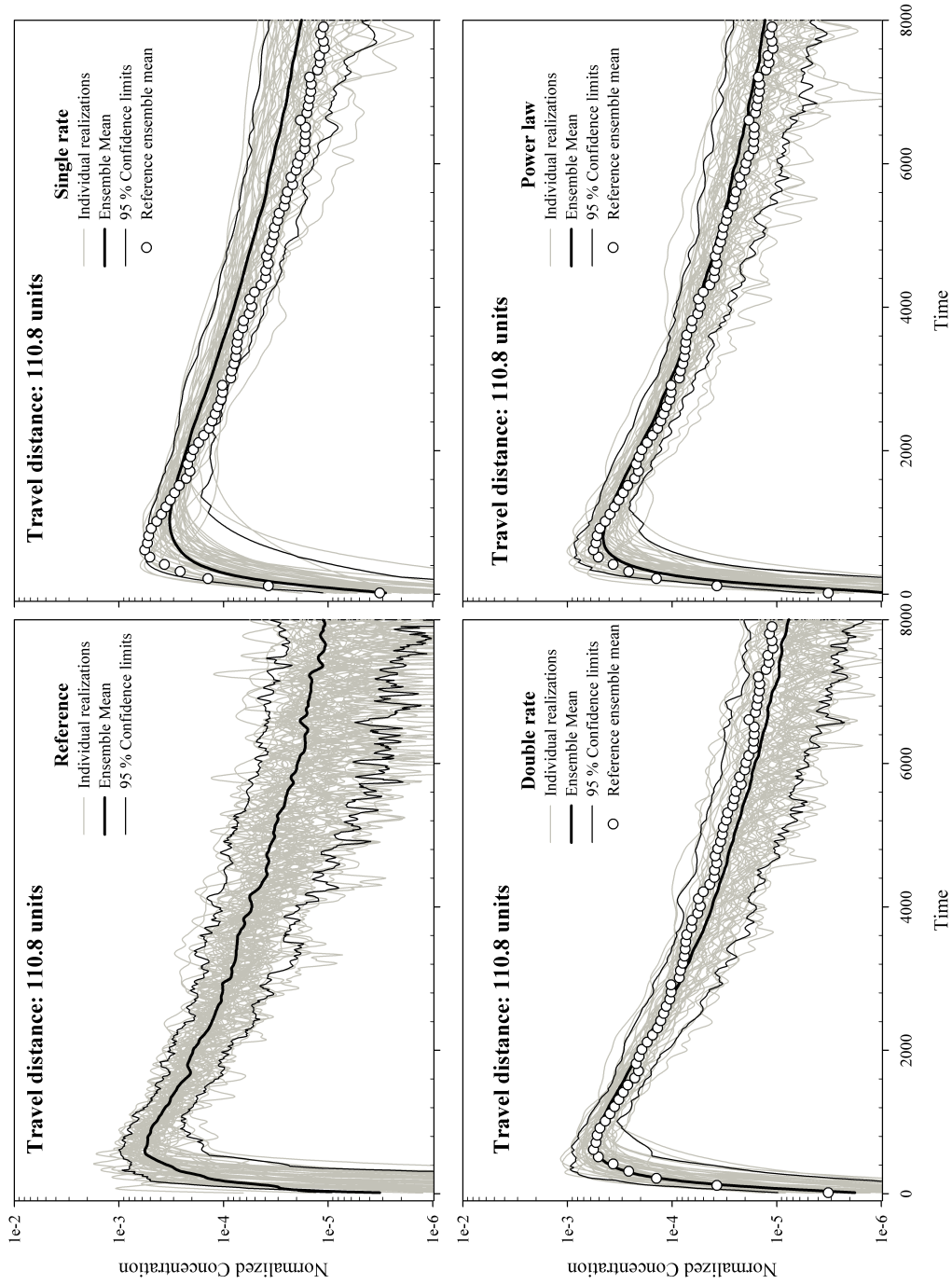


**Figure 3.13.** Ensemble of breakthrough curves obtained at  $x = 110.8$  units for the different upscaled models contrasted against the reference solution. The 95% confidence interval refer to the ensemble of 50 realizations.

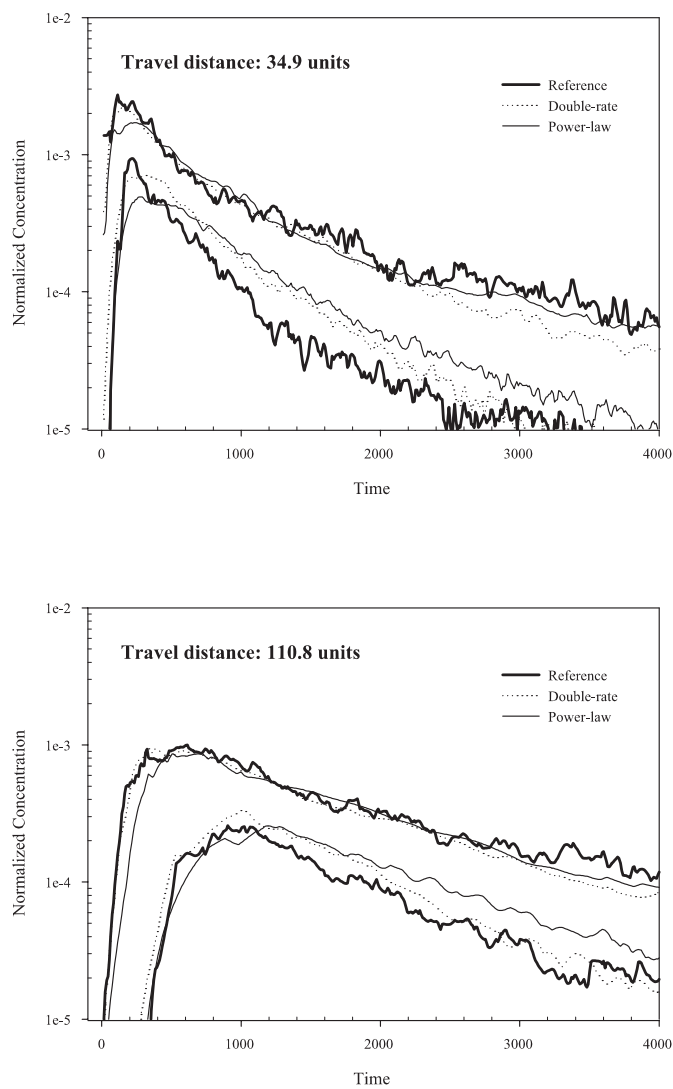


**Figure 3.14.** Propagation of uncertainty: Comparison of the reference confidence interval with those obtained using the upscaled models at two different control planes.

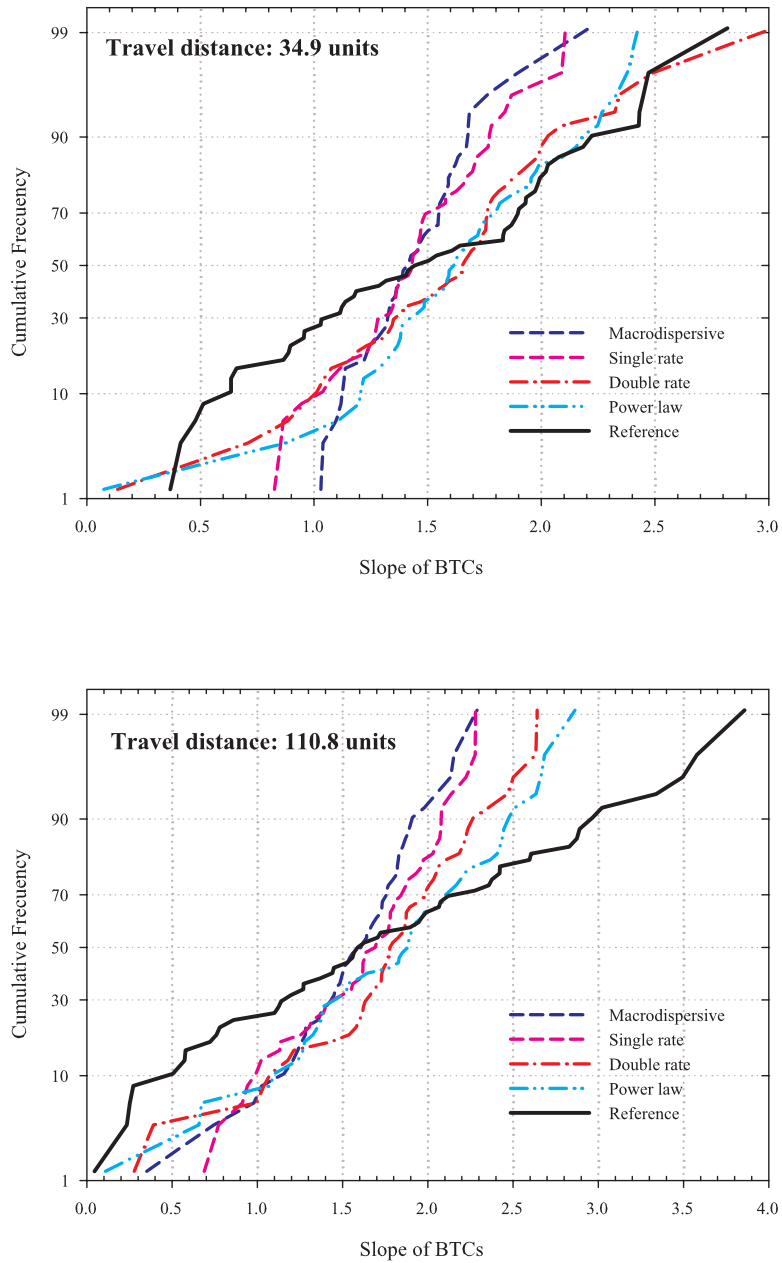


**Figure 3.15.** Cumulative frequency distribution of the late-time slope of BTCs for the different upscaled models. The late-time slope corresponds to the region of the BTCs comprised between the 60% and 80% of the BTC total mass.

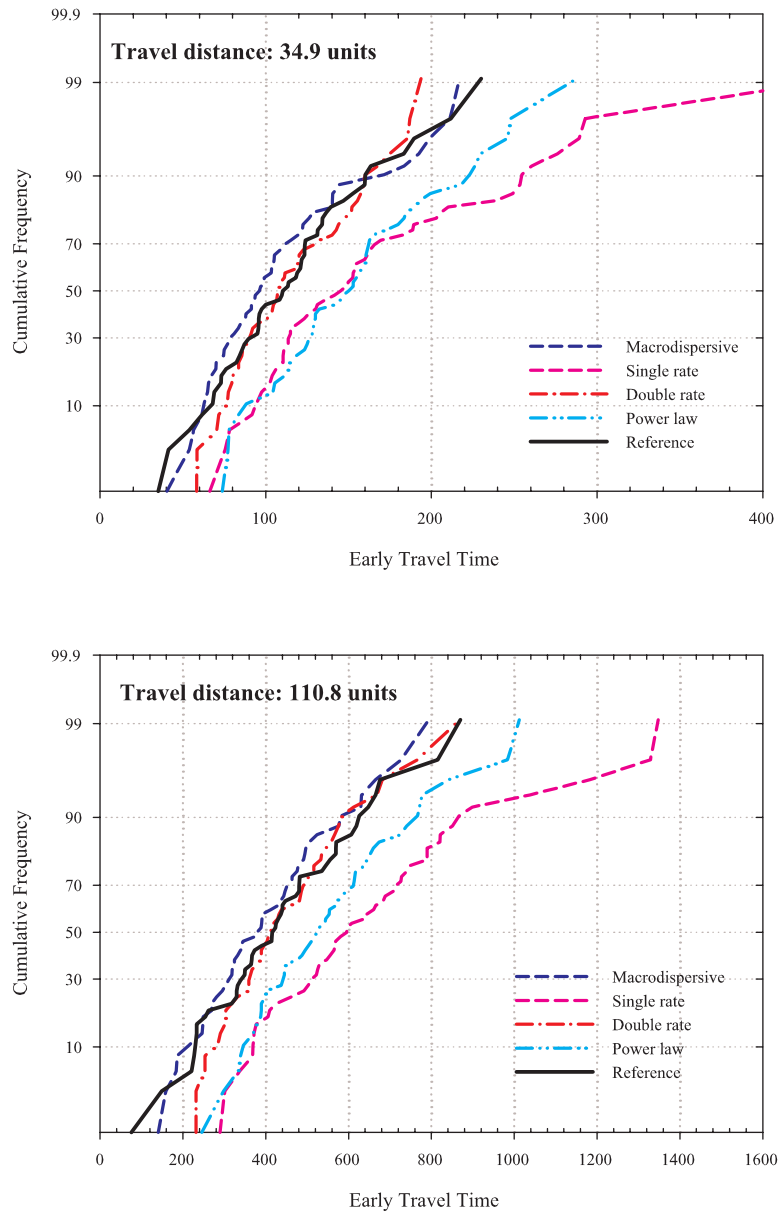


**Figure 3.16.** Cumulative frequency distribution of the early arrival time ( $T_{05}$ ) of BTCs for the different upscaled models.

As soon as particles pass through few blocks, the CDF of the late-time slope associated with the upscaled mass transfer model largely underestimates the dispersion of the corresponding probability density function. This effect increasing with distance.

In regards to the CDF associated with  $T_{05}$ , results show that only the double-rate model is able to properly describe uncertainty for all travel distances. In this case, the truncated power-law model provides a biased estimator of  $T_{05}$ , but still seems to properly capture the general trend depicted by the CDF.

Now, we examine the effect of including a macroscopic transverse dispersion into the upscaled model. This parameter describes the dispersive fluxes taking place in the transverse direction to the block-averaged flow based on a Fickian model. From Figure 3.17 we see that while accounting for transverse dispersive fluxes improves the reproduction of the late-time behavior of the BTCs, it causes an excess of dilution into the system (reduction of peak concentrations). Again, this is attributed to the Fickian assumption.

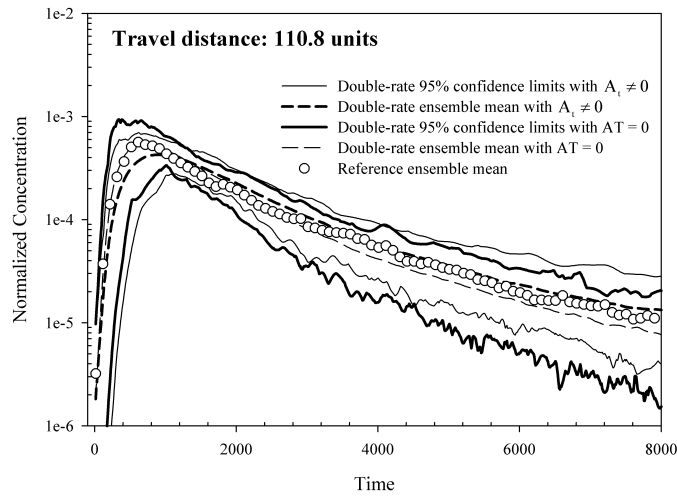


**Figure 3.17.** Comparison of the simulated ensemble of BTCs obtained with and without transverse macrodispersivity.

### 3.6 Summary and Conclusions

We have investigated the use of upscaled mass transfer models as a tool for upscaling solute transport in a general numerical modeling framework. This was achieved by comparing Monte Carlo simulations of solute transport at two

different support scales. Transport phenomena at the computational scale was described by means of a multirate mass transfer model.

The performance of the upscaled models was evaluated from two different perspectives. First, we analyzed the reproduction of the ensemble mean behavior of the main features associated with the simulated BTCs. Importantly, results showed that an appropriate description of the residence time distribution for all blocks of the numerical model provides an upscaled transport model that is capable to reproduce the ensemble mean behavior of the BTCs. In particular, the truncated power-law model provided an excellent reproduction of the effective spreading as well as the ensemble mean slope of the BTCs for all time scales. Yet, it slightly underestimated the first arrival of mass particles at control planes as well as the maximum concentration of the BTCs. In this context, the double-rate mass transfer model, which involved the same number of degrees of freedom as the truncated power-law, gave more consistent estimates of the first arrival and the concentration peak. However, as a drawback and consistent with theory, this model was found not able to properly describe the slope of the BTCs at all time scales ( $t > T_{80}$ ). Remarkably, the single-rate model did not capture any of the main features of the BTCs, giving then a sign of caution to the use of this widely employed model in field applications.

Then, we examined the effect of upscaling on model uncertainty. We found that a complete reproduction of uncertainty was not provided by any of the upscaled transport models, which substantially underestimated the uncertainty associated with the late-time behavior of BTCs and the peak of concentrations. Essentially, this was the result that a truthful reproduction of a BTC associated with an individual realization cannot in general be satisfied. The reason mostly lies on the poor description (lack of memory) of the dispersive mass fluxes transverse to the block-averaged flow direction. While using mass transfer models as a tool for upscaling can preserve the residence time distribution of mass particles in the system, the lack of memory in space prevents the model from reproducing mass fluxes in all directions. In particular, the reproduction of mass fluxes taking place at the interface between two blocks of the upscaled model are not satisfied by upscaling. Thus, results indicate that the lack of directionality involved in the memory term associated with mass transfer models prevents upscaling from reproducing uncertainty and mass fluxes at block interfaces. In this case, a proper description of the non-Fickian nature of dispersive mass fluxes should also be included into the constitutive transport equation.

### 3.7 References

- Adams, E. E., L. W. Gelhar (1992), Field study of dispersion in a heterogeneous aquifer 2. Spatial moment analysis, *Water Resources Research*, 28(12), 3293–3307.
- Benson, D. A., S. W. Wheatcraft, and M. M. Meerschaert (2000), Application of a fractional advection-dispersion equation, *Water Resources Research*, 36(6), 1403–1412.
- Berkowitz, B., and H. Scher (1998), Theory of anomalous chemical transport in fracture networks, *Physical Review E*, 57(5), 5858–5869.
- Berkowitz, B., J. Klafter, R. Metzler, and H. Scher (2002), Physical pictures of transport in heterogeneous media: Advection-dispersion, random-walk, and fractional derivative formulations, *Water Resources Research*, 38(10), 1191, doi:10.1029/2001WR001030.
- Berkowitz, B., A. Cortis, M. Dentz, and H. Scher (2006), Modeling non-fickian transport in geological formations as a continuous time random walk, *Reviews of Geophysics*, 44, RG2003, doi:10.1029/2005RG000178.
- Carrera, J., X. Sánchez-Vila, I. Benet, A. Medina, G. Galarza, and J. Guimerà (1998), On matrix diffusion: formulations, solution methods and qualitative effects, *Hydrogeology Journal*, 6, 178–190.
- Cushman, J. H., and T. R. Ginn (2000), Fractional advection-dispersion equation: A classical mass balance with convolution-Fickian flux, *Water Resources Research*, 36(12):3763–3766.
- Dentz, M., B. Berkowitz (2003), Transport behavior of a passive solute in continuous time random walks and multirate mass transfer, *Water Resources Research*, 39(5), 1111, doi: 10.1029/2001WR001163.
- Doherty, J. (2004), *Manual for PEST*, 5th edition, Brisbane, Australia: Watermark Numerical Computing.
- Feehley, C. E., C. Zheng, and F. J. Molz (2000), A dual-domain mass transfer approach for modeling solute transport in heterogeneous aquifers: Application to the Macrodispersion Experiment (MADE) site, *Water Resources Research*, 36(9), 2501–2515.
- Fernàndez-Garcia, D., T. H. Illangasekare, and H. Rajaram (2005a), Differences in the scale-dependence of dispersivity and retardation factors

- estimated from forced-gradient and uniform flow tracer tests in three-dimensional physically and chemically heterogeneous porous media, *Water Resources Research*, 41, W03012, doi:10.1029/2004WR003125.
- Fernàndez-Garcia, D., T. H. Illangasekare, and Harihar Rajaram (2005b), Differences in the scale dependence of dispersivity estimated from temporal and spatial moments in chemically and physically heterogeneous porous media, *Advances in Water Resources*, 28, 745–759.
- Fernàndez-Garcia, D., H. Rajaram, and T. H. Illangasekare (2005c), Assessment of the predictive capabilities of stochastic theories in a three-dimensional laboratory test aquifer: Effective hydraulic conductivity and temporal moments of breakthrough curves, *Water Resources Research*, 41, W04002, doi:10.1029/2004WR003523.
- Fernàndez-Garcia and Gómez-Hernández (2007), Impact of upscaling on solute transport: travel times, scale-dependence of dispersivity and uncertainty, *Water Resources Research*, 43, W02423, doi:10.1029/2005WR004727, 2007.
- Gómez-Hernández, J. J., and Srivastava R. M. (1990), ISIM3D: An ANSI-C three-dimensional multiple indicator conditional simulation program, *Computer and Geosciences*, 16(4), 395–440.
- Gómez-Hernández, J. J. (1991), A stochastic approach to the simulation of block conductivity fields conditioned upon data measured at a smaller scale, Ph.D. thesis, Stanford University, CA., 351 pp.
- Gómez-Hernández, J. J., and A. G. Journel (1993), Joint simulation of multi-Gaussian random variables. In: Soares A, editor. *Geostatistics Tróia'92*, vol. 1. Dordrecht, Kluwer, 85–94.
- Gouze, P., T. Le Borgne, R. Leprovost, G. Lods, T. Poidras, and P. Pezard (2008), Non-Fickian dispersion in porous media: Multiscale measurements using single-well injection withdrawal tracer tests, *Water Resources Research*, 44, W06426, doi:10.1029/2007WR006278.
- Guswa, A. J., and D. L. Freyberg (2002), On using the equivalent conductivity to characterize solute spreading in environments with low-permeability lenses, *Water Resources Research*, 38, (8), 1132, doi:10.1029/2001WR000528.
- Haggerty, R., and S. M. Gorelick (1995), Multiple-rate mass transfer for modeling diffusion and surface reactions in media with pore-scale heterogeneity, *Water Resources Research*, 31,(10), 2383–2400.

- Haggerty, R., S.A. McKenna, and L. C. Meigs (2000), On the late-time behaviour of tracer test breakthrough curves, *Water Resources Research*, 36, (12), 3467–3479.
- Haggerty, R., and P. Reeves (2002), STAMMT-L: Solute Transport and Multirate Mass Transfer, Version 1.0, User’s Manual, *ERMS#520308*, Sandia Natl. Lab., Albuquerque, N. M.
- Haggerty, R., C. F. Harvey, C. Freiherr von Schwerin, and L. C. Meigs (2004), What controls the apparent timescale of solute mass transfer in aquifers and soils? A comparison of experimental results, *Water Resources Research*, 40, W01510, doi:10.1029/2002WR001716.
- Harbaugh, A. W., Banta, E. R., Hill, M. C., and McDonald, M. G. MODFLOW-2000, The U.S. Geological Survey Modular Ground-Water Model-user guide to modularization concepts and the ground-water flow process, *Open-file Report 00-92*, 2000.
- Harvey, C., and S. M. Gorelick (2000), Rate-limited mass transfer or macrodispersion: Which dominates plume evolution at the Macrodispersion Experiment (MADE) site?, *Water Resources Research*, 36(3), 637–650.
- Hu, B. X., D.-W. Deng, and J.H. Cushman (1995), Nonlocal reactive transport with physical and chemical heterogeneity: Linear non-equilibrium sorption with random  $K_d$ , *Water Resources Research*, 31(9), 2239–2252.
- Koch, D. L., J. F. Brady (1985), Dispersion in fixed beds, *Journal of Fluid Mechanics*, 154, 399–427.
- Lawrence, A. E., X. Sanchez-Vila, and Y. Rubin, Conditional moments of the breakthrough curves of kinetically sorbing solute in heterogeneous porous media using multirate mass transfer models for sorption and desorption, *Water Resources Research*, 38(11), 1248, doi:10.1029/2001WR001006, 2002.
- Levy, M. and B. Berkowitz (2003), Measurement and analysis of non-Fickian dispersion in heterogeneous porous media, *Journal of Contaminant Hydrology*, 64(3-4), 203–226.
- Liu G., Ch. Zheng, and S. M. Gorelick (2004), Limits of applicability of the advection-dispersion model in aquifers containing connected high-conductivity channels, *Water Resources Research*, 40, W08308, doi: 10.1029/2003WR002735.
- Lu Z., and D. Zhang (2002), On stochastic modeling of flow in multimodal heterogeneous formations, *Water Resources Research*, 38(10), 1190, doi: 10.1029/2001WR001026.

- Mackay, D. M., D. L. Freyberg, P. B. Roberts, J. A. Cherry (1986), A natural gradient experiment on solute transport in a sand aquifer: 1. Approach and overview of plume movement, *Water Resources Research*, 22(13), 2017–2029.
- Meigs L. C., and R. L. Beauheim (2001), Tracer tests in fractured dolomite: 1. Experimental design and observed tracer recoveries, *Water Resources Research*, 37(5), 1113–1128, doi:10.1029/2000WR900335
- Morales-Casique, E., S. P. Neuman, A. Guadagnini (2006), Non-local and localized analyses of non-reactive solute transport in bounded randomly heterogeneous porous media: Theoretical framework, *Advances in Water Resources*, 29(9), 1399–1418.
- Neuman, S. P. (1993), Eulerian–Lagrangian theory of transport in spacetime nonstationary velocity fields: exact nonlocal formalism by conditional moments and weak approximation. *Water Resources Research*, 29(3), 633–645.
- Neuman, S. P., D. M. Tartakovsky (2008), Perspective on theories of non-Fickian transport in heterogeneous media, *Advances in Water Resources*., in press.
- Riva, M., L. Guadagnini, A. Guadagnini, T. Ptak, E. Martac (2006), Probabilistic study of well capture zones distribution at the Luswiesen field site. *Journal of Contaminant Hydrology*, 88, 92–118.
- Riva, M., A. Guadagnini, D. Fernández-García, X. Sanchez-Vila, T. Ptak (2008), Relative importance of geostatistical and transport models in describing heavily tailed breakthrough curves at the Lauswiesen site, *Journal of Contaminant Hydrology*, 101, 1–13.
- Rubin, Y., and A. G. Journel (1991), Simulation of non-Gaussian space random functions for modeling transport in groundwater, *Water Resources Research*, 27(7), 1711–1721.
- Rubin, Y. (1995), Flow and transport in bimodal heterogeneous formations, *Water Resources Research*, 31(10), 2461–2468.
- Salamon, P., D. Fernández-García, and J. J. Gómez-Hernández (2006a), A review and numerical assessment of the random walk particle tracking method, *Journal of Contaminant Hydrology*, 87, 277–305.
- Salamon, P., D. Fernández-García, and J. J. Gómez-Hernández (2006b), Modeling mass transfer processes using random walk particle tracking, *Water Resources Research*., VOL. 42, W11417, doi:10.1029/2006WR004927,2006.

- Salamon, P., Fernàndez-Garcia, D., J. J. Gómez-Hernández (2007), Modeling tracer transport at the MADE site: The importance of heterogeneity, *Water Resources Research.*, 43, W08404, doi:10.1029/2006WR005522.
- Sánchez-Vila, X., J. P. Girardi, and J. Carrera (1995), A synthesis of approaches to upscaling of hydraulic conductivities, *Water Resources Research.*, 31(4), 867–882.
- Sanchez-Vila, X., A. Guadagnini, and J. Carrera (2006), Representative hydraulic conductivities in saturated groundwater flow, *Reviews of Geophysics*, 44, RG3002, doi:10.1029/2005RG000169.
- Wen, X. H., and J. J. Gómez-Hernández (1996), The constant displacement scheme for tracking particles in heterogeneous aquifers, *Ground Water*, 34(1), 135–142.
- Wen, X.-H., and J. J. Gómez-Hernández (1996), Upscaling hydraulic conductivities in heterogeneous media: An overview, *Journal of Hydrology*, 183 (1–2), ix–xxxii.
- Willmann, M., J. Carrera, and X. Sanchez-Vila (2008), Transport upscaling in heterogeneous aquifers: What physical parameters control memory functions?, *Water Resources Research*, doi:10.1029/2007WR006531, in press.
- Wood, B. D., F. Cherblan, M. Quintard, and S. Whitaker (2003), Volume averaging for determining the effective dispersion tensor: Closure using periodic unit cells and comparison with ensemble averaging, *Water Resources Research*, 39(8), 1210, doi:10.1029/2002WR001723.
- Zheng, C., and P. P. Wang, *MT3DMS: A Modular Three-Dimensional Multi-Species Model for Simulation of Advection, Dispersion, and Chemical Reactions of Contaminants in Groundwater Systems: Documentation and User's Guide*, SERDP-99-1, U. S. Army Engineer Research and Development Center, Vicksburg, MS, 1999.
- Zinn, B., and Ch. F. Harvey (2003), When good statistical models of aquifer heterogeneity go bad: A comparison of flow, dispersion, and mass transfer in connected and multivariate Gaussian hydraulic conductivity fields, *Water Resources Research*, 39(3), 1051, doi:10.1029/2001WR001146.



# 4

## Modeling Solute Transport at Large Scale in Heterogeneous Media

### Abstract

We evaluate the use of (multi-rate) mass transfer as the solute transport conceptualization for models in heterogeneous media at the field scale. The non-Fickian transport behavior usually observed in the field, manifested by peaked concentration profiles with pronounced tailing, has questioned the use of the classical advection-dispersion equation to simulate solute transport at large scale with a numerical model. We analyze mass transport simulations at two different support scales and evaluate the performance of the upscaling technique proposed, which consists of introducing a mass transfer process for the simulation at the larger scales, with parameters derived from transport simulations at the smallest scale. The mass transfer process pursues the reproduction of the residence times within each model block. The results indicate that introducing this additional process for the simulation of transport at coarser scales yields good predictions for the main features of the breakthrough curves in comparison to upscaled models in which only flow is upscaled or just an enhanced macrodispersion considered.

## 4.1 Introduction

Hydrogeologic properties in an aquifer vary in space, in many cases over several orders of magnitude. Proper reproduction of this spatial heterogeneity is paramount for proper solute transport predictions. Geostatistics provides the ability to characterize the spatial variation of hydrogeologic properties with a high resolution. However, in practice, modeling transport with such resolution is most frequently unfeasible. Standard techniques for flow upscaling yield models at a coarse scale with homogeneous conductivities within each block, which are capable of a good reproduction of the mean flow behavior of the aquifer. However, for mass transport predictions, removing intra-block heterogeneity in order to obtain a model with a smaller number of blocks calls for some action if proper reproduction of the evolution of the plume of solute is to be achieved. The upscaled model must capture those features of the aquifer architecture that control mass transport (Fernández-García et al., 2007; Guswa and Freyberg, 2002).

In the literature there are a lot of work about hydraulic conductivity upscaling (Wen and Gómez-Hernández, 1996; Renard and de Marsily, 1993; Sánchez et al., 2006). Scheibe and Yabusaki (1998) showed that upscaling of conductivity is effective for reproduction of flow behaviour, but do not necessarily lead the best reproduction of transport behaviour. Since the values of conductivity obtained through upscaling does not contain information about the attribute heterogeneity that controls solute transport.

Much attention has been devoted in recent years to the development of methodologies for the characterization of heterogeneity of the hydrogeologic properties (Carrera, 1993; de Marsily et al., 2005; Gómez-Hernández, 2006), and important theories have been developed in the area of stochastic and/or deterministic hydrogeology to describe the flow and solute transport through an aquifer.

The effect of heterogeneity is to induce an anomalous (non-Fickian) transport behaviour, characterized by asymmetrical plumes and breakthrough curves with large tails. Experimental through (Boggs et al., 1992; Adams and Gelhar, 1992; Feehley et al., 2000; Salamon et al., 2007; Riva et al., 2008) and laboratory (Bajracharya and Barry, 1997; Fernández-García et al., 2005c; Levy and Berkowitz, 2003) data have revealed these characteristics.

The large contrast between high and low conductivities zones makes the solute to travel quickly in the direction of preferential flow paths, whereas in low conductivities areas the solute moves slowly creating tailing; neither of these two effects can be reproduced by the classical advection dispersion equation (ADE) (Adams and Gelhar, 1992; Feehley et al., 2000; Guswa and Freyberg, 2000; Zinn and Harvey, 2003; Berkowitz et al., 2006; Fernández-García et al., 2007; Riva et al., 2008).

Various numerical experiment using synthetic models Guswa and Freyberg (2000); Zinn and Harvey (2003); Liu et al. (2004); Carrera et al. (1998); Willmann et al. (2008), have demonstrated that the quality of solute transport predictions, in particular the late-time behavior of breakthrough curves, is significantly improved when the mass transfer equations are added to the ADE.

Alternative transport formulations based on the ADE have been proposed in the literature for modeling solute transport (Haggerty and Gorelick, 1995; Carrera et al., 1998). Carrera et al. (1998) proposed to add a sink/source term to ADE to account for the exchange of solute mass between high and low conductivity zones. This is formally represented by decomposing the domain into a mobile zone, where the transport phenomena include advection and dispersion, and an immobile zone where advection is negligible (Haggerty and Gorelick, 1995; Carrera et al., 1998; Haggerty et al., 2000). The mass flux between mobile and immobile zones is modeled by a linear mass exchange process controlled by a source/sink term. This term can be expressed as a convolution product of a memory function. The memory function represents the mass flux to the immobile zones per unit volume of aquifer, for a unit change in concentration in the mobile zones (Haggerty et al., 2000; Carrera et al., 1998). The formulation of this term depends on the geometry of the immobile zones and on the variability of mass transfer or diffusion rates (Haggerty et al., 2000). This type of model is commonly referred to as multirate mass transfer models (MRMT), where the term multirate refers to the fact that the immobile zone can be made up of many types of materials, each of which with a different transfer coefficient.

Other models have been developed with the same objective of reproducing the non-Fickian transport behaviour observed in heterogeneous aquifers in recent years. In this context, Berkowitz and Scher (1998); Berkowitz et al. (2000) presented a model based on the continuous time random walk (CTRW). In this model, particle transport in heterogeneous aquifer is represented as a random walk in space and time (Berkowitz and Scher, 1998; Dentz and Berkowitz, 2003; Dentz et al., 2004). Dentz and Berkowitz (2003) demonstrated that the mathematical formulation of MRMT is a special case of CTRW.

Neuman and Tartakovsky (2008); Berkowitz et al. (2006) present extensive reviews of the latest approaches to describe the evolution of the solute transport in porous media.

An interesting real case in which to evaluate these concepts is the MADE experimental site (Adams and Gelhar, 1992). Some transport models have been developed using a very fine discretization over the entire domain in order to capture the aquifer heterogeneity. For example, Salamon et al. (2007) improved a geostatistical interpretation of the flowmeter data, and concluded that the ADE model is capable of describe the extensive tracer spreading, when

small-scale variability of hydraulic conductivity is modeled at the flowmeter measurement support scale. Barlebo et al. (2004) using inverse flow and transport modeling obtained the same results, however the effective hydraulic conductivities product of the calibration phase were 5 times higher than the values measured in the field using the flowmeter. Harvey and Gorelick (2000); Feehley et al. (2000) used the dual-domain mass transfer model to explain the solute transport at the MADE site. Both work compare the mass transfer model with ADE.

Feehley et al. (2000) used ordinary kriging and conditional simulation based on fractional Brownian motion to represent the hydraulic conductivity, then, after calibrating the mass transfer coefficient and the immobile porosity they could reproduce the shape of mass plume. Harvey and Gorelick (2000) developed a transport model to recreate one-dimensional concentration profiles observed using ADE and an analytical homogeneous solution of mass transfer. Results of both works indicate that including mass transfer effects can largely improve the performance of solute transport in comparison with the enhanced macrodispersion model.

Another approach used to simulate the non-Fickian transport behavior at MADE site is the continuous time random walk model (Berkowitz and Scher, 1998). This model was able to reproduce the anomalous breakthrough curves and the non-Gaussian shape of tracer plume observed in the complex geological environment of MADE site.

Riva et al. (2008) analyzed the solute transport at the Lauswiesen forced-gradient trace test experiment. This study consists of a stochastic Monte Carlo analysis to evaluate the structure of the heterogeneity of the aquifer and the application of different numerical transport models including advection, dispersion and/or mass transfer processes to recreate the tailed multilevel breakthrough curves. They concluded the same as Salamon et al. (2007) on the fact that the ADE can describe the behaviour transport anomalous at a small support scale combined with a high-resolution description of heterogeneity.

Several researchers [e.g (Guswa and Freyberg, 2002; Carrera et al., 1998; Zinn and Harvey, 2003; Liu et al., 2004; Willmann et al., 2008; Riva et al., 2008)] have shown that to model the behaviour of non-reactive solute transport observed in heterogeneous medium is better to use coarse models incorporating a mass transfer process. In this framework, the scope of this work is to evaluate the use of MRMT as the constitutive transport model to simulate the large scale behavior of solute transport within a given aquifer. We will analyze a formulation of MRMT and compare the results at two different support scales. At the finest scale, we run the transport model considering only advection, then we obtain two upscaled models at two different support scales and compare the solute transport predictions using an enhanced macrodispersion model, and an MRMT in which mass transfer can occur into two

immobile domains (double-rate model). In the upscaled models, both the enhanced macrodispersion and the parameters associated with the double-rate mass transfer model are computed by matching, blockwise, the residence times of the solute within the block to those observed in the fine scale simulations. The enhanced macrodispersion and the parameters defining the mass transfer process are heterogeneous within the aquifer, with each block having their own values; this is contrary to other models reported in the literature that use homogeneous block values for the transport parameters (e.g., Harvey and Gorelick, 2000; Zinn and Harvey, 2003; Willmann et al., 2008)

## 4.2 Solute Transport Experiments

### 4.2.1 Experimental Design

We consider a synthetic case to simulate a typical field tracer test, where the mass of solute is introduced instantaneously into a steady-state flow field from an injection point. The flow domain is a 2D square of 240 units in each side. The aquifer is confined and under steady-state flow. No-flow boundary conditions were set at the top and bottom limits while constant head boundaries were set at the other sides, imposing a mean hydraulic gradient of 0.01 along  $x$ .

The aquifer is heterogeneous with respect to transmissivity  $T$ . For displaying purposes we will use  $\ln T = G(\mathbf{x})$ . Each of the three scenarios analyzed are generated as described below over a grid of 240 by 240 cells of 1 unit by 1 unit size. The solution of advective transport at this scale will represent the reference case. Then, two upscaling exercises will be performed, corresponding to a mild and a strong homogenization. In the first case each block of 5 by 5 cells will be replaced by a homogenous block and in the second case upscaling occur within each block of 15 by 15 cells. The upscaled models are of 48 by 48 blocks and 16 by 16 blocks respectively.

The focus of the work is no the performance of the upscaling techniques being compared. However, it also necessary —and very important— to up-scale the flow field. For this purpose, each block is assigned a homogeneous diagonal transmissivity tensor  $T^v$ , which is computed from the heterogeneous scalar values within the block using the approach known as simple Laplacian with skin (Gómez-Hernández, 1991; Wen and Gómez-Hernández, 1996). Essentially, for a given realization of  $G(\mathbf{x})$ , the grid-block being upscaled plus a skin area surrounding it is isolated from the rest of the blocks in the aquifer, then a small flow problem is solved on this small area to derive the components of a diagonal tensor that matches the average specific discharge to the average gradient. Wen and Gómez-Hernández (1996); Renard and de Marsily (1993); Sánchez et al. (2006) present an extensive review of the different methods for

hydraulic conductivity upscaling. In this study the skin was arbitrarily set to 12 units in each direction of the block, which was checked to be enough for a good reproduction of average fluxes at the block scale.

#### 4.2.2 Reference Transmissivity Field

We will analyze the performance of the two transport upscaling techniques for three different scenarios. The upscaling techniques imply to compute transport parameters associated to transport processes at the block scale in order to reproduce the solute residence times observed at the fine scale within each of the upscaled blocks. The two techniques analyzed are enhanced macrodispersion, in which the ADE is used to model transport at the block scale but an enhanced macrodispersion coefficient has to be determined, and double rate mass transfer, in which a multirate mass transfer process is added to ADE to model transport, in this case, besides an enhanced macrodispersion, the fraction rates of the two immobile phases and of the mobile phase, and the transfer coefficients have to be determined, too.

In all three scenarios, transmissivities are modeled as a composite media made up of a background material following a multiGaussian distribution within which lenses with a different conductivity distribution are embedded. The contrast between background and lenses is the most important difference among the three scenarios. The lenses are oriented in the main flow direction.

Let  $M_1$  represent the background material and  $M_2$  the lens material. To identify the aquifer volume occupied by each material we use a binary random function defined as

$$I(\mathbf{x}) = \begin{cases} 1 & \mathbf{x} \in M_2 \\ 0 & \mathbf{x} \in M_1 \end{cases} \quad (4.1)$$

The volumetric proportion of material  $M_2$ , denoted as  $p_2$ , defines the mean and variance of the indicator random variable, respectively written as  $\langle I(\mathbf{x}) \rangle = p_2$  and  $\sigma_I^2 = p_2 p_1$ , where  $p_1$  is the volumetric proportion of  $M_1$  ( $p_1 = 1 - p_2$ ). We consider that the lens family (material  $M_2$ ) occupies 20% of the domain, i.e.,  $p_2 = 0.2$  and  $p_1 = 0.8$ . The indicator variable was further characterized with an anisotropic covariance function,

$$C_I(|\mathbf{r}|) = \sigma_I^2 \exp \left( -\sqrt{\left(\frac{r_x}{\lambda_x^I}\right)^2 + \left(\frac{r_y}{\lambda_y^I}\right)^2} \right) \quad (4.2)$$

where  $\lambda_x^I$  and  $\lambda_y^I$  are the longitudinal and transverse correlation scales of the indicator variable set to 16 units and 1 unit, respectively.

The background fields  $G_1(\mathbf{x})$  associated to  $M_1$  were generated using the sequential Gaussian simulation program, GCOSIM3D (Gómez-Hernández and

Journal, 1993), whereas the lens family  $I(\mathbf{x})$  was generated using the indicator sequential simulation program ISIM3D (Gómez-Hernández and Srivastava, 1990). In all scenarios the lenses were assigned a constant value. The fields  $G_1$  and  $I$  were generated independently.

The composite media is finally obtained as  $Y(\mathbf{x}) = (1 - I(\mathbf{x}))G_1(\mathbf{x}) + I(\mathbf{x})G_2$  (where  $G_2$  is a homogeneous field of constant logtransmissivity). Figure 4.1 illustrates the steps involved in the stochastic generation of a composite random field.

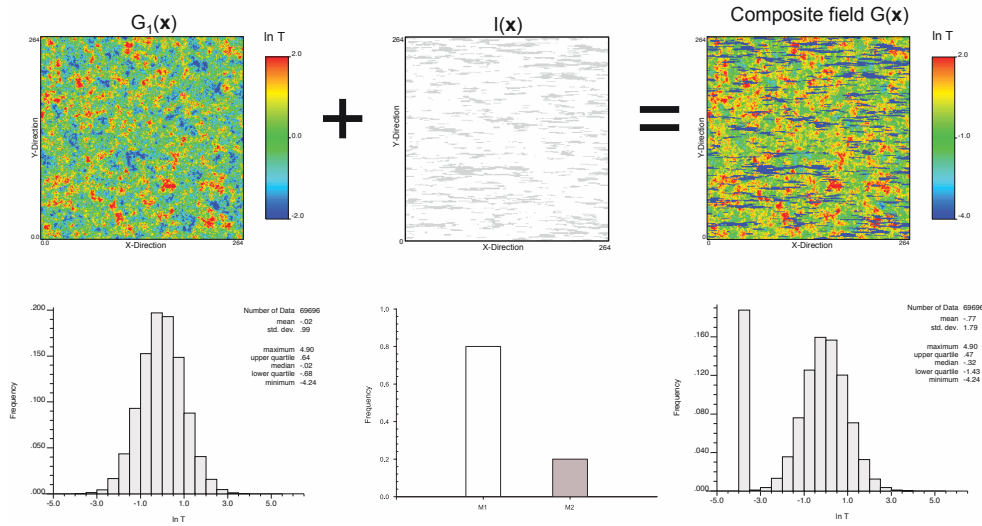


**Figure 4.1.** Representation of the steps involved in the stochastic generation of a composite transmissivity field.

For the first scenario, the background material  $M_1$  is heterogeneous and described by a log-transmissivity characterized with a multi-Gaussian distribution of mean zero and variance 9 following an anisotropy exponential covariance function given by

$$C_{G_1}(|\mathbf{r}|) = \sigma_{G_1}^2 \exp \left( -\sqrt{\left(\frac{r_x}{\lambda_x^{G_1}}\right)^2 + \left(\frac{r_y}{\lambda_y^{G_1}}\right)^2} \right) \quad (4.3)$$

where  $\mathbf{r} = (r_x, r_y)$  is the separation vector between two points of the aquifer,  $\sigma_{G_1}^2$  is the variance of  $G_1(\mathbf{x}) = \ln T_1(\mathbf{x})$  equal to 9, and  $\lambda_x^{G_1}$  and  $\lambda_y^{G_1}$  are the longitudinal and transverse correlation scales set to 40 and 4 units, respectively and aligned with the main flow direction. Figure 4.2 display the realization of  $G_1(\mathbf{x})$  for first scenario of  $M_1$ .

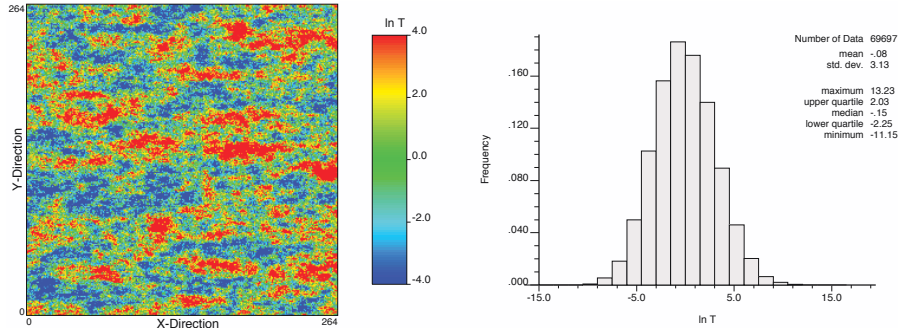


**Figure 4.2.** Illustration of the realization of the reference natural log of transmissivity  $G_1(\mathbf{x})$  for the first scenario

For the second scenario, the field  $G_1(\mathbf{x})$  is characterized by a multi-Gaussian distribution with zero mean and unit variance, following an isotropic exponential covariance function.

$$C_{G_1}(|\mathbf{r}|) = \sigma_{G_1}^2 \exp\left(-\frac{|\mathbf{r}|}{\lambda}\right) \quad (4.4)$$

where the correlation scale is set to 4 units.  $G_1(\mathbf{x})$  of  $M_1$ . The field is shown in the figure 4.3.

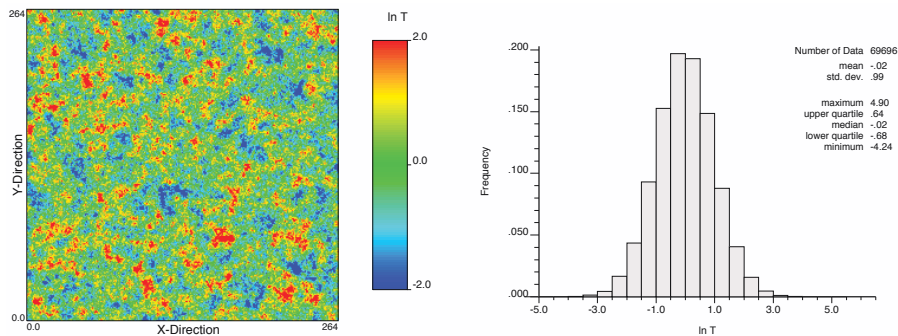


**Figure 4.3.** Illustration of the realization of the reference natural log of transmissivity  $G_1(\mathbf{x})$  for the second scenario

In all scenarios we considered that the variation within  $G_2$  is of lesser importance compared with the contrast between  $G_1$  and  $G_2$ , and we therefore assigned a constant log transmissivity value to  $M_2$  of 2.0 and -4.0 and 4.0 for scenarios 1, 2 and 3 respectively. Figure 4.4 shows the composite random field for the first scenario, which also shows the histogram and univariate statistics. The semivariogram of  $\ln T$  for the  $x$  and  $y$  directions in the composite field are shown in figure 4.5, to which an anisotropic exponential covariance

has been fit with integral scales in the  $x$  and  $y$  directions of  $\lambda_x^G = 32.8$  units and  $\lambda_y^G = 3.2$  units.

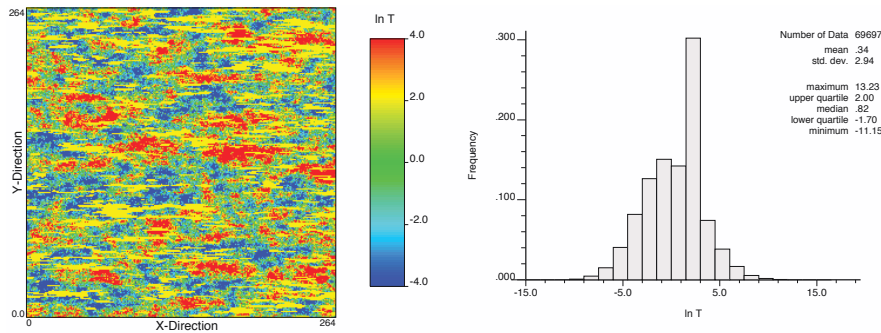


**Figure 4.4.** Transmissivity structure and histogram for the first composite field.

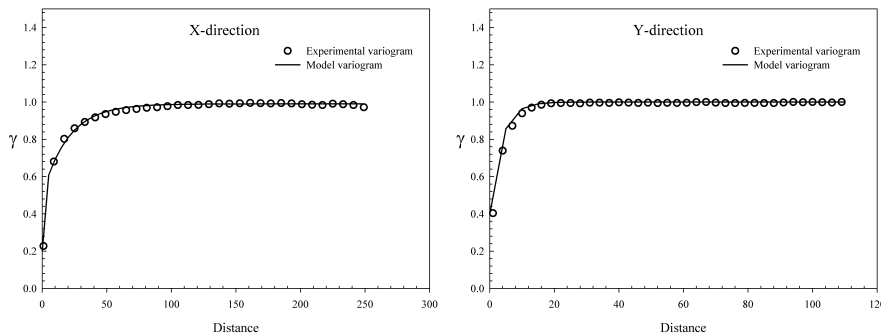


**Figure 4.5.** Experimental and model variograms for the  $\ln T$  in the first scenario for the  $x$  and  $y$  directions.

Figure 4.6 shows the cumulative breakthrough curves at an  $x$ - control plane located at  $x = 159.9$  units obtained in the realization of  $G_1$  and in the composite realization  $G$  for scenario 1. We observe the influence of the lenses in the transport behavior of the solute, in particular the different slopes after a certain time.

The second composite transmissivity field is shown in figure 4.7. The composite field has a mean of  $-0.77$  and a variance of  $3.2$ . The semivariogram of  $\ln T$  for the  $x$  and  $y$  direction are shown in figure 4.8. The integral scale of the fitted exponential models in the  $x$  and  $y$  directions are  $\lambda_x^G = 7.0$  units and  $\lambda_y^G = 2.0$ .

Figure 4.9 shows the cumulative breakthrough curves at an  $x$ - control plane located at  $x = 159.9$  units obtained in the realization of  $G_1$  and in the composite realization  $G$  for scenario 2. We observe the influence of the low

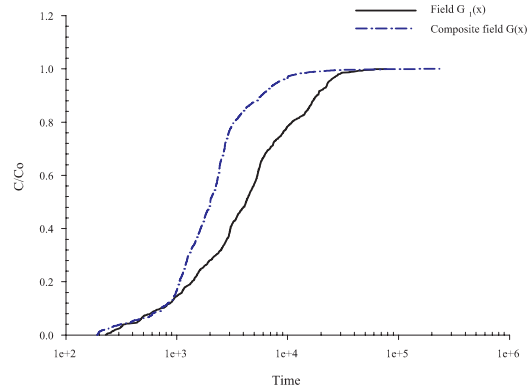


**Figure 4.6.** Cumulative mass flux breakthrough curves obtained at a given  $x$ -control plane ( $x = 159.9$  units) computed on the transmissivity field  $G_1(\mathbf{x})$  and on the associated composite medium  $G(\mathbf{x})$  for scenario 1

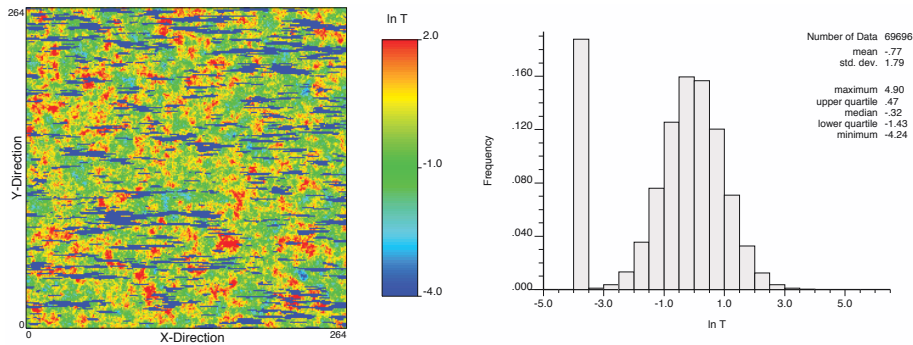


**Figure 4.7.** Transmissivity field and histogram for the composite field in the second scenario.

conductivity lenses in the transport behavior of the solute, in particular the very different tails.

The third field test was generated by multiplying by  $-1.0$  the second field. In this way the lenses change from poorly conductive to highly conductive while the distribution of the background transmissivities remains the same. The field is shown in figure 4.10. The integral scale in the  $x$  and  $y$  directions for field 3 are the same as in field 2. Figure 4.11 shows the cumulative breakthrough curves at an  $x$ -control plane located at  $x = 159.9$  units obtained for the composite realizations in scenarios 2 and 3. For the same background distribution we observe the large influence that the conductivity of the lenses has in the shape of the breakthrough curves.

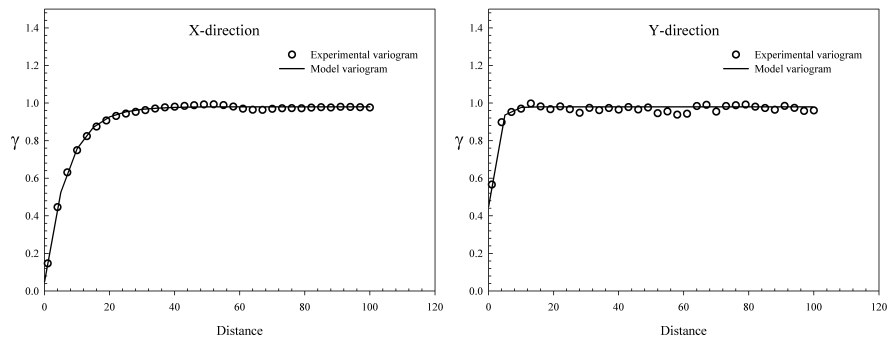


**Figure 4.8.** Experimental and model variograms for the  $\ln T$  in the second scenario for the  $x$  and  $y$  directions.

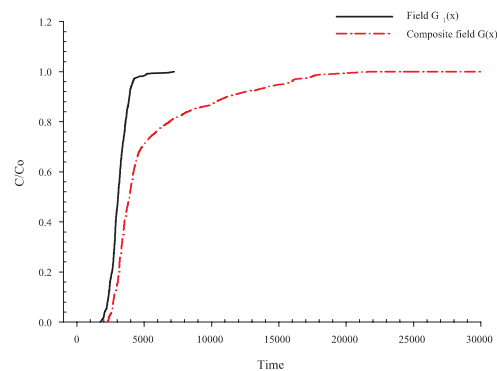


**Figure 4.9.** Cumulative mass flux breakthrough curves obtained at a given  $x$ -control plane ( $x = 159.9$  units) computed on the transmissivity field  $G_1(\mathbf{x})$  and its associated second composite medium  $G(\mathbf{x})$  for scenario 2.

The three scenarios display very different transport behavior. We will try to match this behavior with the proposed upscaling technique and will conclude when it is really necessary to include a double rate mass transfer process in the transport simulation and when just an enhance macrodispersion model would suffice.

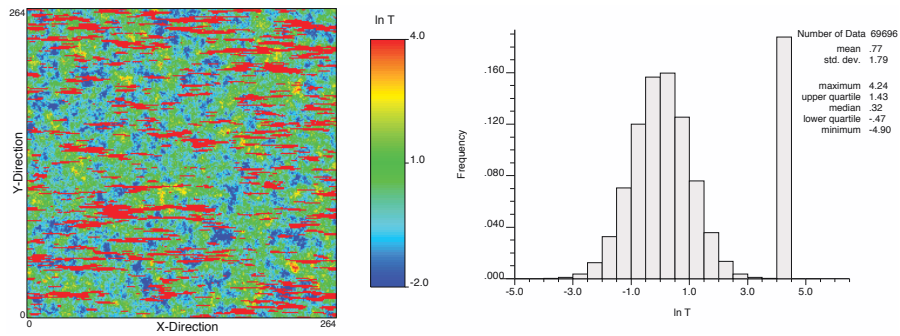


Figure 4.10. Transmissivity field and histogram for the third composite field.

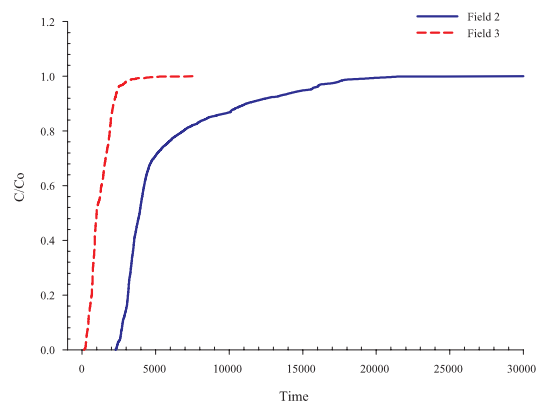
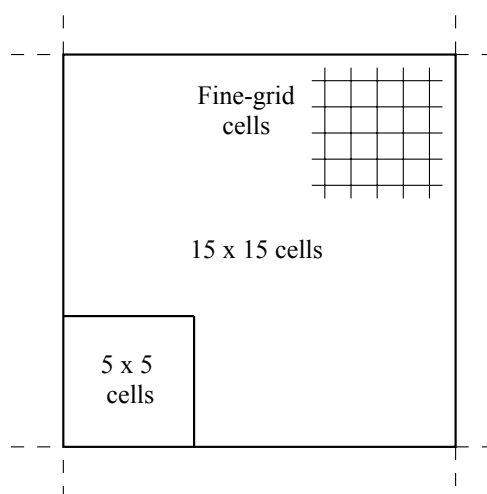


Figure 4.11. Cumulative mass flux breakthrough curves obtained at a given  $x$ -control plane ( $x = 159.9$  units) computed on the transmissivity fields for scenarios 2 and 3.

### 4.2.3 Flow and Transport Solution

Three type of numerical grids are used to simulate the flow and solute transport: a fine grid with 1 unit side square cells that provides the reference solution and two coarse grid with 5, and 15 units side square grid-blocks respectively that are used to test the upscaling algorithm (see figure 4.12). The fine-grid is designed on the same support in which the transmissivity fields were generated.



**Figure 4.12.** Different size of blocks used in the upscaling process

The flow problem was solved with MODFLOW2000 (Harbaugh et al., 2000) at all scales. The solute transport was solved with the random walk particle tracking code RW3D (Fernández-García et al., 2005a,b; Salamon et al., 2006). RW3D was used to simulate advective transport at the fine scale to obtain the reference solutions and it was used to simulate advective-dispersive and mass transfer transport in the upscaled models.

Simulation of solute transport with mass transfer is based on the particle tracking methodology presented by Salamon et al. (2007). Basically, transport is simulated by injecting a large number of mass particles into the system, each particle representing a small portion of the plume solute. Advection is simulated by moving particles along flowlines, whereas dispersion is emulated by a Brownian motion. Mass-transfer process are incorporated by switching the state of the particles between mobile/immobile states according to appropriate transition probabilities.

In each case we simulated the behaviour of the released solute for a period of time,  $t = 3000$ . For this purpose 40,000 particles, where each particle was assigned the same mass, and were uniformly distributed over the 15 x 150 units

rectangular source area is indicated in the figure 4.13. For each movement, the time step was adapted based on a grid Courant number of 0.01 (Wen and Gómez-Hernández, 1996).

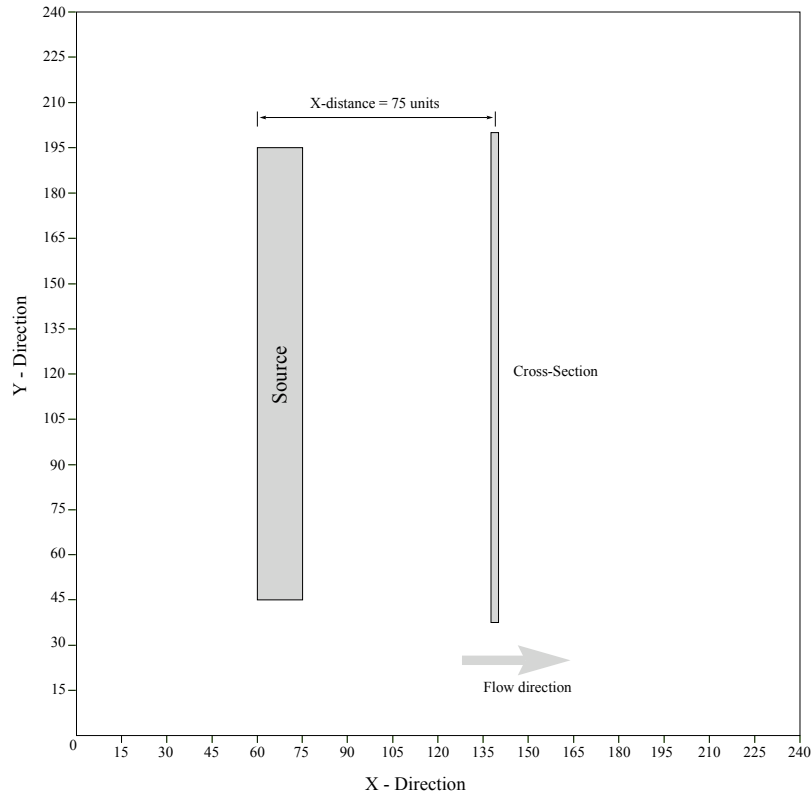


**Figure 4.13.** Plan view of the location of the injection area and location of the control plane, at 75 units along the  $x$  direction from the injection.

#### 4.2.4 Flow and Transport Parameters

Transport parameter values to each grid-block are obtained with the upscaling technique presented in chapter 3. We recall that the proposed technique consists of replacing each block of heterogeneous transmissivities by a homogeneous block, with a homogeneous transmissivity tensor with homogeneous values of the parameters associated to the memory function that is used to represent the mass exchange between the mobile and immobile phases. Block transport parameters are estimated by analyzing the residence time distribution of the particles traversing the block, these travel times are determined using fine-scale simulations.

## 4.3 Results and discussion

### 4.3.1 Overview of Plume Behavior

For each of the three scenarios, Figure 4.14 shows the spatial distribution of the solute plume computed on the reference field at  $t = 300$  and for the upscaled models using a block of 5 by 5 units. In the latter case we consider the double rate mass transfer model and an enhanced macrodispersion transport model. Likewise Figure 4.15 shows the same results but when using an upscaling block of 15 by 15 units. To represent the plume in each figure, the number of particles falling in each cell of a square grid of 1 unit cells were counted and accumulated to get the total mass within the cell.

At the fine scale, transport is purely advective, therefore solute spreading is due entirely to heterogeneity. At the large scale we can observe that this spreading is far from Fickian, the plume displays high asymmetry, fingering, particles accelerate following fast paths. It is only in the second scenario with the very low conductive lenses that the plume displays a more regular shape, although at time  $t = 300$  it has not traveled as far as in the other scenarios.

We can use relative entropy to quantify the performance of the upscaled models. The relative entropy measures the difference between two distributions  $p$  and  $q$  over the same space (Kullback, 1959). For two particle distributions defined over the same set of  $n$  blocks, the relative entropy (**RE**) between the two distributions is defined by

$$\mathbf{RE}(t) = \sum_{i=1}^n p_i \ln \frac{p_i}{q_i} \quad (4.5)$$

where the frequencies  $q_i$  and  $p_i$  represent the fraction of particles in each cell, i.e.,  $q_i = n_i/N_p$ , where  $n_i$  is the number of particles in the block and  $N_p$  is the total number of particles found within the system. **RE** is zero only when two distributions of particles are identical.

**RE** computed for each of the three scenarios and at various times are presented in figure 4.16. Within each graph the entropy of each of the upscaling models for two block sizes and two transport models relative to the reference simulations are shown. For the calculation of the **RE** the domain is discretized over a square fine-grid formed by 240 x 240 cells of 1 unit side.

For scenarios 1 and 3, we could say that both transport models (enhanced macrodispersion and double-rate mass transfer) perform similarly in the reproduction of the evolution of the reference plume, with the macrodispersion model working slightly better for scenario 1 and an upscaling block size of 5 by 5 units. However, in scenario 2, where the lenses are of low conductivity, the double rate mass transfer model works clearly better than the enhanced macrodispersion for the two upscaling block sizes.

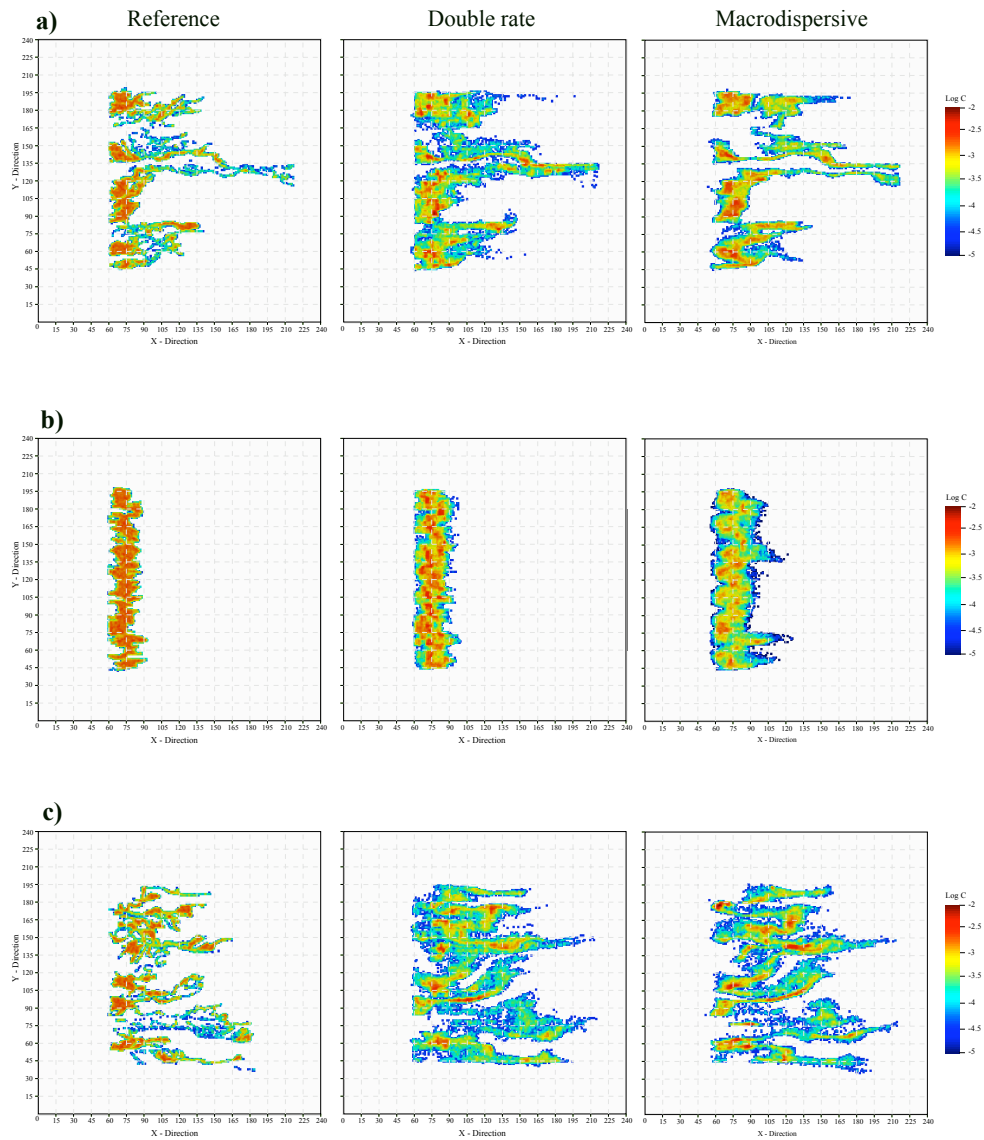


**Figure 4.14.** Log concentration distribution of solute mass for the three scenarios. Comparison between the simulations in the reference field and in the upscaled fields with blocks of 5 by 5 cells using two different transport models at the coarse scale. (a) First scenario, (b) second scenario and (c) third scenario.

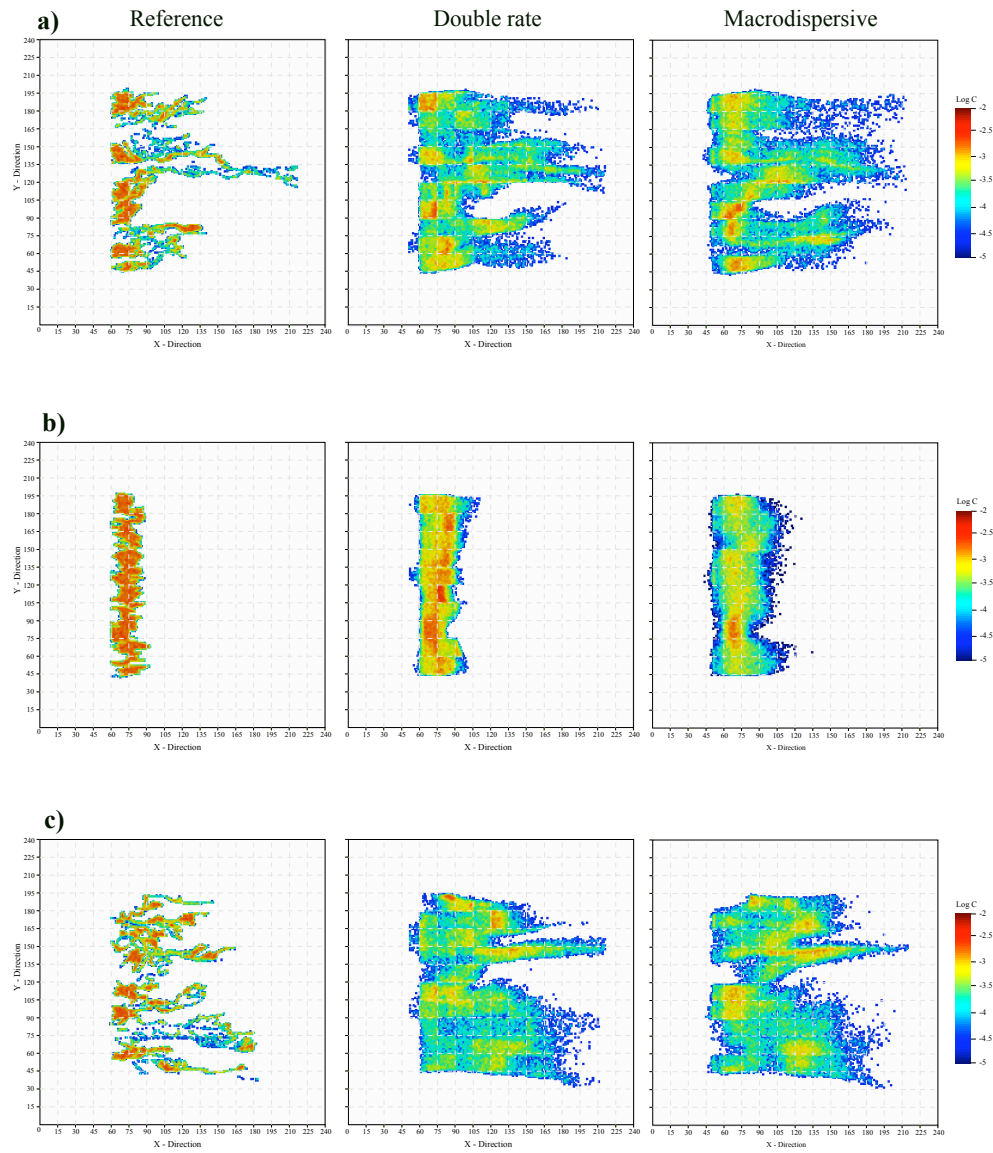


**Figure 4.15.** Log concentration distribution of solute mass for the three scenarios. Comparison between the simulations in the reference field and in the upscaled fields with blocks of 15 by 15 cells using two different transport models at the coarse scale. (a) First scenario, (b) second scenario and (c) third scenario.

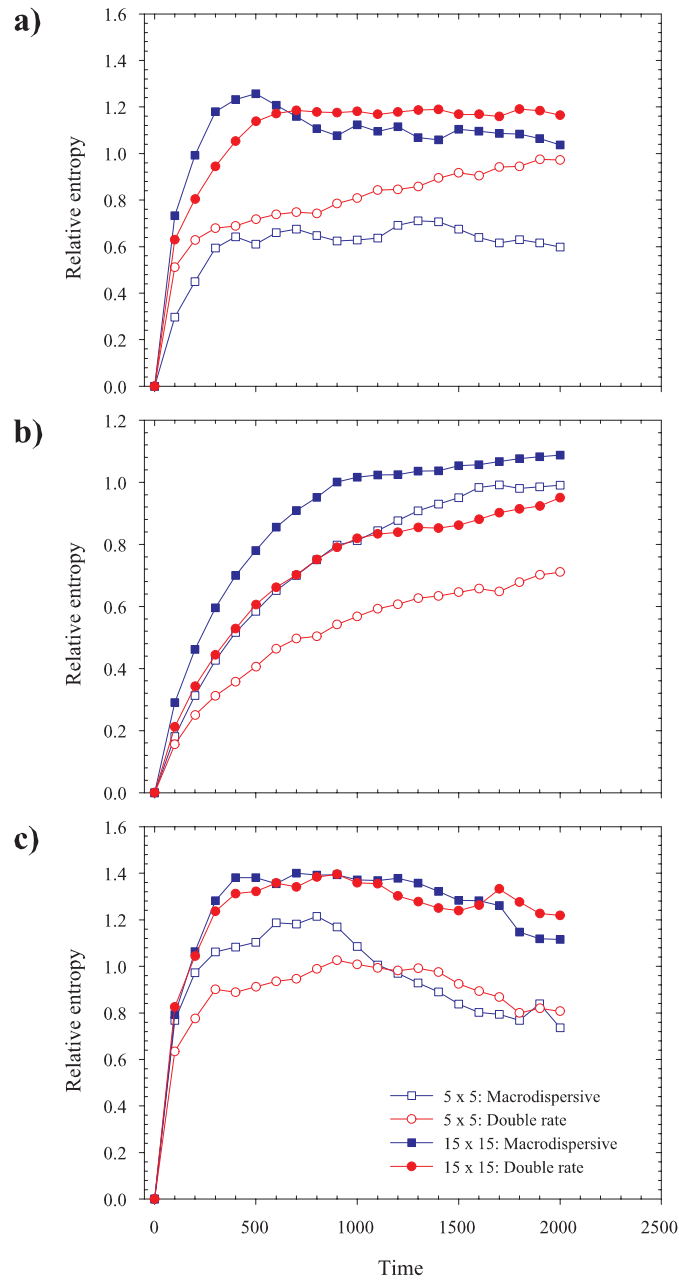


**Figure 4.16.** Comparison of the temporal evolution of relative entropy of double rate and macrodispersion models for the three scenarios. In all cases, entropy is computed relative to the reference case

A preliminary conclusion from this figure is that including mass transfer in the upscaling process is justified when there are low conductivity inclusions, which, conceptually, are equivalent to having an immobile phase in which particles are retarded. But, when the inclusions are of high conductivity, using a simpler enhanced macrodispersion model could suffice.

### 4.3.2 Longitudinal Mass Distribution

Next we will compare the longitudinal mass distribution at two different times for the reference simulations and the upscaled ones. Each profile is obtained by integrating 1 unit wide vertical slices and normalizing the value by the total mass.

Figures 4.17 and 4.18 show the longitudinal mass distribution profiles at times  $t = 300$  and  $t = 600$  for the two transport models and the two support scales. Analyzing these figures we reach similar conclusions as we did after seen the relative entropy values. Double rate transport models work clearly better for scenario 2, and very similarly to enhanced macrodispersion for scenarios 1 and 3. However, in the case of upscaling with blocks of 15 by 15 units, we observe a non-physical back-dispersion induced by the enhanced macrodispersion model in all three scenarios.

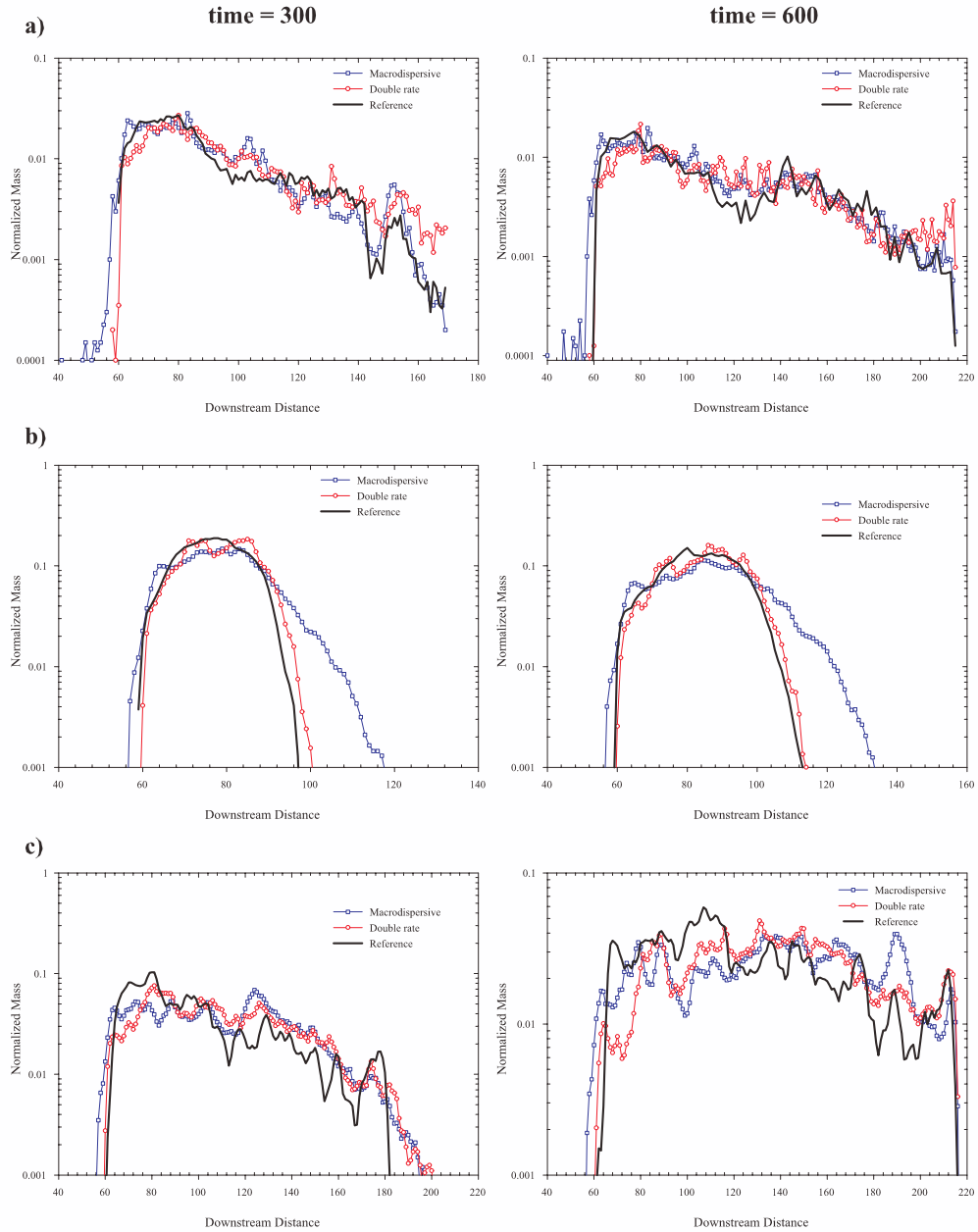
Figure 4.19 shows the breakthrough curves at a control plane located at a horizontal distance of 75 units from the injection point. To compute the curve we determine the total number of particles crossing the control section after each time step. The same conclusion as before can be drawn, double rate models always work better than macrodispersion models, with this superiority begin more apparent for scenario 2. Although neither the peak concentration nor the late-time slope are perfectly matched in scenarios 1 and 3. (For scenario 2, the peak had not arrived yet to the control plane at  $t = 2000$ ).

### 4.3.3 Dilution Index

Finally we have analyzed the dilution index, i.e, the relative volume of aquifer occupied by the solute plume. As seen in Figures 4.14 and 4.15 the plumes simulated in the upscaled models are much more spread than the reference, therefore, their dilution will be larger than the dilution in the reference.

The dilution index is a quantitative measure of the plume structure, which gives us another insight about the performance of the upscaling models. The dilution index was proposed by (Kitanidis, 1994) and it is given by

$$I = \frac{E(t)}{E_{max}} \quad (4.6)$$



Size of block: 5 cells

**Figure 4.17.** Longitudinal mass distribution profiles for the reference solution and the upscaled models using 5 by 5 blocks and modeling transport by double rate and enhanced macrodispersion for times  $t = 300$  (left column) and  $t = 600$  (right column). a) Scenario 1, b) scenario 2 and c) scenario 3. Injection point at  $x = 60$  units

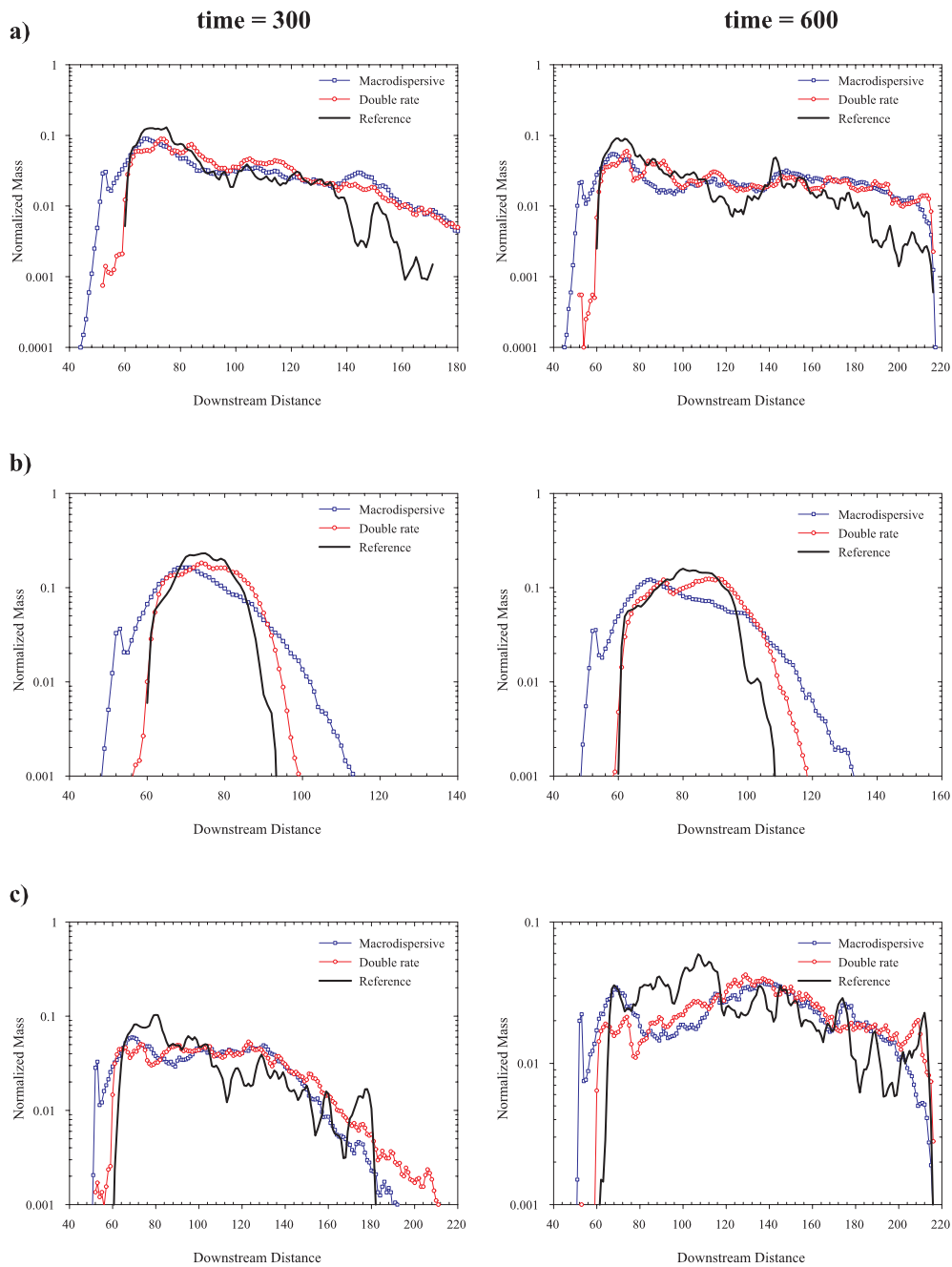


**Figure 4.18.** Longitudinal mass distribution profiles for the reference solution and the upscaled models using 15 by 15 blocks and modeling transport by double rate and enhanced macrodispersion for times  $t = 300$  (left column) and  $t = 600$  (right column). a) Scenario 1, b) scenario 2 and c) scenario 3. Injection point at  $x = 60$  units

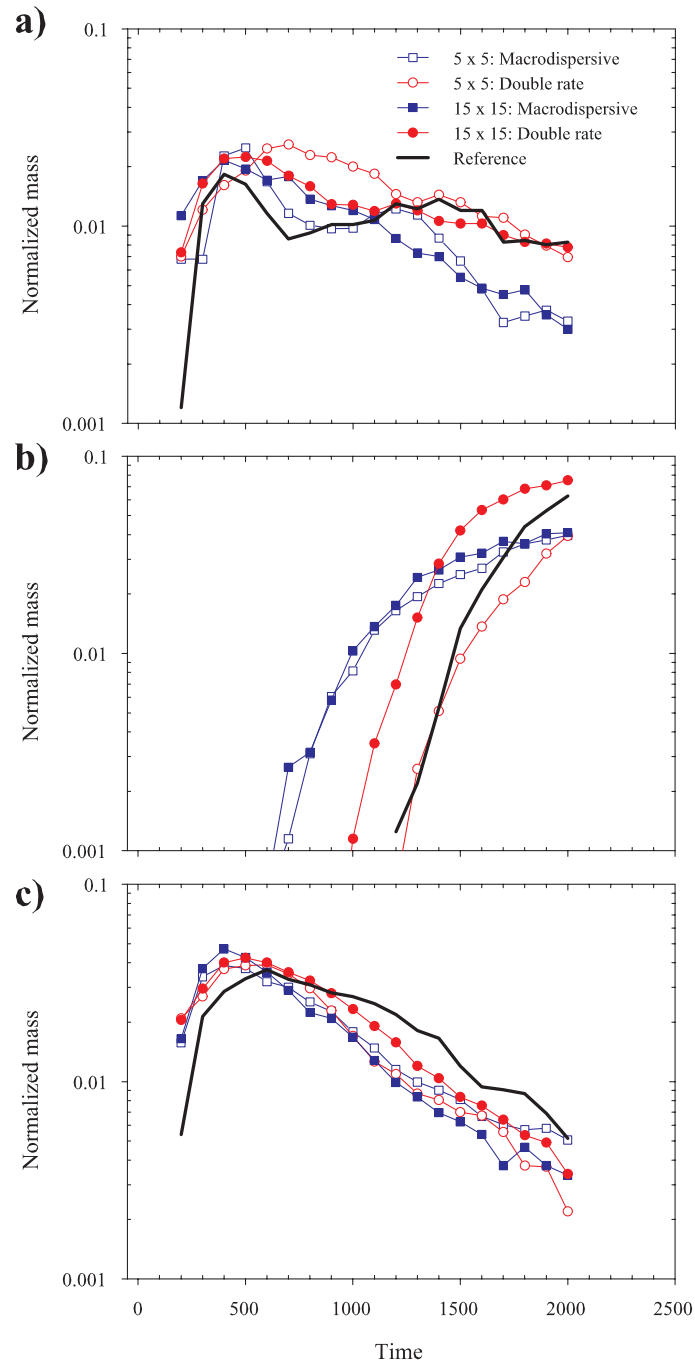


**Figure 4.19.** Comparison of the breakthrough curves at a control plane 75 units horizontally from the injection. (a) Scenario 1, (b) scenario 2 and (c) scenario 3.

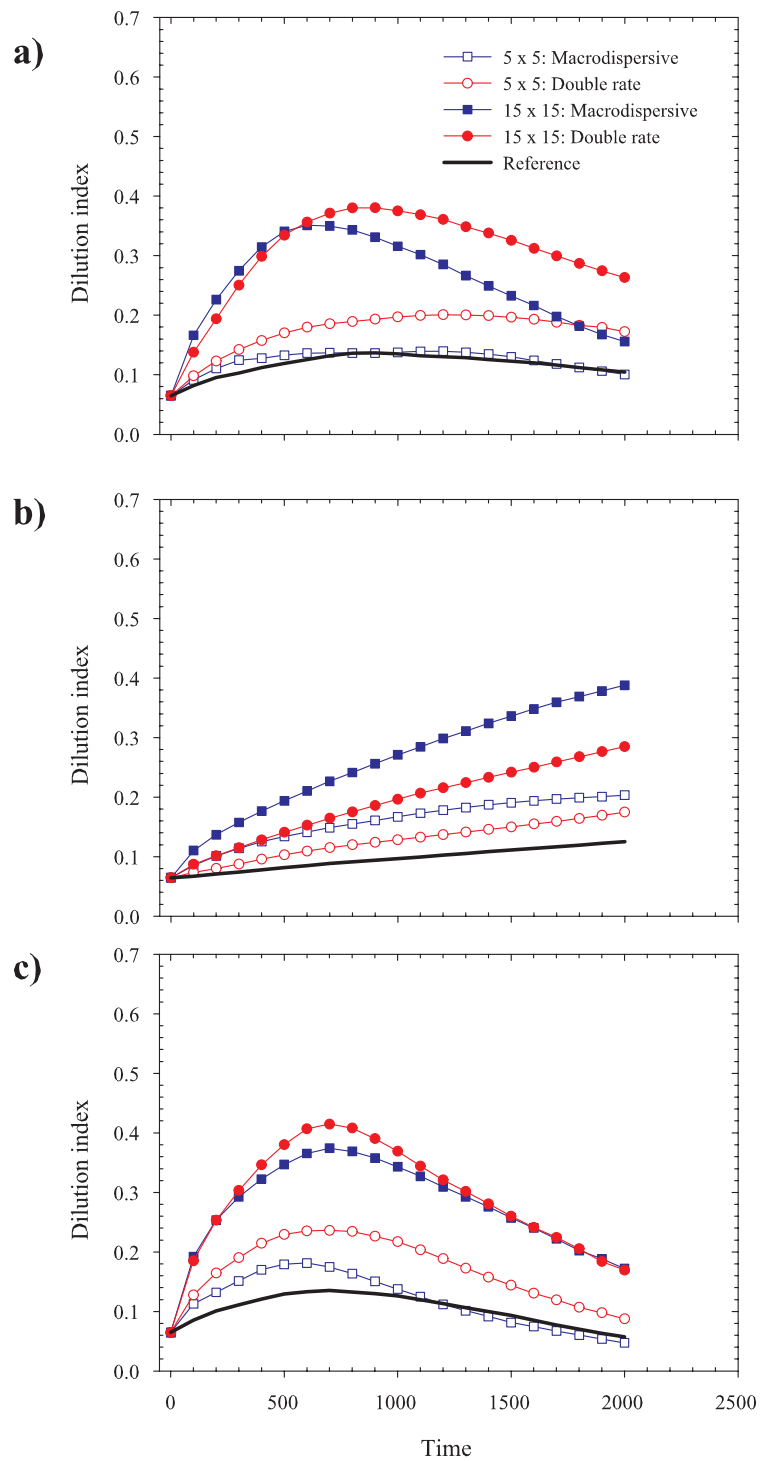


**Figure 4.20.** Comparison of the temporal evolution of the dilution index. (a) Scenario 1, b) scenario 2 and c) scenario 3.

where  $E(t)$  for a plume discretized over a set of  $m$  cells, each of which with a volume of  $\Delta V$ , is given as

$$E(t) = \Delta V \exp \left[ - \sum_{k=1}^m P_k(t) \ln(P_k(t)) \right] \quad (4.7)$$

where  $P_k(t)$  is the fraction of solute mass within the discretization cell with respect to the total mass of solute in the aquifer at time  $t$ . From a practical point view  $I$  expresses the ratio of the volume occupied by the solute mass in a region to the total aquifer volume at time  $t$ , indeed, if all mass would be uniformly distributed over just  $m_1$  cells, the value of  $E$  would be  $m_1 \Delta V$ .  $E_{max}$  is its maximum value that would correspond to maximum dilution when all mass is uniformly distributed over the entire aquifer, that is,  $m \Delta V$ . Thus, values of  $I$  near 1 indicate complete dilution, whereas values near 0 indicate incomplete dilution.

Figure 4.20 displays the evolution of  $I$  with time for the double rate and macrodispersive models and for the two upscaling sizes, it also shows the dilution in the reference case. To compute the dilution index the aquifer is discretized into 240 x 240 square cells of 1 unit size.

We can see that, for the reference case the dilution index goes from close to zero at the injection time (incomplete dilution) then reaches a maximum, and starts to decrease as soon as the mass starts exiting the aquifer. The dilution in the upscaled models is, in general considerably higher, except for scenarios 1 and 3 for which the enhanced macrodispersion upscaling approach gives very similar dilution index as in the reference. It is also observed that the larger the size of the upscaling block, the larger the dilution.

## 4.4 Summary and Conclusions

In this section we have analyzed how the upscaling techniques based on the introduction of additional process for modeling transport at the coarse scale perform. We have compared reference simulations of advective transport at a fine scale with those obtained from coarsened models at different degrees of upscaling under different scenarios. All scenarios have the same structure: a background heterogeneous multiGaussian field with embedded lenses of homogeneous transmissivities. The difference among the scenarios is the contrast between the lens transmissivity and the mean background conductivity. In scenario 1 the lenses have a conductivity value within the range of variability of the background values, in scenario 2, the lenses are much less conductive than the background, and in scenario 3, the lenses are much more conductive than the background.

Upscaling was performed at two different coarsening degrees. In one case each group of 5 by 5 cells was replaced by a homogeneous block, and in the other case, the upscaling was performed over groups of 15 by 15 cells. Both flow and transport upscaling had to be carried out. In flow upscaling the group of heterogeneous scalar transmissivities was replaced by a homogeneous transmissivity tensor. In transport upscaling, the model to simulate transport included additional processes; we considered two different transport models, the first one simply included an enhanced macrodispersion, and in the second one, in addition, the possibility of mass transfer into two immobile domains with different mass transfer rates is included.

As a general conclusion we can say that mass transport upscaling with blocks of 5 by 5 cells using the double rate mass transfer model provides quite good reproduction of most of the general characteristics of the solute plume both in space and time. This model only fails in the reproduction of the dilution, which is substantially larger in the upscaled model than in the reference one. When upscaling is performed with 15 by 15 blocks the results are not as satisfactory. Recall that the correlation lengths in the scenarios 2 and 3 were 7 along  $x$  and 2 along  $y$ , thus this upscaling block is larger than the correlation length. In any case, at the 15 by 15 block size, the double rate mass transfer model gives an acceptable approximation of the spatiotemporal distribution of the reference plume except for the dilution index.

It has also been observed that for the two scenarios in which the lenses accelerate, rather than retard, the particles, the enhanced macrodispersion transport model gives results very close to those obtained by the double rate mass transfer model.

We conclude that solute upscaling can be satisfactorily performed using appropriate flow upscaling and including multiple rate mass transfer for the simulation of the solute transport on the upscaled model as long as the blocks are not larger than the correlation scale of the underlying reference field. We also conclude that the enhanced macrodispersion is a good alternative to the multiple rate mass transfer when the heterogeneity is not characterized by the presence of very low transmissivities embedded within the aquifer that will act as retardation sites for the solute.

## 4.5 References

- Adams, E. E., L. W. Gelhar (1992), Field study of dispersion in a heterogeneous aquifer 2. Spatial moment analysis, *Water Resources Research*, 28(12), 3293-3307.

- Bajracharya, K., and D. A. Barry (1997), Nonequilibrium solute transport parameters and their physical significance: numerical and experimental results, *Journal of Contaminant Hydrology*, 24, 185–204.
- Barbelo, H. C., M. C. Hill, and D. Rosbjerg (2004), Investigating the Macrodispersion Experiment (MADE) site in Columbus, Mississippi, using a three-dimensional inverse flow and transport model, *Water Resources Research*, 40, W04211m doi:10.1029/2002WR001935.
- Berkowitz, B. and H. Scher(1998), Theory of anomalous chemical transport in random fracture networks, *Physical Review E*, 57(5) 5858–5869.
- Berkowitz, B. , H. Scher, and S.E. Silliman (2000), Anomalous transport in laboratory-scale, heterogeneous porous media, *Water Resources Research*, 36(1), 149–158.
- Berkowitz, B., A. Cortis, M. Dentz, and H. Scher (2006), Modeling non-fickian transport in geological formations as a continuous time random walk, *Reviews of Geophysics*, 44, RG2003, doi:10.1029/2005RG000178.
- Boggs, J. M., S. C. Young, and L. M. Beard (1992), Field study of dispersion in a heterogeneous aquifer 1. Overview and site description, *Water Resources Research*, 28(12), 3281–3291.
- Carrera, J, An Overview of uncertainties in modeling groundwater solute transport, *Journal of Contaminant Hydrology*, 13, 23–48.
- Carrera, J., X. Sánchez-Vila, I. Benet, A. Medina, G. Galarza, and J. Guimerà (1998), On matrix diffusion: formulations, solution methods and qualitative effects, *Hydrogeology Journal*, 6, 178–190.
- Cushman, J. H., and T. R. Ginn (2000), Fractional advection-dispersion equation: A classical mass balance with convolution-Fickian flux, *Water Resources Research*, 36(12), 3763—3766.
- de Marsily, G., F. Delay, J. Gonçalvès, P. Renard, V. Teles, and S. Viollette (2005), Dealing with spatial heterogeneity, *Hydrogeology journal*,13, 161–183.
- Dentz, M., and B. Berkowitz (2003), Transport behavior of a passive solute in continuous time random walks and multirate mass transfer, *Water Resources Research*, 39(5), 1111, doi:10.1029/2001WR001163.
- Dentz, M., A. Cortis, H. Scher, and B. Berkowitz (2004), Transport behavior of solute transport in heterogeneous media: transition from anomalous to normal transport, *Advances in Water Resources*, 27, 155–173.

- Doherty, J. (2004), *Manual for PEST*, 5th edition, Brisbane, Australia: Watermark Numerical Computing.
- Feehley, C. E., C. Zheng, and F. J. Molz(2000), A dual-domain mass transfer approach for modeling solute transport in heterogeneous aquifer: Application to the Macrodispersion Experiment (MADE) site, *Water Resources Research*, 36(9), 2501–2515.
- Fernández-García, D., T. H. Illangasekare, and H. Rajaram (2005a), Differences in the scale-dependence of dispersivity and retardation factors estimated from forced-gradient and uniform flow tracer tests in three-dimensional physically and chemically heterogeneous porous media, *Water Resources Research*, 41, W03012, doi:10.1029/2004WR003125.
- Fernández-García, D., T. H. Illangasekare, and Harihar Rajaram (2005b), Differences in the scale dependence of dispersivity estimated from temporal and spatial moments in chemically and physically heterogeneous porous media, *Advances in Water Resources*, 28, 745–759.
- Fernández-García, D., H. Rajaram, and T. H. Illangasekare (2005c), Assessment of the predictive capabilities of stochastic theories in a three-dimensional laboratory test aquifer: Effective hydraulic conductivity and temporal moments of breakthrough curves, *Water Resources Research*, 41, W04002, doi:10.1029/2004WR003523.
- Fernández-García and Gómez-Hernández (2007), Impact of upscaling on solute transport: travel times, scale-dependence of dispersivity and uncertainty, *Water Resources Research*, 43, W02423, doi:10.1029/2005WR004727, 2007.
- Gómez-Hernández, J. J., and Srivastava R. M. (1990), ISIM3D: An ANSI-C three-dimensional multiple indicator conditional simulation program, *Computer and Geosciences*, 16(4), 395–440.
- Gómez-Hernández, J. J. (1991), A stochastic approach to the simulation of block conductivity fields conditioned upon data measured at a smaller scale, Ph.D. thesis, Stanford University, CA., 351 pp.
- Gómez-Hernández, J. J., and A. G. Journel (1993), Joint sequential simulation of multi-Gaussian fields, in *Geostatistics Troia '92*, edited by A. Soares, vol. 1, 85–94, Kluwer.
- Gómez-Hernández, J. J. (2006), Complexity *Ground Water*, 44(6), 782–785.
- Guswa, A. J., and D. L. Freyberg (2002), On using the equivalent conductivity to characterize solute spreading in environments with low-permeability lenses, *Water Resources Research*, 38(8), 1132, doi:10.1029/2001WR000528.

- Guswa, A. J., and D. L. Freyberg (2000), Slow advection and diffusion through low permeability inclusions, *Journal of Contaminant Hydrology*, (46), 205–232.
- Haggerty, R., and S. M. Gorelick (1995), Multiple-rate mass transfer for modeling diffusion and surface reactions in media with pore-scale heterogeneity, *Water Resources Research*, 31(10) 2383–2400.
- Haggerty, R., S.A. McKenna, and L. C. Meigs (2000), On the late-time behaviour of tracer test breakthrough curves, *Water Resources Research*, 36(12), 3467–3479.
- Haggerty, R., and P. Reeves (2002), STAMMT-L: Solute Transport and Multirate Mass Transfer, Version 1.0, User’s Manual, *ERMS#520308*, Sandia Natl. Lab., Albuquerque, N. M.
- Harbaugh, A. W., Banta, E. R., Hill, M. C., and McDonald, M. G. MODFLOW-2000, The U.S. Geological Survey Modular Ground-Water Model-user guide to modularization concepts and the ground-water flow process, *Open-file Report 00-92*, 2000.
- Harvey, C., and S. M. Gorelick (2000), Rate-limited mass transfer or macrodispersion: Which dominates plume evolution at the Macrodispersion Experiment (MADE) site?., *Water Resources Research*, 36(3), 637–650.
- Herr M., G. Schafer, K. Spitz K. (1989), Experimental studies of transport in porous media with local heterogeneities, *Journal of Contaminant Hydrology*, 4, 113–205.
- Kullback, S. (1959), *Information of Theory and Statistics*. Wiley, New York.
- Kitanidis, P. K. (1994), The concept of the dilution index, *Water Resources Research*, 37(7), 2011–2026.
- Levy M. and Brian Berkowitz (2003), Measurement and analysis of non-Fickian dispersion in heterogeneous porous media, *Journal of Contaminant Hydrology*, 64, 203–226.
- Liu, G., C. Zheng, and S. M. Gorelick (2004), Limits of applicability of the advection-dispersion model in aquifers containing connected high-conductivity channels, *Water Resources Research*, 40, W08308, doi:10.1029/2003WR002735.
- Lu Z., and D. Zhang (2002), On stochastic modeling of flow in multimodal heterogeneous formations, *Water Resources Research*, 38(10), 1190, doi:10.1029/2001WR001026.

- Metzler, R. and J. Klafter (2000), The random walk's guide to anomalous diffusion: A fractional dynamics approach, *Physical reports*, 339, 1–77.
- McLaughlin, D. and F. Raun, Macrodispersivity and large-scale hydrogeologic variability, *Transport in porous media*, 42(1-2), 133–144.
- Morales-Casique, E., S. P. Neuman, A. Guadagnini (2006), Non-local and localized analyses of non-reactive solute transport in bounded randomly heterogeneous porous media: Theoretical framework, *Advances in Water Resources*, 29(9), 1399–1418.
- Neuman, S. P. (1993), Eulerian-Lagrangian theory of transport in spacetime nonstationary velocity fields: exact nonlocal formalism by conditional moments and weak approximation, *Water Resources Research*, 29(3), 633–645.
- Neuman, S. P., D. M. Tartakovsky (2008), Perspective on theories of non-Fickian transport in heterogeneous media, *Advances Water Resources*, in press.
- Salamon, P., D. Fernández-García, and Gómez-Hernández,(2007), A review and numerical assessment of the random walk particle tracking method, *Journal of Contaminant Hydrology*, 87(3-4), 277–305.
- Salamon, P., D. Fernández-García, and Gómez-Hernández,(2007), Modelig tracer transport at the MADE site: The importance of the heterogeneity, *Water Resources Research*, 43, W08404, doi:10.1029/2006WRR005522.
- Sánchez-Vila, X., J. P Girardi, and J. Carrera (1995), A synthesis of approaches to upscaling of hydraulic conductivities, *Water Resources Research*, 31(4), 867–882.
- Sánchez-Vila, X., A. Guadagnini, and J. Carrera (2006), Representative Hydraulic conductivities in saturated groundwater flow, *Rev. Geophys*, 44, RG3002, doi:10.1029/2005WRR000169.
- Sheibe TD, and S. Yabusaki (1998) Scaling of flow and transport behaviour in heterogeneous groundwater systems, *Advances in Water Resources*, 22(3),223–238.
- Renard P., and G. de Marsily (1997), Calculating equivalent permeability: A review, *Advances in Water Resources*, 20(5-6), 253–278
- Riva, M., A. Guadagnini, D. Fernández-García, X. Sanchez-Vila, T. Ptak (2008), Relative importance of geostatistical and transport models in describing heavily tailed breakthrough curves at the Lauswiesen site, *Journal of Contaminant Hydrology*, 101, 1–13.

- Rubin, Y., and A. G. Journel (1991), Simulation of non-Gaussian space random functions for modeling transport in groundwater, *Water Resources Research*, 27(7), 1711–1721.
- Rubin, Y. (1995), Flow and transport in bimodal heterogeneous formations, *Water Resources Research*, 31(10), 2461–2468.
- Wen, X. H., and J. J. Gómez-Hernández (1996), The constant displacement scheme for tracking particles in heterogeneous aquifers, *Ground Water*, 34(1), 135–142.
- Wen, X.-H., and J. J. Gómez-Hernández (1996), Upscaling hydraulic conductivities in heterogeneous media: An overview, *Journal of Hydrology*, 183 (1–2), ix–xxxii.
- Willmann, M., J. Carrera, and X. Sanchez-Vila (2008), Transport upscaling in heterogeneous aquifers: What physical parameters control memory functions?, *Water Resource Research*, doi:10.1029/2007WR006531.
- Zinn, B., and C. F. Harvey (2003), When good statistical models of aquifer heterogeneity go bad: A comparison of flow, dispersion, and mass transfer in connected and multivariate Gaussian hydraulic conductivity fields, *Water Resources Research*, 39(3), 1051, doi:10.1029/2001WR0

# 5

## Conclusions and Future Research

### 5.1 General Conclusions

The hydrogeologic properties of an aquifer often exhibit a high degree of spatial variability over a range of scales because of the heterogeneous nature of geologic formations. This implies that to predict the behavior of flow and transport a good characterization of the spatial variability is needed. Geostatistics provides the ability to characterize the spatial variation of hydrogeologic properties with high resolution. However, in hydrogeological modeling practice, due to the high computational demands to run flow and transport at such resolutions it is often necessary to reduce the dimensions of the problem. We have proposed a new technique for the upscaling of solute transport based on the modification of the constitutive transport equation at the coarse scale.

The proposed upscaling technique is based on the experimental evidence that plumes observed in field tests generally exhibit asymmetry and large tails, impossible to reproduce with an advection-dispersion model based on Fick's law. This is so, because mass transport is very much affected by the presence of high and low velocity zones, where the contaminant can travel quickly or get stagnant.

This non-Fickian behavior observed on field tests has moved researchers to investigate alternative formulations to the advection-dispersion equation (ADE). As reviewed in chapter 2, the approaches that can be proposed are:

Multirate mass transfer (MRMT), Time-Depend Macrodispersive (TDM), Continuous time random walk (CTRW) and Fractional Advection-Dispersion Transport (FADT). We have analyzed the use of the MRMT to model transport at the coarse scale after upscaling. We believe that the distribution of residence times within a given heterogeneous block can be easily captured by a homogeneous block with constant MRMT parameters. We replace a heterogeneous description of the transmissivity spatial variation with the fitting of a few parameters in the MRMT model. Contrary to similar proposals by other researchers we assume that the MRMT parameters are heterogeneous in space, and thus, they are fitted for each of the upscaling blocks.

Chapters 3 and 4 evaluate the proposed upscaling technique and compare with alternative techniques to conclude that solute upscaling can be performed using a double rate mass transfer approach for modeling transport at the coarse scale as long as the blocks are not larger than the correlation scale of the underlying heterogeneous transmissivity. We also conclude that this approach will work particularly well when there is an important fraction of very low transmissivity zones, as is the case of scenario 2 analyzed in chapter 4.

The major drawback of the proposed method, from a practical point of view, is that it can be computational expensive because since it requires to solve flow and transport at the fine scale. This is only of interest when running complex models that are to be used to simulate a more computational demanding problem, e.g., reactive transport with many species and reactions.

## 5.2 Future Research

The following future studies are suggested:

The extension of the methodology to three dimensions is important; flow and transport are always three dimensional and the issue of low and high velocity zones has less impact in 3D. It is also important to find an alternative to solve the flow and transport problem at the fine scale to determine the residence time of particles within the upscaling blocks. This could be solved in a way similar to how upscaling of flow is solved: by using a skin around the block being upscaled within which to solve a fine scale flow and transport problem. This skin should be large enough to impose a boundary conditions at the block sides as similar as possible to the ones the block really has.

The problem of reproducing dilution call for extending the memory function used in the modeling of transport in the upscaled models from just using the information about past concentrations within the block, to concentrations in the nearby blocks. That is, the memory function currently is only temporal, it should be made spatiotemporal.

Furthermore, it is important to test the methodology in a real-case study, such the one performed at the MADE site.



# A

## Calibration of Mass Transfer Parameters

This appendix describes the numerical details involved in the calibration process of mass transfer parameters. The objective function minimized by PEST included the estimates of the distribution function obtained at different times as well as the low-order temporal moments of  $f_\tau(\tau)$ , formally written as

$$J(\mathbf{P}) = \sum_{i=1}^{N_{obs}} \omega_i [F_\tau(t_i) - F_{\tau,m}(t_i; \mathbf{P})]^2 + \lambda_1 [\bar{\tau} - \bar{\tau}_m(\mathbf{P})]^2 + \lambda_2 [\sigma_\tau^2 - \sigma_{\tau,m}^2(\mathbf{P})]^2 \quad (\text{A.1})$$

where  $\mathbf{P}$  is a vector of parameters (see Table 3.1),  $N_{obs}$  is the number of time observations,  $F_\tau(t_i)$  is the sample cumulative distribution function of residence times at time  $t_i$ .  $F_{\tau,m}$  is the analytical solution (3.17),  $\bar{\tau}$  and  $\sigma_\tau^2$  are the sample mean and variance of the residence time distribution,  $\bar{\tau}_m$  and  $\sigma_{\tau,m}^2$  are the analytical solutions of the mean and variance of the residence time distribution, and  $\{\omega_i, \lambda_1, \lambda_2\}$  are the weights of the observations, mean and variance of the residence time. The number of estimated parameters depends on the selected upscaled mass transfer model. The analytical solution of the mean and variance of the residence time distribution can be easily obtained from (3.17) as

$$\bar{\tau}_m(\mathbf{P}) = - \lim_{p \rightarrow 0} \frac{d\bar{f}_\tau(p)}{dp} = \frac{L_b}{v_m} (1 + \beta) \quad (\text{A.2})$$

$$\sigma_{\tau,m}^2(\mathbf{P}) = \lim_{p \rightarrow 0} \frac{d^2 \ln \bar{f}_\tau(p)}{dp^2} = \frac{2A_\ell}{v_m^2} (1 + \beta)^2 L_b + \frac{2L_b}{v_m} \beta \int_0^\infty \frac{f(\alpha)}{\alpha} d\alpha \quad (\text{A.3})$$

These results are consistent with the temporal moment analysis conducted by Lawrence et al. (2006).

## A.1 Reference

Lawrence, A. E., X. Sanchez-Vila, and Y. Rubin, Conditional moments of the breakthrough curves of kinetically sorbing solute in heterogeneous porous media using multirate mass transfer models for sorption and desorption, *Water Resources Research*, 38(11), 1248, doi:10.1029/2001WR001006, 2002.